



DEVELOPMENT OF PROTEIN EXTRACTS -LOADED NANOCARRIERS
COMBINATION WITH MICROSPICULES FOR TRANSDERMAL DELIVERY



A Thesis Submitted in Partial Fulfillment of the Requirements
for Doctor of Philosophy (PHARMACEUTICAL TECHNOLOGY)
Department of PHARMACEUTICAL TECHNOLOGY
Graduate School, Silpakorn University
Academic Year 2021
Copyright of Silpakorn University

การพัฒนานาโนแคโรอีร์บรรจุสารสกัดโปรตีนร่วมกับเข็มนาคไมครอนเพื่อนำส่งทาง
ผิวหนัง



โดย
นางสาวกฤษณาพร ตันเสถียร

วิทยานิพนธ์นี้เป็นส่วนหนึ่งของการศึกษาตามหลักสูตรปรัชญาดุษฎีบัณฑิต
สาขาวิชาเทคโนโลยีสารสนเทศ แบบ 1.2 ปรัชญาดุษฎีบัณฑิต
ภาควิชาเทคโนโลยีสารสนเทศ
บัณฑิตวิทยาลัย มหาวิทยาลัยศิลปากร
ปีการศึกษา 2564
ลิขสิทธิ์ของมหาวิทยาลัยศิลปากร

DEVELOPMENT OF PROTEIN EXTRACTS -LOADED
NANOCARRIERS COMBINATION WITH MICROSPICULES FOR
TRANSDERMAL DELIVERY



By
MISS Kritsanaporn TANSATHIEN

A Thesis Submitted in Partial Fulfillment of the Requirements
for Doctor of Philosophy (PHARMACEUTICAL TECHNOLOGY)
Department of PHARMACEUTICAL TECHNOLOGY
Graduate School, Silpakorn University
Academic Year 2021
Copyright of Silpakorn University

Title Development of protein extracts -loaded nanocarriers combination
with microspicules for transdermal delivery
By Kritsanaporn TANSATHIEN
Field of Study (PHARMACEUTICAL TECHNOLOGY)
Advisor Professor PRANEET OPANASOPIT , Ph.D.

Graduate School Silpakorn University in Partial Fulfillment of the
Requirements for the Doctor of Philosophy

.....Dean of graduate school
(Associate Professor Jurairat Nunthanid, Ph.D.)

Approved by

.....Chair person
(Associate Professor Prasopchai Patrojanasophon , Ph.D.)

.....Advisor
(Professor PRANEET OPANASOPIT , Ph.D.)

.....Co advisor
(Assistant Professor NOPPARAT
NUNTHARATANAPONG , Ph.D.)

.....Co advisor
(Assistant Professor Worranan Rangsimawong , Ph.D.)

.....External Examiner
(Assistant Professor Sureewan Duangjit , Ph.D.)

60353801 : Major (PHARMACEUTICAL TECHNOLOGY)

Keyword : protein extract, nanocarriers, microspicules, transdermal delivery

MISS KRITSANAPORN TANSATHIEN : DEVELOPMENT OF PROTEIN EXTRACTS -LOADED NANOCARRIERS COMBINATION WITH MICROSPICULES FOR TRANSDERMAL DELIVERY THESIS ADVISOR : PROFESSOR PRANEET OPANASOPIT, Ph.D.

Proteins extracted from natural products are hydrophilic macromolecules which limited the ability to passively penetrate through the skin. The combination of penetration enhancing techniques such as nanocarriers and sponge microspicules might improve the transdermal delivery of extracted proteins. In this study, the aim was to extract the macromolecular proteins and growth factors from natural products, deer antler velvet (DAV) and porcine placenta (PPE), using the probe-sonication method. The percent yields, protein content, growth factors (FGF, EGF, IGF-1, TGF- β 1) and amino acid contents of the dry powder extract were determined. The bioactivities of these extracts on skin cells (normal human skin fibroblasts (NHFs) and human keratinocyte cells (HaCaTs)) and hair cells (human dermal papilla cells (HFDPCs)) were evaluated. Afterwards, the development of drug delivery systems (lipid based nanocarriers, polymer based nanocarriers and microspicules) for enhancing transdermal delivery of bioactive macromolecular protein was performed. The *in vitro* skin permeation study was used to evaluate the effective delivery system of macromolecular protein. For the *in vivo* human study, the effective formulations loading DAV or PPE were applied on the scalp skin of healthy human volunteers. Results presented that DAV and PPE extract containing proteins, growth factors, and amino acids improved both skin and hair regeneration by inducing bioactivities on skin and hair cells such as proliferation, migration, regeneration effect, anti-oxidant, anti-inflammation, and dermal papilla cell aggregation. To develop an effective transdermal delivery system of bioactive macromolecules, nanocarriers, and dermabrasion techniques were selected to enhance the skin permeation of macromolecular proteins. Niosomes (NIs) that exhibited the suitable physicochemical properties and the ability to deliver entrapped macromolecular protein through the skin more than other nanocarriers were chosen to develop the formulation with microspicules (MSs). High skin permeation of macromolecular proteins from NIs serum MSs was related to high deposition of entrapped compounds in skin and hair follicles, indicating that transdermal and transfollicular routes were the skin permeation pathways of this formulation. After applying DAV or PPE loaded NI serum MS on the skin for 14 and 30 days, increasing skin hydration and decreasing erythema index represented the improvement of skin condition without skin irritation. Furthermore, the formulation significantly increased hair elongation and melanin index, indicating the enhancement of hair growth promotion. In conclusion, proteins extracted from DAV and PPE act as the potent bioactive compounds to regenerate the skin and hair cells, which the suitable delivery system by using nanocarriers and microneedling techniques might play an important role to deliver bioactive compounds into and through the skin and hair follicles, resulting in an effective skin regeneration and hair growth promotion of natural product extract.

ACKNOWLEDGEMENTS

My dissertation would not be successful without someone to help and support me. Firstly, I would like to express my deep gratitude to my thesis advisor, Prof. Dr. Praneet Opanasopit, for supporting my Ph.D. study and related research. Throughout the research period, she helped me point out a solution to the problems.

In addition, I would like to express my sincere thanks to my thesis co-adviser, Assist. Prof. Dr. Nopparat Nuntharatanapong and Assist. Prof. Dr. Worranan Rangsimawong, for commenting and reviewing the work. This allows me to better carry out my work and write research.

Next, I sincerely thank you for this great opportunity from a scholarship and the facilities sponsors, The Thailand Research Funds through the Royal Golden Jubilee Ph.D. Program (Grant No. PHD/0192/2561), for financial support and Faculty of Pharmacy, Silpakorn University for facility support.

Moreover, I would like to express my deep gratitude to Professor Dr. Mont Kumpugdee Vollrath and the expert scientists at Berliner Hochschule für Technik (BHT), Berlin, Germany for providing research experience abroad and various facilitation and assistance while living abroad.

Also, I would like to give a special thanks to my colleagues, the Pharmaceutical Development of Green Innovation Group (PDGIG), for supporting laboratory techniques and their encouragement.

Finally, I would like to thank my family for supporting me. It allows me to go through difficult times.

For any mistake or inadequate information that may find in this dissertation, certainly, the responsibility is entirely my own.

MISS Kritsanaporn TANSATHIEN

TABLE OF CONTENTS

	Page
ABSTRACT.....	D
ACKNOWLEDGEMENTS.....	E
TABLE OF CONTENTS.....	F
LIST OF TABLES.....	K
LIST OF FIGURES.....	L
LIST OF ABBREVIATIONS.....	1
CHAPTER 1.....	8
INTRODUCTION.....	8
1.1 Statement and significance of the research problem.....	8
1.2 Aims and objectives.....	11
1.3 The research hypothesis.....	11
CHAPTER 2.....	12
LITERATURE REVIEWS.....	12
2.1 Aging skin and hair.....	12
2.2 Peptides, GFs and cytokines used in skin and hair rejuvenation.....	15
2.3 Natural resource extracts.....	15
2.3.1 DAV extract.....	15
2.3.2 Porcine placenta extract (PPE).....	16
2.4 Bioactivities for regenerative effect on skin and hair aging.....	17
2.4.1 Cell proliferation.....	17
2.4.2 Cytoprotective effect.....	18
2.4.3 Intracellular ROS reduction.....	18
2.4.4 Regenerative effect from UVB-irradiation.....	18
2.4.5 Cell migration.....	19
2.4.6 Anti-inflammation.....	19

2.4.7 Hair cell aggregation	20
2.5 Nanocarrier systems.....	20
2.5.1 Lipid-based nanocarriers	21
2.5.1.1 LI	21
2.5.1.2 NI.....	22
2.5.1.3 PEGylated lipid-based nanocarriers	22
2.5.2 Polymer-based nanocarriers	23
2.5.2.1. Chitosan (CS) NP	23
2.5.2.2. Chitosan-maleimide (CS-MHA) NP	23
2.6 Transdermal drug delivery of a macromolecular compound.....	24
CHAPTER 3	26
MATERIALS AND METHODS	26
3.1 Materials	26
3.2 Equipments	27
3.3 Methods	28
3.3.1 Extraction of DAV and PPE.....	28
3.3.1.1 Extraction method of DAV	28
3.3.1.2 Extraction method of PPE	28
3.3.1.3 Determination of %yield, total protein content, GFs, and amino acid content.....	29
3.3.1.3.1 Determination of %yield.....	29
3.3.1.3.2 Determination of total protein content.....	29
3.3.1.3.3 Polyacrylamide gel electrophoresis (SDS-PAGE) analysis.....	29
3.3.1.3.4 Determination of GFs content	29
3.3.1.3.5 Determination of amino acids.....	30
3.3.2 Determination of DAV and PPE bioactivity for skin and hair rejuvenation	30
3.3.2.1 Measurement of cell viability and cell proliferation on skin and hair cells.....	30

3.3.2.2 Determination of cell migration on skin cells	31
3.3.2.3 Evaluation on the repair of UVB-induced skin damage determination	31
3.3.2.3.1 Determination of cell viability of damaged-skin.....	31
3.3.2.3.2 Determination of procollagen I and MMP9 content in the damaged-skin	31
3.3.2.4 Determination of protective effect of the extracts on skin cells...	32
3.3.2.5 Intracellular reduction of ROS activity in skin cells	32
3.3.2.6 Anti-inflammatory activities	32
3.3.2.6.1 <i>In vitro</i> lipoxygenase (LOX) inhibition assay	32
3.3.2.6.2 Effect on the reduction of intracellular TNF- α	33
3.3.2.7 Determination of hair cell aggregation.....	33
3.3.3 Development of nanocarriers containing macromolecule for transdermal delivery	33
3.3.3.1 Preparation of macromolecule-loaded nanocarriers.....	33
3.3.3.1.1 Preparation of LI and pegylated liposome (PEG-LI)	33
3.3.3.1.2 Preparation of NI and pegylated niosome (PEG-NI).....	34
3.3.3.1.3 Preparation of CS-TPP NP and CS-MHA-TPP NP.....	34
3.3.3.2 The characterization of macromolecule-loaded nanocarriers.....	34
3.3.3.3 <i>In vitro</i> skin permeation and deposition studies	35
3.3.4 Development of NIs loaded MSs serum.....	36
3.3.4.1 Preparation of NIs loaded MSs serum.....	36
3.3.4.2 <i>In vitro</i> skin permeation study of NIs loaded MSs serum	36
3.3.4.3 CLSM study.....	36
3.3.5 Stability test.....	36
3.3.6 <i>In vivo</i> human study	37
3.3.7 Statistical analysis	38
CHAPTER 4	39
RESULTS AND DISCUSSION	39
4.1 Appearance and SDS-PAGE analysis of DAV and PPE.....	39

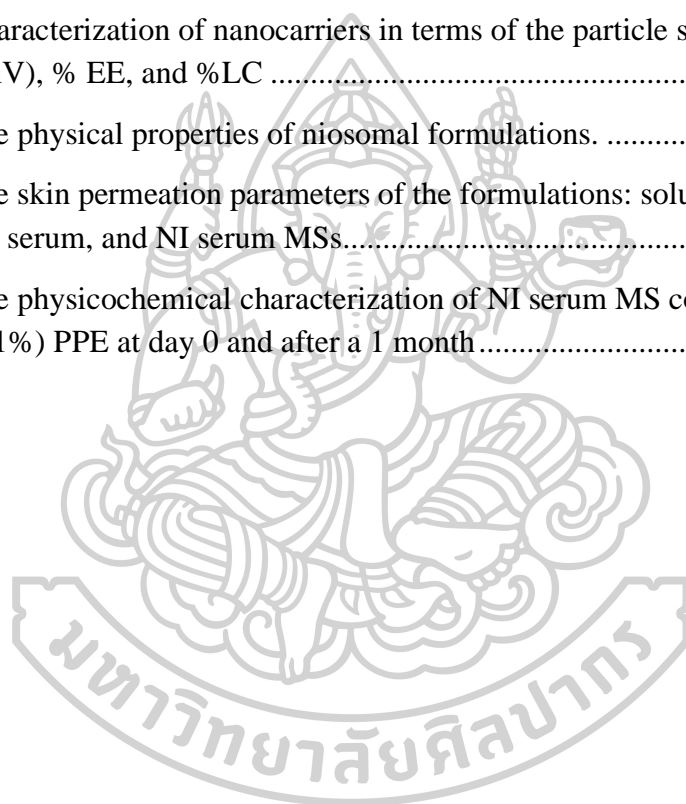
4.2 Quantitative analysis of % Yield, total protein, GFs (FGF2, EGF, IGF-1, and TGF- β 1) and amino acids in DAV and PPE	39
4.3 Bioactivities of DAV and PPE on skin and hair rejuvenation.....	40
4.3.1 Effect of DAV and PPE on cell viability of NHFs, HaCaTs, and HFDPCs	40
4.3.2 Effect of DAV and PPE on cell proliferation of NHFs, HaCaTs, and HFDPCs.....	41
4.3.3 Effect of DAV and PPE on skin cell migration.....	42
4.3.4 Repair of UVB-induced skin damage	43
4.3.5 Protective effect of DAV and PPE on skin cells	45
4.3.6 Effect of DAV and PPE on intracellular ROS reduction	48
4.3.7 Effect of DAV and PPE on anti-inflammation.....	49
4.3.7.1 Effect of DAV and PPE on inhibition of LOX enzyme	49
4.3.7.2 Effect of DAV and PPE on intracellular TNF- α reduction	50
4.3.8 Effect of DAV and PPE on the aggregation of hair cell	51
4.4 Development of nanocarriers for incorporation of a macromolecular protein ..	51
4.4.1 Physicochemical properties of nanocarriers.....	51
4.4.2 <i>In vitro</i> skin permeation and drugs deposited in the skin.....	52
4.5 Development of BSA-FITC-NIs loaded MSs serum.....	54
4.5.1 Physicochemical properties of niosomal formulations loaded BSA-FITC	54
4.5.2 <i>In vitro</i> skin permeation of niosomal formulations loaded BSA-FITC....	55
4.5.3 CLSM study	56
4.6 Stability study	60
4.7 <i>In vivo</i> human study.....	62
CHAPTER 5	66
CONCLUSION.....	66
5.1 Effect of DAV and PPE on skin and hair regeneration	66
5.2 Effect of nanocarriers and dermabrasion techniques on skin permeation for macromolecules	66

5.3 The effectiveness of DAV and PPE-loaded NI serum with sponge MSs for skin and hair regeneration	67
REFERENCES	68
APPENDIX.....	79
APPENDIX A.....	80
APPENDIX B	90
VITA.....	93



LIST OF TABLES

	Page
Table 1 The compositions of LI and PEG-LI	33
Table 2 The compositions of NI and PEGylated NI.....	34
Table 3 Percent yield, total protein content and the quantitative content of GFs (IGF-1, EGF, TGF- β 1, and FGF2), and amino acids in DAV and PPE	40
Table 4 Characterization of nanocarriers in terms of the particle size (nm), PDI, zeta potential (mV), % EE, and %LC	52
Table 5 The physical properties of niosomal formulations.	54
Table 6 The skin permeation parameters of the formulations: solution, base, NI solution, NI serum, and NI serum MSs.....	56
Table 7 The physicochemical characterization of NI serum MS containing (0.2%) DAV or (0.1%) PPE at day 0 and after a 1 month.....	61



LIST OF FIGURES

	Page
Figure 1 Overview of major signaling pathways in the intrinsically and extrinsically aged skin (28).....	13
Figure 2 Factors affecting the homeostasis and aging of humans (7).....	13
Figure 3 Hair growth and aging processes (12, 32, 33).....	14
Figure 4 The schematic of nanocarriers for dermal or transdermal drug delivery (84).....	20
Figure 5 The structure of liposomal vesicle composed of phospholipid bilayers and entrapped both lipophilic (●) and hydrophilic (◆) compounds (86).....	21
Figure 6 The feature of niosomal vesicle (89).....	22
Figure 7 Image of polymeric NP types: polymeric nanosphere and polymeric nanocapsule (21).....	23
Figure 8 The schematic of transdermal drug delivery and penetration pathways: transcellular, intercellular, and follicular pathways (16).....	24
Figure 9 The schematic of a diagram represented the strategies applied for the increment of skin penetration (91).....	25
Figure 10 Image of protein separation by SDS-PAGE electrophoresis.....	29
Figure 11 Image of process for content determination of GFs by ELISA.....	30
Figure 12 Image of appearance and proteins analysis using electrophoresis technique (SDS-PAGE) of DAV (A) and PPE (B).....	39
Figure 13 The %cell viability of NHFs (A), HaCaTs (B) and HFDPCs (C) treated with DAV (●) and PPE (✕) at various concentrations (1-4,000 µg/mL). * expresses the significant difference between the treatment compound ($p < 0.05$)......	41
Figure 14 The % cell proliferation of skin and hair cells treated with DAV and PPE for 24 h (✕), 48 h (□), and 72 h (▲): (A-1 and A-2) NHFs cell proliferation, (B-1 and B-2) HaCaTs cell proliferation, and (C-1 and C-2) HFDPCs cell proliferation. * represents the significant difference value compared to time 24 h ($p < 0.05$)......	42
Figure 15 Image-based monitoring of human skin fibroblasts migration at 0, 24 and 48 h for untreated cell (A), cells treated with TGF-β1 (B), DAV 2000 µg/mL (C), and	

- PPE 1000 $\mu\text{g/mL}$ (D). All images were obtained at a magnification of $4\times$ objective lens.43
- Figure 16 The % cell viability of UVB-irradiated cells treated with DAV (A) and PPE (B). The mark (+) indicated the samples exposure to the substance, while the mark (-) presented the samples have not been exposed to the substance. For statistical symbols, # and * demonstrate the significant difference value between the control non-UVB-irradiated group and control UVB-irradiated group, respectively.44
- Figure 17 The extracellular procollagen I ($\text{pg}/\mu\text{g}$) level of the extracts-treated UVB-exposed NHFs cells (A) and an intracellular procollagen I ($\text{pg}/\mu\text{g}$) level of the extracts-treated UVB-exposed NHFs (B) compared with the control group (non-treatment). * exhibits statistically significant difference from the control ($p < 0.05$). .45
- Figure 18 The extracellular MMP9 ($\text{mg}/\mu\text{g}$) level of the extracts-treated UVB-exposed HaCaTs cells (A) and an intracellular MMP9 ($\text{mg}/\mu\text{g}$) level of the extracts-treated UVB-exposed HaCaTs (B) compared with the control group (non-treatment). * show statistically significant difference from the control ($p < 0.05$).45
- Figure 19 Protective effect of DAV (A) and PPE (B) on skin cells prior to $200 \mu\text{M}$ t-BHP-exposed for 4 h. The mark (+) indicated the samples exposure to the substance, while the mark (-) presented the samples have not been exposed to the substance. # and * demonstrate a significant difference value from the control non-t-BHP-exposed group and the control t-BHP-exposed group, respectively.47
- Figure 20 % Intracellular ROS reduction on HaCaTs pretreated with DAV, PPE and positive control ($100 \mu\text{M}$ quercetin) after inducing ROS production with 1mM t-BHP. The mark (+) indicated the samples exposure to the substance, while the mark (-) presented the samples have not been exposed to the substance. # and * present the significant difference value compared to control non-treatment with t-BHP group and control t-BHP-induced HaCaTs cells group ($p < 0.05$), respectively.49
- Figure 21 Effect of non-treatment group (negative control), $300 \mu\text{M}$ of ASA (positive control), PPE (200 and $1,000 \mu\text{g/mL}$), and DAV (200 and $1,000 \mu\text{g/mL}$) on intracellular $\text{TNF-}\alpha$ ($n=3$). The mark (+) indicated the samples exposure to the substance, while the mark (-) presented the samples have not been exposed to the substance. * exhibits the significant difference value from control ($p < 0.05$).50
- Figure 22 Effects of DAV and PPE on HFDPCs aggregation: (A1-A4) control group at time 0, 24, 48, 72 h, (B1-B4) the cells treated with $2,000 \mu\text{g/mL}$ of DAV at time 0, 24, 48, 72 h, and (C1-C4) the cells treated with $1,000 \mu\text{g/mL}$ of PPE at time 0, 24, 48, 72 h.51
- Figure 23 The cumulative permeation profile of BSA-FITC loaded nanocarriers: LI (---■---), PEG-LI (---□---), NI (---▲---), PEG-NI (---△---), CS-TPP NP (---◆---), CS-MHA-TPP

- NP (—◇·-) at various time interval (0-8 h) compare to solution (—●—) (n=3). * presents the significant difference value compare to BSA-FITC solution.53
- Figure 24 The profile of BSA-FITC deposited in the skin ($\mu\text{g}/\text{mL}$) in various types of nanocarriers containing BSA-FITC: LI, PEG-LI, NI, PEG-NI, CS-TPP NP, and CSM-TPP NP compared to BSA-FITC solution (N=3). * expresses the significant difference from solution form ($p < 0.05$).54
- Figure 25 The cumulative BSA-FITC permeation-time profiles of NI serum MSs (—●—), NI serum (—■—), NI solution (—▲—), base (—□—), and solution (—*—). The data represent average \pm S.D. (n = 3). * presents significant difference values from solution (p -value < 0.05).56
- Figure 26 The x-z axis serial images from CLSM of skins treated with BSA-FITC solution (A), BSA-FITC-loaded Rh-PE-probed NI (B), and BSA-FITC-loaded Rh-PE-probed NI serum MSs (C) for 8 h. The images show green fluorescence of BSA-FITC and red fluorescence of Rh-PE (10 \times objective lens).59
- Figure 27 CLSM images of the skin cross-section after being treated with (A) BSA-FITC solution and BSA-FITC-loaded Rh-PE-probed nanocarriers: (B) NI solution and (C) NI serum MSs for 8 h. The images show (1) bright field, (2) green fluorescence of BSA-FITC, (3) red fluorescence of Rh-PE and (4) overlay of (2) and (3) (10x objective lens).60
- Figure 28 Appearance of NI serum MS containing (0.1%, w/v) PPE (A) or61
- Figure 29 Images of change in the length of hair: non-treatment (A-C) at day 0 (A) (79.7x magnification), day 14 (B) (80.4x magnification), and day 30 (C) (14.4x magnification), after applying NI serum MSs containing (0.2%, w/v) DAV (D-F) at day 0 (D) (77.2x magnification), day 14 (E) (24x magnification), and day 30 (F) (10x magnification), and after applying NI serum MSs containing (0.1%, w/v) PPE (G-I) at day 0 (D) (69x magnification), day 14 (E) (19.8x magnification), and day 30 (F) (19.8x magnification).63
- Figure 30 The percentage of hair elongation (%), A), %MI (B) skin hydration (%Hydration, C) and, %EI (D), after treatment with NI serum MSs containing DAV extract for 14 days and 30 days. The data represents average \pm S.D. (n = 12). * present significance difference value from control (untreated skin) ($p < 0.05$).64
- Figure 31 The percentage of hair elongation (%), A), %MI (B), skin hydration (%Hydration, C), and %EI (D) after treatment with NI serum MSs containing PPE extract for 14 days and 30 days. The data represents average \pm S.D. (n = 12). * present significance difference value from control (untreated skin) ($p < 0.05$).65

LIST OF ABBREVIATIONS

AAPH	2,2'-Azobis(2-amidinopropane) dihydrochloride
ABTS	3-ethylbenzothiazoline-6-sulfonic acid
AGA	androgenetic alopecia
ALT	alanine aminotransferase
ANOVA	one-way analysis of variance
ASA	aspirin
AST	aspartate aminotransferase
bFGF	basic fibroblast growth factor
BCA	bicinchoninic acid
BSA	bovine serum albumin
BSA-FITC	bovine serum albumin-fluorescein isothiocyanate
$\text{Ca}_5(\text{PO}_4)_3\text{OH}$	calcium hydroxyapatite
CD4^+	the cluster of differentiation 4 positive cells
CD8^+	the cluster of differentiation 4 positive cells
CHCl_3	chloroform
CH_3COOH	acetic acid
Chol	cholesterol
CLSM	confocal laser scanning microscope
cm^2	square centimeters
CO_2	carbon dioxide
CS	chitosan
CS-MHA	chitosan-maleimide
Da	dalton
DAV	deer antler velvet
DCF	dichlorofluorescein
DEJ	dermal-epidermal junction
DMEM	Dulbecco's Modified Eagle's Medium

DMSO	dimethyl sulfoxide
DNA	deoxyribonucleic acid
DP	dermal papillae
DPPH	2,2-diphenyl-1-picrylhydrazyl
ECM	extracellular matrix
EDTA 2Na	ethylene diamine
EE	entrapment efficiency
e.g.	exempi gratia (Latin); for example
EGF	epidermal growth factor
EI	erythema index
ELISA	enzyme-linked immunosorbent assay
ER	enhancement ratio
et al.	and others
etc	Et cetera
ETOH	Ethanol
FBS	fetal bovine serum
FDA	The United States Food and Drug Administration
Fe ²⁺	ferrous ion
Fe ³⁺	ferric ion
Fe ₂ (SO ₄) ₃	ferric sulfate
FGF	fibroblast growth factor
FGF2	human fibroblasts growth factor basic
FIR	far infrared
FI	fluorescence intensity
FOX	ferrous oxidation–xylenol orange
FRAP	ferric reducing antioxidant power
g	gram(s)
GAG	sulfated-glycosaminoglycan
GFs	growth factors
GL	Glycine-leucine

h	hour(s)
HaCaTs	immortalized human keratinocytes
H ₂ DCF-DA	2',7'-dichlorodihydrofluorescein diacetate
H ₂ DCF	2',7'-dichlorodihydrofluorescein
HFDPCs	human follicle dermal papilla cells
H ₂ SO ₄	sulfuric acid
IC ₅₀	The half-maximal inhibitory concentration
i.e.	id est (Latin); that is
Ig	immunoglobulin
IGF	insulin-like growth factor
IGF-1	insulin-like growth factor-1
IGFBP	insulin-like growth factor binding protein
IL	interleukin
iNOS	inducible NO synthase
KCl	potassium chloride
kDa	kilodalton
KH ₂ PO ₄	potassium dihydrogenphosphate
kHz	kilohertz
kJ	kilojoule
Kp	permeation coefficient
LA	linoleic acid
LC	loading capacity
LG	leucine-glycine
LI	liposome
LOX	lipoxygenase
LPS	lipopolysaccharide
M	molarity
MeOH	methanol
MHA	6-maleimidohexanoic acid
mg	milligram(s)

MI	melanin index
Microcare PHC	Phenoxyethanol (and) Chlorphenesin (and) Water (and) Glycerin
min	minute(s)
mL	milliliter(s)
mM	millimolar
MMPs	matrix metalloproteinases
MMP1	matrix metalloproteinase1
MMP2	matrix metalloproteinase2
MMP3	matrix metalloproteinase3
MMP8	matrix metalloproteinase8
MMP9	matrix metalloproteinase9
MMP10	matrix metalloproteinase10
MMP11	matrix metalloproteinase11
MMP13	matrix metalloproteinase13
MMP18	matrix metalloproteinase18
MMP19	matrix metalloproteinase19
mRNA	messenger ribonucleic acid
MS	sponge spicule extract powder
MTT	3-(4,5-Dimethylthiazol-2-yl)-2,5-diphenyltetrazolium
mV	millivolt(s)
MW	molecular weight
NaCl	sodium chloride
NAD ⁺	nicotinamide adenine dinucleotide
Na ₂ HPO ₄	disodium hydrogen phosphate
NaOH	sodium hydroxide
NHFs	normal human skin fibroblasts
ng	nanogram
NI	niosome
NK	natural killer

NLC	nanostructured lipid carrier
nm	nanometer(s)
nmol	nanomole(s)
NP	nanoparticle
O.D.	optical density
PBS	phosphate buffer saline
PC	Egg phosphatidylcholine
PDGF	platelet derived growth factor
PDI	polydispersity index
PEG	polyethylene glycol
PEG-NI	pegylated niosome
PEG-LI	pegylated liposome
PEG2000-DSPE	N-(carbonyl-methoxypolyethyleneglycol-2000)- 1,2-distearoyl-sn-glycero-3-phosphoethylene sodium salt
pH	potentia hydrogenii (Latin); potential for hydrogen
pI	isoelectric point
pg	picogram
PPE	porcine placenta extract
Pre-mRNA	pre-mature ribonucleic acid transcript
Rh-PE	Lissamine™ Rhodamine B 1,2-Dihexadecanoyl- sn-Glycero-3-Phosphoethanolamine, Triethylammonium Salt
ROS	reactive oxygen species
rpm	revolutions per minute
SC	stratum corneum
S.D.	standard deviation
SDS	sodium dodecyl sulfate
SDS-PAGE	sodium dodecyl sulfate-polyacrylamide gel electrophoresis
SEPIMAX ZEN™	Polyacrylate Crosspolymer-6

SLN	solid-lipid nanoparticle
Span [®] 20	sorbitan laurate
t-BHP	<i>tert</i> -butyl hydroperoxide
TEWL	transepidermal water loss
TGF- β	transforming growth factor- β
TGF- β 1	transforming growth factor- β 1
Th1	T helper cell 1
Th2	T helper cell 2
Th17	T helper cell 17
TIMP	tissue inhibitor of metalloproteinase
Tnnt1	troponin T1
TPP	sodium tripolyphosphate
Treg	regulatory T
Trypsin-EDTA	trypsin-ethylenediaminetetraacetic acid
TNF- α	tumor necrosis factor-alpha
Tnni 1	troponin I
Tpm2	tropomyosin 2
UV	ultraviolet
UVA	ultraviolet A
UVB	ultraviolet B
UVC	ultraviolet C
UVR	ultraviolet radiation
VEGF	vascular endothelial growth factor
V	volt(s)
W	watt(s)
w/v	weight by volume
μ g	microgram(s)
μ L	microliter(s)
μ m	micron; micrometer(s)
μ M	micromolar

%	percentage(s)
TM	trademark
®	registered trademark
°C	degree Celsius



CHAPTER 1

INTRODUCTION

1.1 Statement and significance of the research problem

Aging affects the lifespan of human, which the loss of physiological integrity and impaired of functions can be defined. The biological of aging is time-dependent functional decline to bring the pathologies associated with aging. Current molecular and cellular research show nine hallmarks of aging: genomic instability, telomere attrition, epigenetic alterations, loss of proteostasis, deregulation of nutrient sensing, mitochondrial dysfunction, cellular senescence, stem cell exhaustion and alteration in intercellular communication (1).

Skin is the largest organ of human body and has multiple functions such as the protection of the body form physical, chemical and microbiological agents, the sensation of signals such as pressure or touch detection, vibration, heat or cold, and pain, as well as regulatory response. When entering the state of skin aging, the changing of morphological and physiological cause many functions to become progressively worse (2). Skin aging or cutaneous aging is divided into intrinsic and extrinsic process. Intrinsic or chronological aging is genetically determined. For the histology of this process, the epidermis layer is thinner with a flattening of the dermal-epidermal junction, resulting in loss of surface area and a decrease in epidermal cell turnover. While the dermis becomes atrophic, leading to reduced numbers of fibroblasts and decreased the number and diameter of collagen fiber bundles. Extrinsic aging causes by external factors such as sun exposure or photoaging as well as pollution, resulting in epidermal atrophy, fragmentation of collagen and elastic fibers and elastosis. The clinical signs of aging skin are dryness, rhytids or wrinkles, irregular pigmentation, loss of elasticity, telangiectasia, and areas of purpura (3).

Ultraviolet (UV) ray is a natural component of sunlight and invisible to the human eyes. There are divided into three types according to wavelength: ultraviolet A (UVA) (315–400 nm), ultraviolet B (UVB) (280–315 nm), and ultraviolet C (UVC) (100–280 nm). UVB directly affects the deoxyribonucleic acid (DNA) damage, whereas UVA indirectly damages DNA (4). Apart from UV-induced skin aging, the environmental pollutions such as motor vehicle emissions, fossil fuel combustion, forest fires and air pollution or chemical agents at industrial sites are also exogenous factor to induce the aging of skin. An exposure to these exogenous factors has been shown to be a major contributing factor to the production of reactive oxygen species (ROS), as one type of free radical, and the generation of oxidative stress through a variety of mechanisms (5). ROS affects the cellular signaling pathway, resulting in the increase of matrix metalloproteinases (MMPs) and proinflammatory cytokines expression, causing dermal extracellular matrix (ECM) degradation. Collagen is the principal structural protein in the ECM of the dermis, which the decreasing of collagen production and increasing MMP activity in chronic UV exposure leads to a significant collagen destruction. Collagen levels are further reduced due to alterations in gene expression resulting in a decrease of procollagen synthesis (6). Currently, Kanaki et al (2016) reported the biomarkers of aging as the biological parameters to

predict the pathologies and body function changes of aged skin such as DNA, proteins, immunological biomarkers, hormones, metabolic markers, inflammatory markers, oxidative stress markers, and apoptosis markers. In human skin aging, the free radical or the oxidative stress theories can explain the mechanism of aging process. Another important overexpression of ROS is strongly triggered the inflammation by inducing the stimulation of inflammatory mechanism of the organism. (2). In the free radical, oxidative and mitochondrial theories of aging, an aging process caused by the accumulation of oxidative damage in biomolecules. Normally, the functional organisms show a balance between free radicals or ROS and antioxidant defenses. If they loss of balance, it leads to the production of the oxidative stress. This situation results in oxidative cell injury, which the mitochondrial level causes a loss of bioenergetic competence, and a deterioration of cell function (7). Besides, inflammation is a causative agent in aging known as inflamm-aging (8). With aging the level of pro-inflammatory compounds increase and it is higher than the level of anti-inflammatory compounds, leading to show the inflammatory stress. Moreover, aging seems to be associated with an oxidative and inflammatory stress (7).

Apart from skin, hair is a derivative of epidermis layer. It can be divided into two parts: the follicle in the skin and the hair shaft, which is visible on the body surface. In humans, its main functions are the skin protection and sexual and social communication. The development of hair is a dynamic and cyclic process, depending on the duration of growth cycles. Hair follicles grow in repeated cycles (9), which hair growth cycle can be divided into 3 major phases: anagen phase, catagen phase, and telogen phase. Anagen phase refers to active growth phase, which accounts for 85 - 90 percent of the hair growth cycle. Catagen phase refers to the period of involution. Telogen phase is a phase of relative quiescence. Hair pigmentation, also known as hair color, is a variation of amount and type of melanin pigment production. The melanin is synthesized in melanosomes, and then transferred from melanocytes to keratinocytes of skin and hair (10). In age-related hair changes, it involved with the progressive degeneration of hair fibers, decreasing of the melanocyte function or graying, and reducing of the hair production in androgenetic and senescent alopecia. Hair aging is caused by in intrinsic and extrinsic factors. Intrinsic factors are related to individual genetic such as familial premature graying, and androgenetic alopecia (AGA), while extrinsic factors are ultraviolet radiation (UVR), air pollution, smoking, nutrition, and lifestyle (11). Oxidative stress is related with the aging process as described above. For the effect of oxidative stress on the aging of hair, it involved with a combination of pre-emerging and post-emerging factors on hair fiber. Sources of oxidative stress with impact on the pre-emerging fiber include oxidative metabolism, smoking, UVR and inflammation from microbial, pollutant or irritant origins. Sources of oxidative stress that impact the post-emerging fiber such as UVR, chemical insults and oxidized scalp lipids (12).

Growth factors (GFs) are endogenous signaling molecules that regulate cellular processes of migration, proliferation, differentiation and metabolism. The major GFs involved in skin regeneration are epidermal growth factor (EGF), platelet derived growth factor (PDGF), basic fibroblasts growth factor (basic FGF), transforming growth factor- β (TGF- β), insulin-like growth factor (IGF) and vascular endothelial growth factor (VEGF) families (13). For skin aging strategies, peptides

and GFs are one type of cell regulators and have direct effects on collagen metabolism and production, including migration, proliferation, and differentiation (14). However, GFs present some critical limitations due to their low stability and high molecular weight (MW). To overcome the limitations, drug delivery systems have been developed to improve the stability and the skin permeability of the GFs (13).

Transdermal delivery system has been studied for drug transportation through the skin barrier into the target of action, which this route has many advantages such as avoiding first pass metabolism, improving patient compliance, reducing side effects, etc (15). Skin is the largest organ of the human body and composed of three layers: epidermis, dermis and hypodermis. In the epidermis, stratum corneum (SC) is the important barrier for permeation of compounds through the skin (16). Therefore, the properties of compounds such as high MW (> 500 dalton (Da)), very low or high partition coefficient and low solubility in water and lipid may limit the skin permeation (17). For penetration pathways, the mechanism of molecules to move across the SC can be divided into three routes: transcellular, intercellular and transfollicular pathways (18). Many pharmaceutical and cosmetic industries have been developed potential transdermal drug delivery system to transport active macromolecular compounds (e.g., proteins, peptides and genes) for treatment of cutaneous disease or skin rejuvenation (19).

In the past, the majority of newly and potentially potent protein and peptide drugs was developed to improve therapeutic effect of therapeutic protein such as human insulin, interleukin (IL)-2, calcitonin, EGF, etc. The approaches to enhance percutaneous proteins or peptides delivery are passive diffusion, chemical permeation enhancers, iontophoresis, electroporation, ultrasound and others (20). Chaulagain et al. (2018) reported that the strategies for improving passive transport of proteins were the use of carrier support adjuvants, nanocarriers and miscellaneous (21). Nanocarriers and encapsulation technologies were mostly studied for protein transdermal delivery. Encapsulation was the entrapment of the compounds within phospholipid or polymeric delivery system such as liposomes (LIs), niosomes (NIs), nanoparticles (NPs), etc. The advantages of protein encapsulation in the delivery systems include slow or controlled release of protein, improvement of protein stability, and promotion of cutaneous delivery (22). The composition of nanocarriers such as lipid, surfactants, and skin penetration enhancer could affect the skin permeation by disrupting the lipid bilayer structure of SC and increasing the dermal permeability. Moreover, creating micron-scale pores in the SC (e. g. microneedle) has been reported to associate the transport of large molecules through the skin (23).

Therefore, the aim of this study was to extract the macromolecular proteins and GFs from natural products, deer antler velvet (DAV) and porcine placenta, using probe-sonication method. The % yields, protein content, GFs (human FGF basic (FGF2), human EGF, human insulin-like growth factor-1 (IGF-1), human transforming growth factor- β 1 (TGF- β 1)) concentrations and the component of amino acids of the dry powder extracts were determined. The bioactivities of the extracted proteins (GFs) on skin cells (normal human skin fibroblasts (NHFs) and immortalized human keratinocytes (HaCaTs)), and hair cells (human follicle dermal papilla cells (HFDPCs)) such as cell proliferation, regenerative effect and intracellular ROS were evaluated. Afterwards, development of drug delivery systems (lipid based nanocarrier, polymer based nanocarrier and microspicules (MSs)) for enhancing transdermal

delivery of bioactive macromolecular protein was performed. After applying the macromolecular protein, the changes of skin structure and permeation enhancement were investigated. Finally, the *in vivo* transdermal delivery efficiency of the developed natural protein extract-loaded nanocarriers in combination with MSs cream/serum base products were performed in healthy human volunteers.

1.2 Aims and objectives

1. To extract proteins (GFs) from DAV and porcine placenta, and determine the *in vitro* bioactivities.
2. To develop protein extracts-loaded nanocarriers in combination with MSs for transdermal delivery
3. To evaluate the physicochemical properties, *in vitro* skin permeation, and the penetration mechanism of protein extracts-loaded nanocarriers combined with MSs.
4. To evaluate the *in vivo* human studies of protein extracts-loaded nanocarriers combination with MSs for transdermal delivery.

1.3 The research hypothesis

1. Proteins (GFs) can be extracted from DAV and porcine placenta, and have many bioactivities such as proliferation, regenerative, antioxidant, migration, and anti-inflammation activities.
2. Different physicochemical properties of the nanocarriers (particle size, size distribution, surface charge, entrapment efficiency (EE), and loading capacity (LC)) and the combination with MSs have an influence on *in vitro* skin permeation of the extracted protein.
3. The combination of nanocarrier systems and MSs can facilitate penetration of the hydrophilic protein extracts through the skin and improve the skin and hair regeneration effect.

CHAPTER 2

LITERATURE REVIEWS

2.1 Aging skin and hair

Aging affects the lifespan of a human, it leads to the loss of physiological integrity and functional impairment of the cells, tissues, or organs. Aging is a time-dependent process of functional decline led to increased vulnerability disease (1). Skin and hair aging are common problems that are concerned by many people and research is needed to improve the quality of life of the elder.

Skin is composed of epidermis, dermis and hypodermis. The epidermis consisting of keratinocytes continues the proliferation process in the basal layer. It is attached to the dermal-epidermal junction (DEJ) or the epidermal basement membrane. The dermis plays an important role to support the epidermis, and provides tensile strength as well as resilience properties of the skin. The dermis contains the skin appendages and hair follicle associated with sebaceous glands. It is mainly composed of ECM and fibroblasts, which can be divided into the papillary dermis and reticular dermis. The papillary dermis connected to the DEJ is enclosed by loose type I and type III collagen and elastin fibers. It contains a high density of fibroblasts regulating the production and modulation of ECM. The ECM maintain the structural integrity of the dermis. The reticular dermis comprises dense bundles of type I collagen fibers (24). Moreover, the ECM controls cellular functions (for example differentiation, proliferation, migration) and cell survival (25). Therefore, the collagen fibers that are found around 70% in the dermis layer maintain the strength and toughness of the skin, while elastin fibers affect the elasticity and flexibility of the skin. The ECM of the dermis layer is degraded by MMPs. There are outstanding in three types as follows: collagenases, gelatinases, and stromelysins. The collagenases such as matrix metalloproteinase-1 (MMP1), matrix metalloproteinase-8 (MMP8), Matrix metalloproteinase-13 (MMP13), and matrix metalloproteinase-18 (MMP18) facilitate the cleavage of interstitial collagen. The gelatinases (matrix metalloproteinase-2 (MMP2) and matrix metalloproteinase-9 (MMP9)) break basement membrane collagens and denature the collagen structure. The stromelysins, for example, matrix metalloproteinase-3 (MMP3), matrix metalloproteinase-10 (MMP10), matrix metalloproteinase-11 (MMP11), and matrix metalloproteinase-19 (MMP19) degrade basement membrane collagens, proteoglycans and matrix glycoprotein (26). Mechanisms of skin aging are dominantly involved with the progressive loss of skin cells and the degradation of ECM (27). An overview of common signaling pathways of skin aging is presented in **Figure 1**.

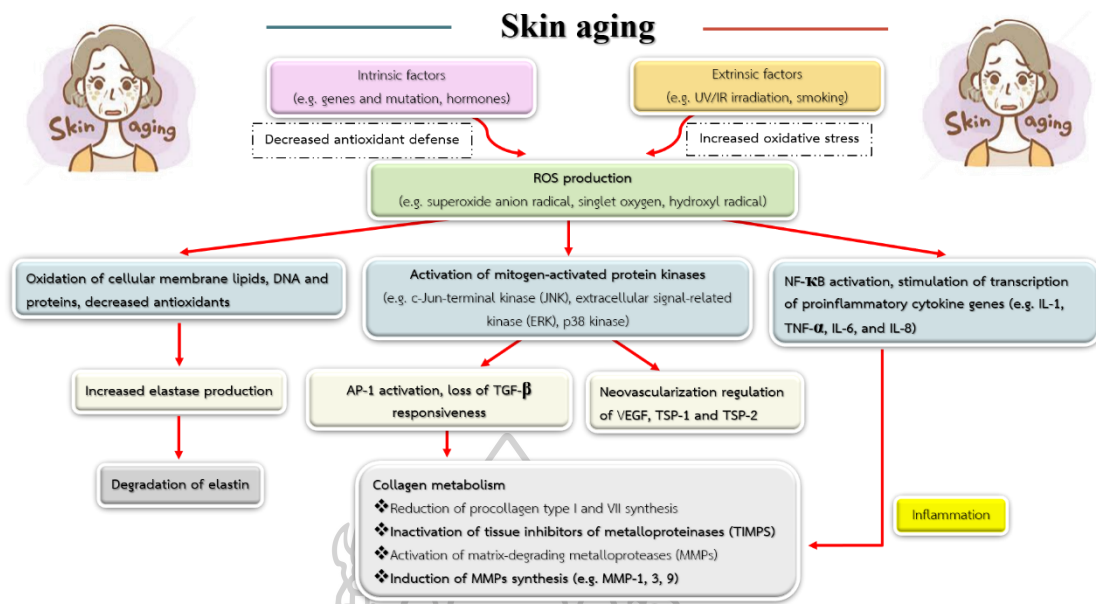


Figure 1 Overview of major signaling pathways in the intrinsically and extrinsically aged skin (28).

Human skin aging is generally divided into the intrinsic and extrinsic aging processes. Intrinsic or chronological aging is genetically determined that occurs during the normal aging process, while extrinsic aging is caused by environmental factors. A genetically aging has been reported to appear less than the extrinsic aging as shown in **Figure 2**. Thus, many studies have focused on the effect of the active compounds on the anti-aging process accelerated by environmental influences.

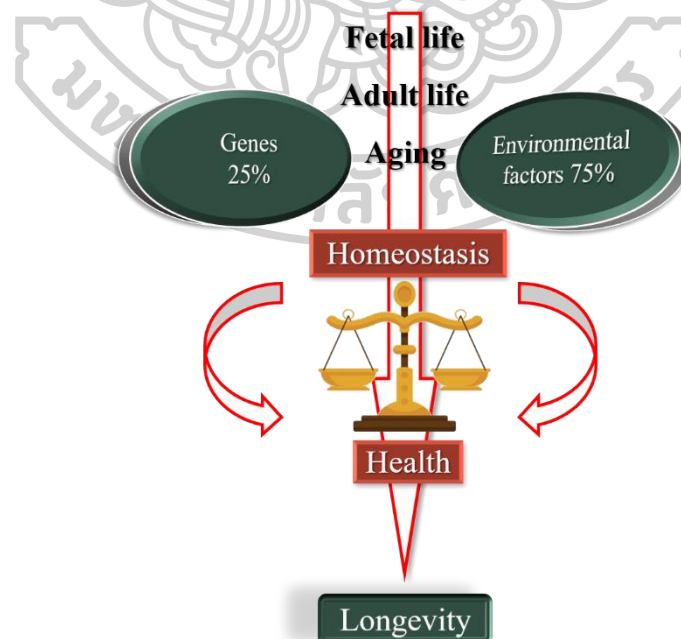


Figure 2 Factors affecting the homeostasis and aging of humans (7)

The major exogenous environmental factors such as sunlight, UV radiation and the toxicity substance are photo-oxidative stress. Aging leads to a thinning and declined barrier function of the epidermis, whereas the dysfunction of the dermis layer and remodeling of the ECM have also been reported. In a recent report, Tigges et al. (2014) explained the hallmarks of extrinsic aging in dermal fibroblasts as follows: DNA damage and genome instability, telomere shortening and irreparable DNA damage at telomeres, disruption of post-transcriptional pre-mature ribonucleic acid transcript (pre-mRNA) processing, epigenetic alterations, loss of proteostasis, mitochondrial damage and dysfunction, cellular senescence, altered intercellular communication, alterations of the cytoskeleton, adaptation or maladaptation to extrinsic stress, disruption of circadian regulation/decrease of nicotinamide adenine dinucleotide (NAD⁺) and sirtuin activity, genome-wide alterations in gene expression networks, and proteome changes (29).

In part of the hair, the structure of hair follicles is derived from basal cells of the epidermis layer. The hair follicles were generated from epidermal-mesenchymal interaction to form the dermal papillae (DP). The DP is located at the base of the hair follicle. In hair follicle development, it can be divided into three major phases: anagen, catagen, and telogen. The anagen phase refers to the active growth phase of around 85%-90% of hair follicles. The DP is surrounded by hair matrix cells and resides deep in the subcutaneous fat. The catagen phase refers to the period in which there is a massive loss of cells by apoptosis. In this phase, the DP moves up to the dermis as the epithelial strand regresses. At the end of catagen, the DP comes to rest immediately adjacent to these cells that will form the next lower hair follicle. Finally, the telogen phase is a phase of relative quiescence with no active hair production (26, 30). During the late telogen to early anagen transition, signals from the DP stimulate the hair germ and quiescent bulge stem cells to become activated (31). Age-related hair changes involved the progressive degeneration of hair fibers, decrease of melanocyte function or graying, and decrease in hair production in androgenetic and senescent alopecia. Hair aging is characterized in by intrinsic and extrinsic factors. Intrinsic factors are related to individual genetics such as familial premature graying, and AGA, while extrinsic factors are UVR, air pollution, smoking, nutrition, and lifestyle (11). as seen in **Figure 3**.

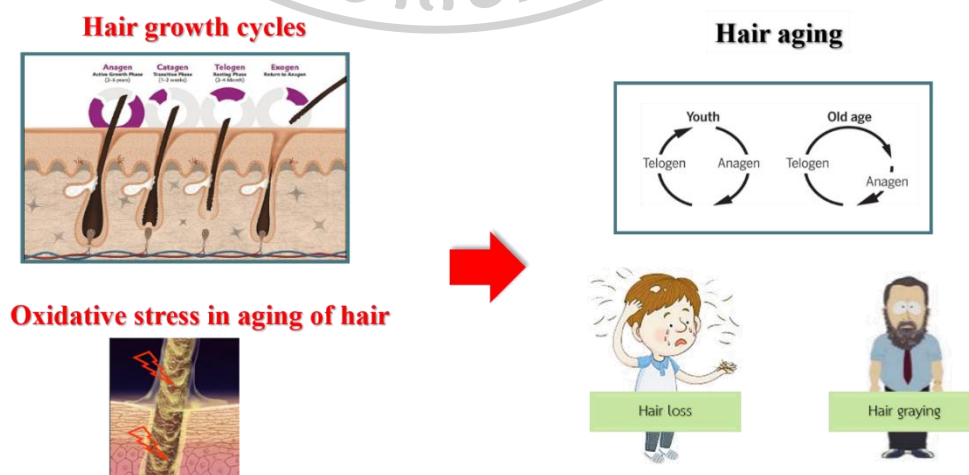


Figure 3 Hair growth and aging processes (12, 32, 33)

2.2 Peptides, GFs and cytokines used in skin and hair rejuvenation

Peptides are short-chain amino acids that act as a trigger in the cellular and biochemical processes of aging. Peptides stimulate cell growth, migration, and collagen production and also decreased collagen breakdown, resulting in the improvement of aged skin (34). GFs and cytokines were applied in cosmeceutical or pharmaceutical formulations. These compounds are composed of a large group of regulatory proteins that attach to cell surface receptors and serve as chemical messengers. This interaction occurred in inter and intracellular signaling pathways that regulate cell growth, proliferation, and differentiation. A summary of major pathways involved in skin aging can describe that the extrinsic and intrinsic factors induced the breakdown of the collagen and elastin fibers in the dermis. GFs and cytokines are dominantly up-regulated collagen synthesis and down-regulate collagen degradation (35). Besides, GFs appear to be important in the control of the hair growth cycle and exerting activities on skin-derived cells (36).

2.3 Natural resource extracts

2.3.1 DAV extract

Antlers are the bony skeleton of the skull, and velvet antlers are the growing phase of the horns borne on the heads of the male deer. Velvet antlers have been found in various species of deer family such as Cervidae, Tragulidae, and Moschidae, where Cervidae was mostly studied in many research. The previous reports, the scientists studied the bioactive components in many species of deer such as white-tailed deer (*Odocoileus leucurus*), red deer (*Cervus elaphus*), elk (*E. davidianus*), sambar deer or rusa unicolor deer (*Cervus unicolor swinhoeti*), and sika deer (*Cervus nippon*). The constituents of DAV are mainly composed of protein, GFs, amino acids, polypeptides, polysaccharides, fatty acids, phospholipids, mineral elements, ash, collagen, complex carbohydrates, biological bases, and calcium hydroxyapatite ($\text{Ca}_5(\text{PO}_4)_3\text{OH}$). Velvet antlers have been used for medicinal purposes for centuries. They exert many pharmacological effects including immunomodulatory, anti-cancer, anti-fatigue, antiosteoporosis, anti-inflammatory, anti-oxidation, wound healing, regeneration promoting, anti-heart failure, and anti-aging effects (37-39). Ko et al. (1986) reported that velvet antlers of red deer containing EGF can proliferate fibroblast cells in a dose-dependent manner (40). Supercritical carbon dioxide (CO_2) and co-solvent extraction of DAV were performed and many components were found such as uracil, hypoxanthine, uridine, *p*-hydroxybenzaldehyde, estradiol, and progesterone. The extract showed antioxidant-related activities by carbohydrates protection from hydroxyl radical-mediated degradation, scavenging hydroxyl radical, and inhibiting lipid peroxidation (41). Uronic acid, sulfated-glycosaminoglycan (GAG), and sialic acid were found in hot water or 70% ethanol-extracted velvet antler extract. The active components showed antioxidant activities on scavenging abilities such as 2,2-diphenyl-1-picrylhydrazyl (DPPH), hydroxyl radical, hydrogen peroxide, and reduction power (42). The antioxidant activities of the protein hydrolysates from aqueous extract were also detected. Low MW peptides had high (3-ethylbenzothiazoline-6-sulfonic acid; ABTS) radical scavenging and ferrous ion (Fe^{2+})-chelating ability, whereas high-MW peptides were more effective in DPPH

radical scavenging and ferric reducing antioxidant power (FRAP) than its low MW (43). Polypeptides constituents from Cervidae have an anti-osteoporotic effect by inhibiting bone loss and controlling the balance between bone resorption and bone remodeling. In addition, the polypeptides from velvet antler can activate epidermal cells, cartilage, and osteoblasts proliferation, as well as decrease cytokines level (44). The peptides (MW < 3 kilodalton (kDa)) derived from a simulated gastrointestinal digest of velvet antler protein showed anti-inflammatory activity. The anti-inflammatory peptides inhibited nitric oxide production in lipopolysaccharide (LPS)-induced macrophages (43). In other species of the Cervidae family, the bioactive compounds have also been found in sika deer. Polypeptides from antler velvet promoted the proliferation of epidermal cells and fibroblast cells (45). Peptides from velvet antler demonstrated the protective effects on acute ischemic myocardial injury in rats. The oral route of velvet antler's peptides provided cardioprotective activity via antioxidant and anti-lipid peroxidation properties (46). Besides, purified polypeptide (MW 3.2 kDa) from velvet antler extract might have an essential role in both cell-mediated immunity and humoral immunity. The immunomodulatory effects were confirmed by stimulating the growth of splenocytes, inducing natural killer (NK) cells cytotoxicity and facilitating their killing, up-regulation of the cluster of differentiation 4 positive cells (CD4⁺) and/or the cluster of differentiation 8 positive cells (CD8⁺), including T helper cell 1 (Th1)-grouped cytokines up-regulation and T helper cell 2 (Th2)-grouped cytokines down-regulation (47). For sambar deer or rusa unicolor deer, velvet antler showed the anti-allergic effects by prevention of allergen-induced airway hyperresponsiveness via elevation the cytokines of regulatory T (Treg), Th1, and T helper cell 17 (Th17), suppression of Th2, and inhibition immunoglobulin (Ig) E production (48). Moreover, the velvet antler extract increased the levels of contraction-related proteins in skeletal muscle fibers of mice such as troponin T1 (Tnnt1), troponin I (Tnni 1), and tropomyosin 2 (Tpm2), leading to delay muscle fatigue (49).

2.3.2 Porcine placenta extract (PPE)

The placenta is a major endocrine organ, which is a reservoir of the nutrients, GFs, peptides, and steroid hormones that moderate maternal physiology. It plays an important role in transporting these nutrients between the mother's body and the fetus, leading to fetal organ development and growth (50). The placental extract contains nucleic acids, amino acids, peptides, vitamins, minerals, trace elements, ECM components, cytokines, and GFs. In a previous study, the placental extract exhibited anti-inflammatory, antioxidation, and anti-fatigue activities including the improvement of health and energy and, accelerate the wound healing process (51). PPE has been widely used in the traditional medicines, foods, and cosmetic fields. PPE consists of 17 amino acids such as glycine, proline, glutamic acid, arginine, aspartic acid, lysine, leucine, serine, valine, phenylalanine, threonine, isoleucine, histidine, tyrosine, methionine, tryptophan and cystine. Oral administration of PPE showed an effective anti-fatigue effect, because the whole extract and its amino acids (glycine, proline, glutamic acid, and arginine) decreased immobility duration, fatigue-related blood parameters (lactic acid, aspartate aminotransferase; AST, alanine aminotransferase; ALT), and inflammatory cytokine levels (tumor necrosis factor alpha; TNF- α) (52). Long-term oral administration of PPE reduced the wrinkle widths

below the eye. The components of PPE such as glycine, proline, hydroxyproline, and glycosaminoglycans might contribute to preventing skin wrinkling (53). For molecular mechanism, PPE inhibited wrinkle formation by decreasing collagen degradation via down-regulation of MMP and up-regulation of tissue inhibitor of metalloproteinase (TIMP) expressions. Moreover, the PPE improved skin hydration by inducing the skin water holding capacity and decreasing the transepidermal water loss (TEWL) from photo-aging (54). The water-soluble protein of PPE improved the skin regeneration effect by stimulating fibroblast proliferation in a concentration-dependent manner. In addition, the outgrowth of fibroblasts was responsible for the high level of GFs such as basic FGF and TGF- β 1 (55), which these GFs were also found in PPE. Hydrolysate PPE also plays an important role in skin rejuvenation because it enhanced the proliferation of skin fibroblasts, procollagen type I, C-peptide production, and down-regulated MMP9 expression (56). Both water-extracted PPE and hydrolysate PPE showed the antioxidant effect by decreasing free radicals scavenging activities: DPPH, ABTS, superoxide, hydroxyl, ROS reduction, and FRAP at higher concentrations (57-59). Hydrolysate PPE showed anti-inflammatory activities by suppressing the production of proinflammatory factors such as inducible NO synthase (iNOS), TNF- α , IL-6, IL-1 β , and caspase-1 activity (60, 61). Dipeptides (Glycine-leucine (GL) and leucine-glycine (LG)) in PPE can inhibit the inflammation process and oxidative stress. Both anti-inflammation and antioxidant effect can refer to anti-fatigue activity, because fatigue is a common symptom in various inflammatory disorder and delay the onset and accelerate recovery of fatigue (60). Thus, the ability of PPE to inhibit the fatigue-associated inflammatory cytokines and oxidative stress might be used as bioactive compound for skin and hair regeneration.

2.4 Bioactivities for regenerative effect on skin and hair aging

2.4.1 Cell proliferation

HaCaTs are the predominant cell type in the epidermis. In normal healthy epidermis, the proliferation rate is probably determined by the transit-amplifying cells and the progeny of the stem cells (62). NHFs are found in the dermis and have an important role in the generation and maintenance of the reconstructed epidermis. Moreover, keratinocyte proliferation was stimulated by soluble factors released from fibroblasts (63).

The initiation of hair follicle morphogenesis has been related to secret molecules alternating from epidermis and dermis, regulated by mesenchymal-epithelial interactions. As development progresses, DP cells are located in the lowest part of the hair bulb, then the DP moves upwards toward the permanent portion of the hair follicle in the regeneration of the hair growth cycle. Thus, the formation of dermal condensates or clusters of the DP is believed to stimulate the proliferation and downgrowth of hair germs (64). DP cell number is associated with the size and shape of the hair. It confirmed that DP has an important role in activating stem cells to initiate the formation of a new hair shaft (65). During human aging, the proliferation rate of cells tends to reduce in the epidermis and dermis layers, leading to a degeneration of skin structure and function. The viability of aged keratinocytes become shorter and fatter than normal cells, whereas corneocytes showed bigger size resulting in a decreased epidermal turnover. Moreover, vascularity and cellularity in the dermis were decreased. The number of mast cells and fibroblasts was also

reduced. A flattening of the dermo-epidermal junction is found more than a third, resulting in the loss of DP (66). Besides, hair loss and hair thinning are caused by the aging condition, which the DP population degeneration was observed (65).

2.4.2 Cytoprotective effect

ROS is byproducts of normal metabolism and environmental stimulators, which reacted to metabolic biomolecules such as lipids, proteins, sugars, and nucleic acids. The harmful effects of ROS cause cell injury or dysfunction, inflammation and degeneration disease states, including aging. The human body has defense mechanisms against free radicals with a protective system by using antioxidant response elements (67). The *tert*-butyl hydroperoxide (t-BHP) as an organic hydroperoxide produces hydroxyl radical to increase DNA oxidation which is the basis of cellular aging related to DNA damage (68). Therefore, t-BHP is commonly used as a model for screening the cytoprotective activities of drugs. It can be metabolized to free radical intermediates and initiate lipid peroxidation and oxidative stress, resulting in decreased viability of cells (69).

2.4.3 Intracellular ROS reduction

ROS is an important pathogenic factor associated with human aging. In the free radical theory of aging, ROS oxidizes cellular constituents (lipids, proteins, and nucleic acids), leading to impair cellular functions and creating an age-related aberrant dermal ECM microenvironment. The elevated ROS contributes to damage or thin skin dermis by increasing broken collagen and reducing collagen production (70). There are many methods for evaluating free radical production in the cells. 2',7'-dichlorodihydrofluorescein diacetate (H₂DCF-DA) has been successfully used to detect the redox state of cells. Its techniques use cell-permeable fluorescent to detect ROS with a fluorescent probe. H₂DCF-DA is a non-fluorescent precursor of 2', 7'-dichlorofluorescein (DCF), which was cleaved to 2', 7'-dichlorodihydrofluorescein (H₂DCF) by intracellular esterases. H₂DCF accumulates intracellularly and subsequent oxidation yields the highly fluorescent product, DCF. Accumulation of DCF in the cells can be monitored by detecting the increment in fluorescence (71).

2.4.4 Regenerative effect from UVB-irradiation

Extrinsic aging or photoaging is caused by environmental exposure, mainly UV irradiation. The sunlight can penetrate the skin and affects the biological responses in both the epidermis and dermis layer. UV ray is a natural component of sunlight and are invisible to the human eyes. It is divided into three types according to wavelength: UVA (315–400 nm), UVB (280–315 nm) and UVC (100–280 nm), and only UVA and UVB can reach the earth's surface. UVB has high energy and can transfer more energy than UVA. Moreover, UVB is approximately absorbed in the epidermis and can reach the papillary dermis. The UVB influences DNA damage because DNA bases can absorb photons from UVB, resulting in increased ROS generation (4). Rising ROS makes the over-expression of MMPs and losses the synthesis of type I procollagen that dominantly component of skin connective tissue in the dermis (72). The main signaling pathway involved in the process of UVB-induced photoaging of dermal fibroblasts showed that increasing ROS decreased the

synthesis of collagen, increased collagen and elastin degradation, and senescence-associated secretory phenotype (73).

Collagen is the essential structural protein in the ECM and skin connective tissue, and type I collagen is the most abundant subtype (85-90%). In photo-aging of skin, UVB induces down regulation of the type-I collagen expression in dermal fibroblasts. Procollagen acts as a precursor molecule of collagen, which is synthesized in dermal fibroblasts and converted into mature collagen after enzymatic processing. UVR directly caused the dermal collagen degradation or inhibited procollagen biosynthesis, leading to reduce the collagen formation (74). In addition, acute UVR exposure stimulates the expression of MMPs in human skin cells. MMPs are one of the most essential families of protease enzymes, which catalyze the breakdown of proteins by hydrolysis reaction. In photodamaged skin, three MMPs (MMP1, MMP3, and MMP9) play an important role in up-regulation in human skin cells, in which MMP9 is regarded as a factor for wrinkle formation in UV-induced cells (25).

2.4.5 Cell migration

Human skin anatomy is composed of three layers: the epidermis, dermis, and hypodermis or subcutaneous adipose tissue. Age correlated with changes in the healing phase, in which the growth factor levels, cell proliferation and migration, and ECM secretion decrease (75). For skin repair, the epidermis is the part restored during the re-epithelialization process, while other components of the skin, for example, the dermis, have important supporting roles in the re-epithelialization process (76). In the case of hair, hair loss is a common symptom of aging in mammals. Cell migration and cell compaction as key processes in hair morphogenesis (77). Cytokines can enhance cell migration, proliferation, differentiation, and metabolic function (78), and tissue regeneration has been measured by *in vitro* cell migration assay.

2.4.6 Anti-inflammation

Excessive production of ROS due to insufficient scavenging activity or an altered mitochondrial function are crucial aspects of skin aging. High levels of ROS lead to oxidative modification and damage to lipids, proteins, and DNA as well as dysregulation of cell signaling pathways, altering cytokine release (79). After that, immune cells are stimulated to migrate, resulting in the exacerbation of inflammation. In the final step, the degradation and synthesis of elastin and collagen fibers occur. The fibroblasts in old age are unable to synthesize these fibers. The inflammatory process causes the aging of the skin with a change in the component of the dermis and epidermis, including skin thickness and elastic properties of the skin. Cytokines play a central role in the manifestation of old skin. TNF- α produced by fibroblasts, keratinocytes, macrophages, and monocytes is a triggers of cytokine inflammatory responses that occur in the skin. The intrinsic or extrinsic stimuli of cutaneous aging promotes the production of TNF- α by skin cells and increases inflammation. TNF- α is a key role in skin aging by inhibiting collagen synthesis and increasing the production of MMP9 and collagen degradation (80).

2.4.7 Hair cell aggregation

For the inductive property in hair-forming ability, DP cells change during the hair cycle and affect the frequency of hair formation. The DP cells induce hair growth and interact with the adult follicular epidermis, resulting in the organization of new hair follicles. The papilla-epidermal interaction is maintained in the epidermis, in which the papilla cell aggregation is surrounded by the epithelial cells and formed by the matrix cells. This new bulb commences generating hair as the follicle lengthens which occurs initially at the anagen stage. Regenerative phenomena have been described by the basic regenerative ability in the papilla and the growth of hair length (81, 82).

2.5 Nanocarrier systems

In the pharmaceutical field, nanocarriers are commonly used in transdermal drug delivery. They can be divided into two types: nanomaterials and nanodevices. Nanomaterials can be distinguished into nanocrystalline and nanostructured materials. Nanostructures are classified as a lipid-based systems, polymers, and non-polymer (83). In this study, lipid- and polymer-based nanocarriers were used to develop the transdermal delivery system for bioactive macromolecules (**Figure 4**).

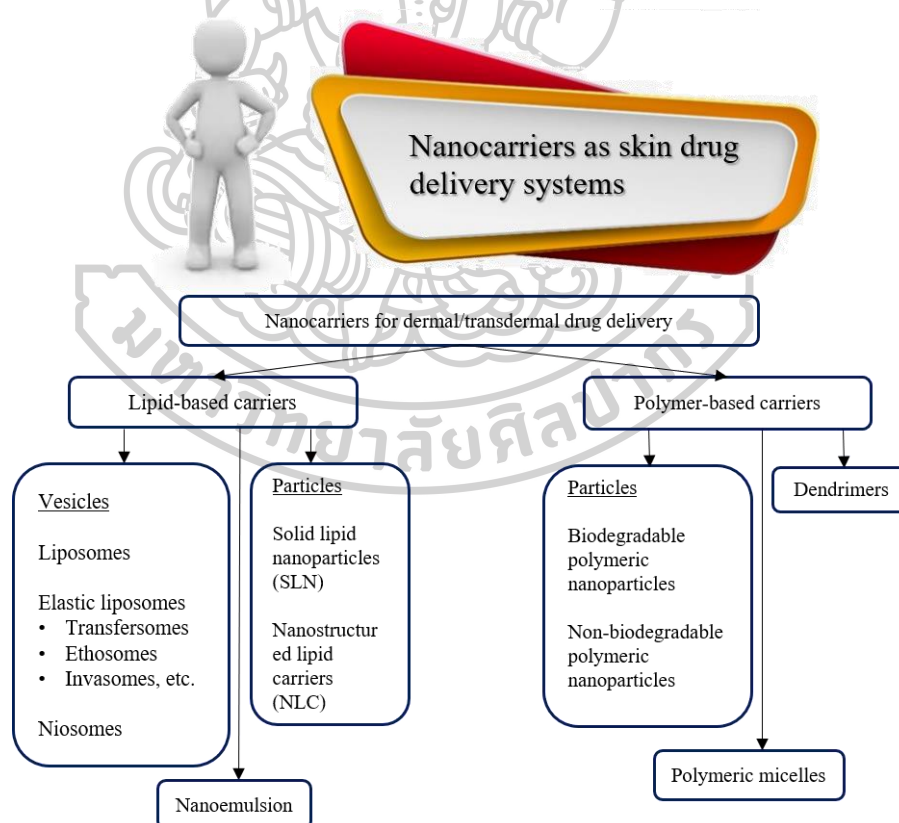


Figure 4 The schematic of nanocarriers for dermal or transdermal drug delivery (84)

2.5.1 Lipid-based nanocarriers

Lipids such as oils, waxes, cholesterol (Chol), sterols, monoglycerides, diglycerides, triglycerides, phospholipids and fat-soluble vitamins are generally used as potential excipients for pharmaceutical and cosmeceutical products (83). The lipid-based nanocarriers are composed of lipid-based NPs (solid-lipid nanoparticles, SLNs, and nanostructured lipid carriers, NLCs) and vesicular nanocarriers (such as LIs, NIs, transfersomes and ethosomes) (85).

2.5.1.1 LI

LIs were discovered by Bangham in the 1960s, the morphology of LIs consists of single or multiple lipid bilayers. They can encapsulate both lipophilic and hydrophilic compounds, in the lipid bilayer and the aqueous core, respectively (**Figure 5**). For the physicochemical properties of LIs, they consisted of phospholipids and amphiphilic molecules that have a hydrophilic head and a hydrophobic chain. LIs can be classified based on the preparation method, size, and lamellarity (86). LIs have been reported as effective delivering systems for the delivery of an active compound through the skin. The benefits of transdermal drug delivery using LIs include (1) LIs are similar to a biological membrane, and they can store water-soluble or amphiphilic and lipophilic compounds, (2) they can interact with the skin lipids; LI bilayers may improve local drug concentrations, (3) they can sustain the release of dermatological active compounds by reservoir effect, (4) they act as penetration enhancers and facilitate dermal delivery, and (5) act as rate-limiting membrane barriers for the modulation of systemic absorption (87). It was reported that LIs enhance drug penetration by (1) the free drug mechanism, (2) penetration enhancement achieved by components of the liposomal formulation, (3) adsorption or fusion of liposomal vesicles with the SC, (4) penetration of intact vesicles into or through the SC, and (4) transfollicular delivery (88).

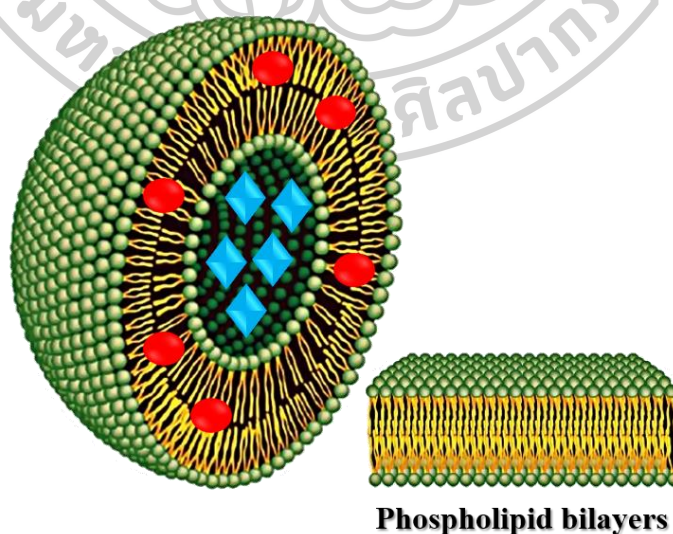


Figure 5 The structure of liposomal vesicle composed of phospholipid bilayers and entrapped both lipophilic (●) and hydrophilic (◆) compounds (86).

2.5.1.2 NI

NIs are spherical vesicles containing amphiphilic molecules surrounded by an aqueous compartment, in which the vesicles can entrap both hydrophilic and hydrophobic molecules (**Figure 6**). These amphiphilic molecules are surfactants and consisted of 2 parts, which are hydrophobic tails and hydrophilic heads. Non-ionic surfactants are suitable for NIs preparation with low skin irritation. Moreover, non-ionic surfactants are biodegradable, biocompatible, and not immunogenic. The level of irritation of surfactant used to form NIs was in the order: cationic > anionic > nonionic. NIs can be prepared from different types of surfactant molecules such as derivatives of alkyl ethers, alkyl esters, and sorbitan fatty acid esters (89). Chol as an additive agent influences the physical properties and structure of NIs. The interaction between Chol and surfactant occurs by the formation of a hydrogen bond between its hydroxyl groups and the alkyl chain of surfactant molecules, leading to escalating the transition temperature of vesicles, enhancing the drug EE and improving stability by altering the fluidity of chains in bilayers (90). Additionally, NIs are percutaneous permeation enhancement, which possible mechanisms of action of surfactant vesicles for dermal and transdermal applications include: (1) drug molecules are released by NIs, (2) NI constituents act as penetration enhancers, (3) NI adsorption and/or fusion with SC, (4) intact NI penetration through the intact skin, and (5) NI penetration through hair follicles and/or pilosebaceous units (91).



Figure 6 The feature of niosomal vesicle (89)

2.5.1.3 PEGylated lipid-based nanocarriers

PEGylation of nanocarriers is related to the coating of nanocarrier surface with polyethylene glycol (PEG) via adsorption, grafting, or entrapment to improve the biocompatibility of the nanocarriers (92). Besides, the incorporation of PEG into nanocarriers increased the pharmacokinetic profile of particulate and macromolecular therapeutics (93). For PEGylation of lipid-based nanocarriers, it is beneficial in the protection of the hydrophobic nanovesicle surface and any surface charge. Moreover, the MW of the PEG chain affected the aqueous solubility of the PEGylated phospholipid molecule and its size (94). In transdermal drug delivery, to enhance

penetration efficiency, the drug penetration depth and drug permeation amount are the critical parameters (95). Surface modification with polymers is one of the strategies for improving the transdermal delivery of nanocarriers. PEG is a commonly used polymers (96). Rangsimawong et al. (2014) reported that grafting PEG onto the membrane of a LI could enhance skin permeation of hydrophilic drug (97).

2.5.2 Polymer-based nanocarriers

Polymeric NPs have been defined as nanosized solid colloidal particles engendered from polymers (Figure 7). The type of polymeric NPs depends on the preparation method which is divided into nanospheres (matrix-type NPs) and nanocapsules (reservoir-type NPs). Moreover, various biodegradable polymers such as synthetic and natural have been developed (21).

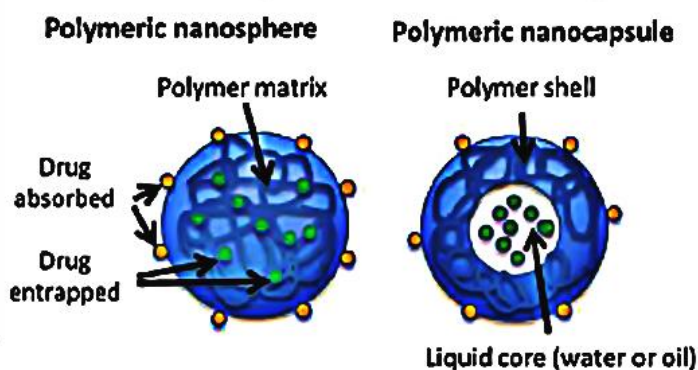


Figure 7 Image of polymeric NP types: polymeric nanosphere and polymeric nanocapsule (21)

2.5.2.1. Chitosan (CS) NP

CS is a mucopolysaccharide with a high degree of biodegradability and biocompatibility. CS had been approved by the United States Food and Drug Administration (FDA) for use in pharmaceutical and food applications. CS is soluble in most organic acidic solutions such as formic, acetic, tartaric, and citric acid (98). CS can enhance transdermal drug delivery by changing the structure of keratin in the SC, resulting in a more loose accumulative structure of keratin and a larger degree of freedom for carbon movement. Moreover, CS increased the water content in the SC, decreased keratinocyte cell membrane potential and improved cell membrane fluidity (99). CS NPs have been reported to have many benefits due to their stability, biocompatibility, low toxicity, and simple preparation technique (100).

2.5.2.2. Chitosan-maleimide (CS-MHA) NP

CS-MHA has been developed by conjugating the amino groups of CS backbone with thiol groups of 6-maleimidoheptanoic acid (MHA) by thiol-Michael addition reaction. This functionalized polymer exhibited low cytotoxicity of on human fibroblast cells (101).

In a recent report, NPs were able to be distributed through the porous pathway of skin through the deep skin such as the groove and hair follicles. Nevertheless, they rarely move from the groove or hair follicles to the viable epidermis and dermis (102).

The factors affecting skin penetration of all nanocarriers are (1) physicochemical properties, (2) vehicle effect, (3) surface area, dose, duration, and frequency of exposure, (4) distribution, (5) skin appendages, (6) skin surface conditions, (7) additional factors of skin penetration and permeation, (8) loss from the skin surface, exfoliation, and wash effect and (9) elimination and photochemical transformation (103).

2.6 Transdermal drug delivery of a macromolecular compound

Transdermal delivery systems have many advantages such as avoiding first-pass metabolism, improving patient compliance, and reducing side effects (104). According to the skin structure, the layers of skin can be divided as epidermis, dermis and hypodermis. Penetration of a substance through the skin surface can be achieved by three main pathways: (1) across the continuous SC, (2) through the sweat duct, or (3) through the hair follicles with their associated sebaceous glands (**Figure 8**). The intact SC is the main barrier structure composed of keratinocytes and intercellular lipids. The structure of the SC is similar to "brick and mortar", in which the keratin-rich keratinocytes act as "bricks" and the intercellular lipids act as "mortar". The drug penetration route via the SC barrier can be divided into the intercellular and transcellular routes (105). Apart from the SC, the hair follicles and appendage route can be the main penetration pathway for many compounds. Therefore, the mechanism of molecules across the SC can be divided into three routes: transcellular, intercellular and transfollicular pathways (106).

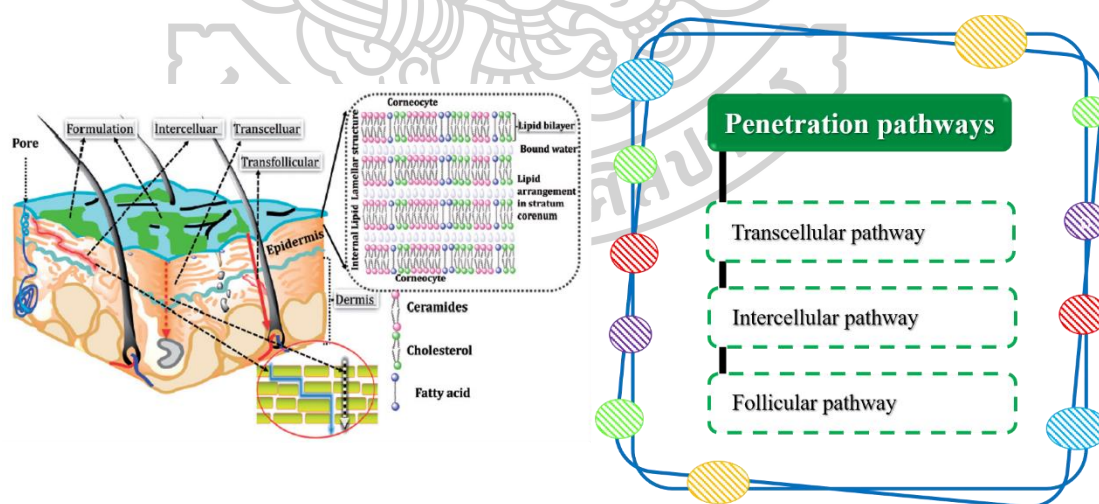


Figure 8 The schematic of transdermal drug delivery and penetration pathways: transcellular, intercellular, and follicular pathways (16)

The properties of compounds (for example, their MW (>500 Da), partition coefficient and solubility in water and lipid) affect the skin penetration ability (107). Transdermal drug delivery has achieved its potential as an alternative to the oral route and hypodermic route. First-generation transdermal delivery candidates are low

molecular-weight and lipophilic compounds and are efficacious at low doses. Second-generation transdermal delivery was developed using chemical enhancers, iontophoresis, and nongravitational ultrasound. Third-generation transdermal delivery uses a combination of chemical enhancers, biochemical enhancers, electroporation, cavitation ultrasound, microneedles, thermal ablation, and microdermabrasion (108). For transdermal delivery of hydrophilic macromolecules such as protein and peptides, proteins cannot passively permeate across the skin, while peptides also have difficulty passively diffusing through the skin, illustrating low permeability of peptides through the SC (20, 109). To overcome the limiting barrier of the skin, Chaulagain et al. (2018) (**Figure 9**) reported the strategies for passive transport of proteins including the use of carrier support adjuvants, nanocarriers and miscellaneous (21). Nanocarriers and encapsulation technologies were mostly studied for the transdermal delivery of protein. Encapsulation was the entrapment of the compounds within phospholipid or polymeric delivery systems such as LIs, NIs, NPs, etc. The beneficial effects of protein loading in these systems include a slow or controlled release of protein, improvement of protein stability, and promotion of cutaneous delivery (22). The composition of nanocarriers could affect skin permeation such as surfactants, which disrupted the lipid bilayer structure of the SC and increased dermal permeability. Moreover, creating micron-scale pores in the SC (e.g., microneedle) can be exploited to transport large molecules (23).

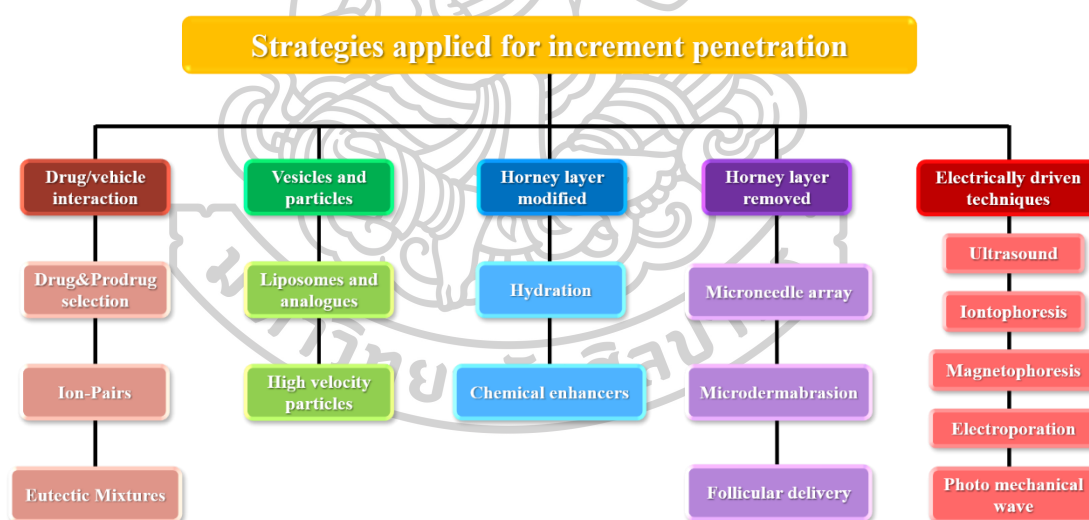


Figure 9 The schematic of a diagram represented the strategies applied for the increment of skin penetration (91)

Sponges or marine *Spongillia* are multicellular marine animals whose structure compose of soft tissue suspended in a jelly-like proteinaceous matrix supported by a hard skeleton. The components of their structure are mainly composed of calcium carbonate, silica and collagen. Sponges also contain a micronized needle-like substance called monoactines or MSs. The MSs can enhance the penetration of substances through the skin by microdermabrasion technique causing damage and removal of the SC layer, creating the pore in the skin. Besides, the MSs have been reported to be biocompatible and are safe to use (110-113).

1
2
3
4
5
6
7
8
9
10
11
12
13
14
15
16
17
18
19
20
21
22
23
24
25
26
27
28
29
30
31
32
33
34
35
36
37
38
39
40
41
42
43

CHAPTER 3

MATERIALS AND METHODS

3.1 Materials

1. DAV (Karakada 2011 Co., Ltd., Ratchaburi, Thailand)
2. PPE (Betagro Co., Ltd, Bangkok, Thailand)
3. 3-(4,5-dimethylthiazol-2-yl)-2,5-diphenyl-2H-tetrazolium bromide (MTT) (Sigma-Aldrich, Co., MO, USA.)
4. Dulbecco's Modified Eagle's Medium (DMEM) (Gibco BRL, Rockville, MD, USA.)
5. Fetal bovine serum (FBS) (Gibco BRL, Rockville, MD, USA.)
6. Trypsin-ethylenediaminetetraacetic acid (Trypsin-EDTA) (Gibco BRL, Rockville, MD, USA.)
7. Alternative to L-glutamine (Glutamax™) (Gibco BRL, Rockville, MD, USA.)
8. Non-essential amino acid (Gibco BRL, Rockville, MD, USA.)
9. Penicillin-streptomycin (Gibco BRL, Rockville, MD, USA.)
10. Bicinchoninic Acid (BCA) protein assay kit (Novagen®, EMD Millipore Crop., USA)
11. Silver stain (ProteoSilver™ Silver Stain Kit, Sigma- Aldrich, Co., St. Louis, MO, U.S.A.)
12. Human insulin-like growth factor-1 (IGF-1) enzyme-linked immunosorbent assay (ELISA) kit (Abcam, ab100545, Cambridge, MA, USA)
13. Human EGF ELISA kit (Abcam, ab100504, Cambridge, MA, USA)
14. Human FGF basic (FGF2) ELISA kit (Abcam, ab99979, Cambridge, MA, USA)
15. Human TGF-β1 ELISA kit (Abcam, ab100647, Cambridge, UK)
16. Human Pro-collagen I alpha I CatchPoint® SimpleStep ELISA kit (Abcam, ab229389)
17. Human MMP9 ELISA kits (Abcam, ab100610)
18. H₂DCFDA (Invitrogen, Thermo Fisher Scientific, USA)
19. Lipoxidase from glycine max (soybean) (Sigma-Aldrich, MO, USA)
20. Linoleic acid (LA) (Sigma-Aldrich, MO, USA)
21. Xylenol Orange disodium salt (Sigma-Aldrich, MO, USA)
22. Human TNF-α ELISA kit (Sigma-Aldrich, MO, USA)
23. Egg phosphatidylcholine (PC) (Lipoid GmbH, Ludwigshafen, Germany)
24. N-(carbonyl-methoxypolyethyleneglycol-2000)-1,2-distearoyl-sn-glycero-3-phosphoethylene sodium salt (PEG2000-DSPE) (Lipoid GmbH, Ludwigshafen, Germany)
25. Sorbitan laurate (Span® 20, Sigma-Aldrich, MO, USA)
26. Chol (Sigma-Aldrich, MO, USA)
27. CS (MW 8000 g/mol and degree of deacetylation = 88%) (OliZac technologies Co., Bangkok, Thailand)
28. 6-maleimidohexanoic acid (MHA) (Sigma-Aldrich, MO, USA)
29. Sodium tripolyphosphate (TPP) (Sigma-Aldrich, MO, USA)

- 44 30. Rhodamine B 1,2-dihexadecanoylsn-glycero-3-phosphoethanolamine
45 triethylammonium salt Rh-PE; LissamineTM) (Invitrogen, Carlsbad, CA, USA)
46 31. Bovine serum albumin-fluorescein isothiocyanate (BSA-FITC) (Sigma-
47 Aldrich, MO, USA)
48 32. Sponge spicule extract powder (MS; 98% plus spicule; 100–180 mesh)
49 (Human Sunshine Bio-Tech Co., Ltd., Hunan, China)
50 33. Serum water gel-based: glycerin (4% w/v), chlorphenesin in phenoxyethanol
51 (microcare PHC) (0.8% v/v), ethylene diamine (EDTA 2Na) (0.05% w/v),
52 polyacrylate crosspolymer-6 (Sepimax ZenTM) (0.54% w/v), and far infrared
53 (FIR) water (5% v/v) (Zen Innovation Group Co., Ltd., Pathum Thani,
54 Thailand)
55 34. Other chemicals and solvents
56 35. Chloroform; CHCl₃ (RCI Labscan, Bangkok, Thailand)
57 36. Methanol; MeOH (Burdick&Jackson[®], Honeywell International Inc., MI,
58 USA)
59 37. Triton[®] X-100 (Amresco[®], Solon, Ohio, USA)
60 38. Sodium chloride; NaCl (Sigma-Aldrich, MO, USA)
61 39. Potassium chloride; KCl (Ajax Finechem Pty Ltd., NSW, Australia)
62 40. Disodium hydrogen phosphate; Na₂HPO₄ (Supelco[®], Darmstadt, Germany)
63 41. Potassium dihydrogenphosphate; KH₂PO₄ (QRëCTM, QRëC Newzealand)
64 42. Acetic acid; CH₃COOH (EMSURE[®], Merch KGaA, Darmstadt, Germany)
65 43. Ethanol; ETOH (EMSURE[®], Merch KGaA, Darmstadt, Germany)
66 44. Dimethyl sulfoxide; DMSO (Fisher chemical, Fisher Scientific U.K., Leics.,
67 UK)
68 45. Sulfuric acid; H₂SO₄ (QRëCTM, QRëC Newzealand)
69 46. Iron (II) sulfate heptahydrate (Riedel-deHaën, Laborchemikalien GmbH,
70 Germany)
71 47. Tris (Amresco[®], Solon, Ohio, USA)
72 48. Sodium hydroxide; NaOH (Scharlau, Barcelona, Spain)
73 49. Hydrochloric acid; HCl (EMSURE[®], Merch KGaA, Darmstadt, Germany)
74 50. Methyl salicylate (P.C. Drug Center Co., Ltd., Bangkok, Thailand)

75 3.2 Equipments

- 76 1. 1.7-mL microcentrifuge tube (Costar[®], Corning incorporated, UT, USA)
77 2. 2.0-mL microtube (AXYGEN[®], Corning Incorporated, China)
78 3. 50-mL centrifuge tube (CentristarTM Cap, Corning Incorporated Life science,
79 Jiangsu, China)
80 4. 15-mL centrifuge tube (CentristarTM Cap, Corning Incorporated Life science,
81 Jiangsu, China)
82 5. 6-wells Cell Culture plate (SPL Life Science Co., Ltd., Gyeonggi-do, Korea)
83 6. 24-wells Cell Culture plate (Costar[®], Corning Incorporated, ME, USA)
84 7. 96-wells Cell Culture plate (Costar[®], Corning Incorporated Life Sciences,
85 Jiangsu, China)
86 8. 96-wells Assay plate, black plate (Costar[®], Corning Incorporated, ME, USA)
87 9. 10-μL microvolume pipette tip (Corning Incorporated, NY, Mexico)
88 10. 200-μL pipet tip (DeckWorksTM, Corning Incorporated, UT, USA)
89 11. 1000-μL pipette tip (TLR112NXL-Q, Thermo scientific, CA, Mexico)

- 90 12. Centrifugal filter units (Amicon[®] Ultra-4 or Ultracel[®]-100K, Cork Ireland,
91 Ireland)
92 13. 90x15 mm Petri Dishes (Biologix[®], Biologix Group Limited, Shandong,
93 China)
94 14. A probe-sonicator (Vibracell[™], VCX 130 PB; Sonics and Materials, Inc.,
95 Newtown, CT, U.S.A.)
96 15. A freeze dryer (FreeZone 2.5 Liter Benchtop Freeze Dry System, MO, USA)
97 16. An amino acid analyzer (L-8900 amino acid analyzer, Hitachi, USA)
98 17. A microplate reader (VICTOR Nivo[™] Multimode Plate Reader, PerkinElmer,
99 Germany)
100 18. An inverted microscope (Nikon[®] T-DH, Nikon, Tokyo, Japan)
101 19. A dynamic light scattering particle size analyzer (Zetasizer Nano-ZS, Malvern
102 Instruments, Worcestershire, UK)
103 20. A cryostat (Leica CM1850, Leica Instrument, Wetzlar, Germany)
104 21. The vertical Franz-type diffusion cells
105 22. A confocal laser scanning microscope (CLSM; an inverted Zeiss LSM 800
106 microscope, Carl Zeiss, Jena, Germany)
107 23. The DermaLab[®] series (SkinLab Combo, Cortex Technology, Hadsund,
108 Denmark)
109 24. A Dino-Lite Edge digital microscope (AM7915 Series, Taiwan)
110 25. Microscope Slides (25.4 x 76.2 mm., SAIL 1828, China)
111 26. Microscope Coverglasses (22 x 22 mm., D.A.T. Scientific Co., Ltd., Thailand)

112 3.3 Methods

113 3.3.1 Extraction of DAV and PPE

114 3.3.1.1 Extraction method of DAV

115 Fresh DAV was grided, then, 1 g of the sample was weighed. Afterward, the
116 extract was diluted with water in a ratio of 1:20, following by sonication using a probe
117 sonicator (Vibracell[™], VCX 130 PB; Sonics and Materials, Inc., Newtown, CT,
118 U.S.A.) at a frequency of 40 kilohertz (kHz) and 40% amplitude for 30 min under an
119 ice bath. The DAV extract was then centrifuged at 3000 rpm, 4°C for 10 min. The
120 supernatant was collected and freeze-dried for 3 days using a freeze dryer (FreeZone
121 2.5 Liter Benchtop Freeze Dry System, MO, USA). The extract powder was kept in a
122 refrigerator (4-8 °C) until used.

123 3.3.1.2 Extraction method of PPE

124 Porcine placenta was mashed with phosphate buffer saline (PBS) pH 7.4 (1:1).
125 Then, 2g of the sample was weighed and mixed with sterile water (2:15). Afterwards,
126 the mixture was extracted using by probe sonication (Vibracell[™], VCX 130 PB;
127 Sonics and Materials, Inc., Newtown, CT, U.S.A.) set at a frequency of 40 kHz and
128 40% amplitude for 30 min under an ice bath. The PPE solution was spined using a
129 centrifuge instrument at 4000 rpm, 4°C for 15 min. The supernatant was collected and
130 freeze-dried using a freeze dryer (FreeZone 2.5 Liter Benchtop Freeze Dry System,
131 MO, USA) for 3 days to obtain the extract powder. PPE was kept in a refrigerator (4-8
132 °C) before use.

133 **3.3.1.3 Determination of %yield, total protein content, GFs, and amino acid**
 134 **content**

135 **3.3.1.3.1 Determination of %yield**

136 Total extract powder was weighed and the percent yield of the extracts was
 137 calculated using **equation (1)**.

138
$$\% \text{ Yield} = (\text{weight of extract powder}) / (\text{weight of fresh material}) \times 100 \dots\dots (1)$$

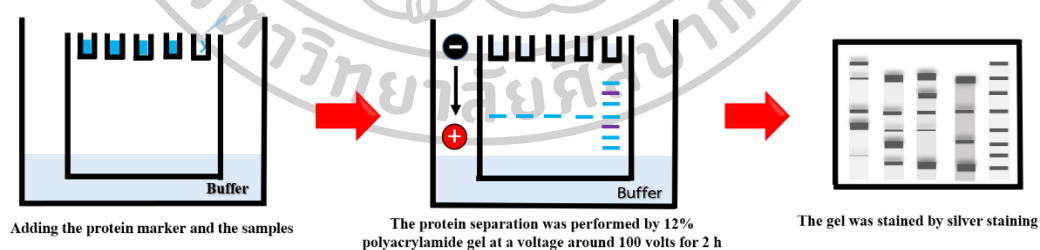
139 **3.3.1.3.2 Determination of total protein content**

140 The total protein content of the extracts was determined by a BCA protein
 141 assay kit (Merck, Darmstadt, Germany) following the procedure specified by the
 142 manufacturer. Protein content was calculated using **equation (2)**.

143
$$\text{Protein content} = (\text{Analyzed protein content}) / (\text{Initial weight of the extract}) \dots\dots (2)$$

144 **3.3.1.3.3 Polyacrylamide gel electrophoresis (SDS-PAGE) analysis**

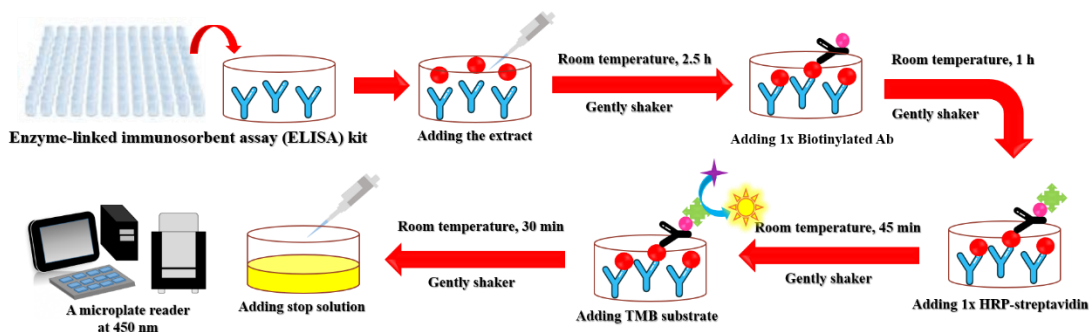
145 Proteins as an active ingredient in DAV and PPE were separated by SDS-
 146 PAGE using 12% polyacrylamide gel. For separation, the denature samples were
 147 loaded onto the gel, which is immersed in an electrophoresis buffer. After that, a
 148 voltage (around 100 V) was applied in order to migrate the negatively charged
 149 molecules through the mesh of the gel in the direction of the positively charged
 150 anode. The proteins were separated by their molecular size. Small molecular proteins
 151 easily migrate through the gel, while larger proteins migrate more slowly than small
 152 proteins (**Figure 10**). At the end of the electrophoresis experiment, all proteins were
 153 analyzed by protein staining using silver staining (ProteoSilver™ Silver Stain Kit,
 154 Sigma, MO, USA) followed the manufacturer protocol.



156 **Figure 10** Image of protein separation by SDS-PAGE electrophoresis

157 **3.3.1.3.4 Determination of GFs content**

158 The contents of IGF-1, EGF, TGF- β 1, and FGF2, which are involved with
 159 skin and hair regeneration, were quantified. Quantitative analysis of these GFs was
 160 analyzed by ELISA kits as the following procedures (**Figure 11**).



161

162 **Figure 11** Image of process for content determination of GFs by ELISA

163 Briefly, the extract solution (100 μ L) was added into ELISA plate, and then
 164 incubated at room temperature for two and a half hours with gentle shaking. After
 165 that, the wells were washed with 1x wash buffer, added 100 μ L of 1x Biotinylated
 166 antibody, and incubated at room temperature for 1 h with gentle shaking. Afterwards,
 167 the wells were washed with 1x wash buffer, added 100 μ L of 1xHRP-streptavidin,
 168 followed by incubated at room temperature for 45 min with gentle shaking. Then, the
 169 wells were washed with 1x wash buffer, filled with 100 μ L of TMB substrate, as well
 170 as incubated at room temperature for 30 min with gentle shaking. Finally, the stop
 171 solution was pipetted in each well to stop the reaction and quickly read the results by
 172 a microplate reader at absorbance 450 nm. The amount of each growth factor was
 173 calculated by using their standard curve. The growth factor content of the extracts was
 174 computed as follows **equation (3)**

175
$$\text{Growth factor content} = C_g/C_i \dots \dots \dots (3)$$

176 Where C_i is the initial weight of each extract as well as C_g is amount of each
 177 growth factor

178 3.3.1.3.5 Determination of amino acids

179 Type of amino acids and their contents in the extracts were analyzed by an
 180 amino acid analyzer (L-8900 amino acid analyzer, Hitachi, USA).

181 3.3.2 Determination of DAV and PPE bioactivity for skin and hair rejuvenation

182 NHFs and HFDPCs were cultured in DMEM supplement with 10% FBS, 1%
 183 GlutamaxTM, 1% penicillin-streptomycin, and 1% nonessential amino acid, while
 184 HaCaTs were cultured in DMEM supplement with 10% FBS and 1% penicillin-
 185 streptomycin in an incubator with 5% CO₂/95% humidified air, at 37°C.

186 3.3.2.1 Measurement of cell viability and cell proliferation on skin and hair cells

187 NHFs and HFDPCs (10⁴ cells/well) or HaCaTs (5x10³ cells/well) were seeded
 188 into a 96-wells plate and incubated in an incubator at 37°C, with
 189 5% CO₂/95% humidified air for 24 h (NHFs and HFDPCs) or 48 h (HaCaTs). After
 190 that, the medium was changed, and the cells were washed with PBS pH 7.4. Various
 191 concentrations of samples were treated on the cells for 24 h. The cell viability was
 192 determined by MTT assay. After the treatment with the samples, the samples were

193 discarded and the cells were washed with PBS pH 7.4. Then, MTT solution (a final
194 concentration of 0.5 mg/mL) was added to the well plate and incubated for 3 h. After
195 that, the MTT solution was replaced by 100 μ L of DMSO in order to dissolve the
196 formazan crystals for 15-20 min with gentle shaking, which were produced from the
197 living cells. The absorbance was measured at 550 nm using a microplate reader
198 (VICTOR Nivo™ Multimode Plate Reader, PerkinElmer, Germany).

199 For cell proliferation, NHFs, HaCaTs, and HFDPCs (5×10^3 cells/well) were
200 cultured into a 96-wells plate and incubated in an incubator at 37°C, with
201 5% CO₂/95% humidified air for 24 h (NHFs and HFDPCs) or 48 h (HaCaTs).
202 Afterwards, the medium was discarded and the cells were washed with PBS pH 7.4.
203 Various concentrations of samples were added to the cells and incubated for at
204 different time interval (24-72 h). The cell proliferation was evaluated using the MTT
205 assay as described above. The percent cell viability and cell proliferation were
206 calculated according to **equation (4)**.

$$207 \quad \% \text{Cell viability or cell proliferation} = \frac{\text{O.D. of sample-blank}}{\text{O.D. of control-blank}} \times 100 \dots (4)$$

208 **3.3.2.2 Determination of cell migration on skin cells**

209 The cell migration was determined by *in vitro* scratch assay. Briefly, 2×10^5
210 cells of NHFs were seeded into in each well of 6-wells plate under humidified
211 atmosphere (37°C, 95% humidified air/5% CO₂) until 70-80% confluence. The straight
212 lines were drawn onto the cells using a 200- μ L pipette tip before discarding the
213 medium. After that, 3 mL of TGF- β 1 (as a positive control), DAV or PPE was added
214 to each well. The images were taken at 0, 24 h and 48 h using an inverted microscope
215 (Nikon® T-DH, Japan).

216 **3.3.2.3 Evaluation on the repair of UVB-induced skin damage determination**

217 **3.3.2.3.1 Determination of cell viability of damaged-skin**

218 NHFs (5×10^3 cells/well) were seeded onto a 96-wells plate and incubated
219 overnight in an incubator at 37°C, 5% CO₂/95% humidified air. After discarding the
220 medium, 100 μ L of PBS was added in the plate and immediately placed it under a
221 UVB lamp (20W) in order to expose to UVB ray at a radiation energy of 6 kilojoule
222 (kJ). Then, the cells were treated with 0-2,000 μ g/mL of DAV or 0-1,000 μ g/mL of
223 PPE for 24 h. The result was analyzed by MTT assay as described above. The %cell
224 viability was calculated using **equation (4)**.

225 **3.3.2.3.2 Determination of procollagen I and MMP9 content in the damaged-skin**

226 For molecular pathway involved with the skin repair, pro-collagen I and
227 MMP9 were determined by an ELISA assay kit following the manufacturer's
228 protocol. Briefly, 2×10^5 cells of NHFs were cultured onto 6-wells plate overnight in
229 an incubator at 37°C, 5% CO₂/95% humidified air. The old medium was discarded and
230 the cells were cleaned with PBS pH 7.4. Afterwards, the plate was added with 1.5 mL
231 of PBS pH 7.4 and immediately exposed to UVB irradiation at a radiation energy of 6
232 kJ. 2,000 μ g/mL of DAV or 1,000 μ g/mL of PPE were treated onto the cells for 24 h.

233 The supernatant and the cell pellets were collected to measure the pro-collagen I and
234 MMP9 contents.

235 **3.3.2.4 Determination of protective effect of the extracts on skin cells**

236 HaCaTs (5×10^3 cells/well) were seeded into 96-wells plate and incubated in an
237 incubator at 37°C, 5% CO₂/95% humidified air for 48 h. Afterward, the medium was
238 changed and washed with PBS pH7.4. At concentrations (0-2,000 µg/mL) of DAV or
239 PPE were prepared and treated on the cells for 1 h. Then, the samples were replaced
240 by 200 µM of t-BHP for 4 h. The cell viability was determined by MTT assay,
241 followed by calculating the % cell viability according to **equation 4** as described
242 above.

243 **3.3.2.5 Intracellular reduction of ROS activity in skin cells**

244 H₂DCFDA is a fluorescent probe which is generally used for determination of
245 intracellular ROS activity. In this study, the method was modified from Wadkhien et
246 al. (2018) (114). Briefly, 2.5×10^4 cells/well of HaCaTs were seeded into 96-black
247 wells plate and incubated under an incubator at 37°C, 5% CO₂/95% humidified air for
248 48 h. In this study, quercetin is a polyphenolic flavonoid and acts as a positive control.
249 Its antioxidant activities have been exhibited via maintaining an antioxidant defense
250 system, inhibiting the level of glutathione, against the key enzymes related to
251 oxidative properties, controlling the signal transduction pathways, and resisting
252 oxidative damage from ROS. (115). Besides, quercetin showed a strong protective
253 capacity against oxidative stress from excess production of ROS (116). The positive
254 control (quercetin 100 µM) or various concentrations (25-1,000 µg/mL) of the
255 samples (DAV or PPE) were added for 1 h. The medium was replaced by 1mM of t-
256 BHP for 1 h. Then, the medium was changed and 20 µM of H₂DCFDA was added to
257 incubate with the cells in the dark, at 37°C for 30 min. The results were measured by a
258 fluorescence microplate reader (VICTOR Nivo™ Multimode Plate Reader,
259 PerkinElmer, Germany) at 485/535 nm (excitation/emission). The percent ROS
260 reduction was calculated according to **equation (5)**.

$$261 \quad \% \text{Intracellular ROS reduction} = (Fl_A) / (Fl_B) \times 100 \dots \dots \dots (5)$$

262 where Fl_A referred to fluorescence intensity of test sample group, and Fl_B was
263 fluorescence intensity of non-treatment group.

264 **3.3.2.6 Anti-inflammatory activities**

265 **3.3.2.6.1 *In vitro* lipoxygenase (LOX) inhibition assay**

266 *In vitro* LOX inhibition assay was determined by the modified method from
267 Chung et al. (2009) (117). Fifty microliters of LOX in 50 mM Tris HCl buffer pH 7.4
268 (final concentration at 167.5 Unit/mL) was incubated with 60 µL of the test sample
269 (PPE or standard inhibitors) at 25 °C for 5 min. For the control group, 50 µL of LOX
270 and 60 µL of the buffer were mixed in the microcentrifuge tube (1.5 mL).
271 Background blank was composed of LOX, buffer, and a substrate (LA). Afterwards,
272 50 µL of LA (final concentration at 30 µM) was mixed together and incubated at 25
273 °C for 20 min in the dark. Two hundred and forty microliters of ferrous

274 oxidation–xylenol orange (FOX) reagent was added in each microcentrifuge tube (1.5
275 mL), the Ferric ion (Fe^{3+})-dye complex was developed for 30 min at 25 °C. The
276 absorbance was measured using a microplate reader (VICTOR Nivo™ Multimode
277 Plate Reader, PerkinElmer, Germany) at 590 nm. The percentage of LOX inhibition
278 was calculated using **equation (6)**.

$$279 \quad \% \text{ LOX inhibition} = (\text{O.D.}_A - \text{O.D.}_B) / \text{O.D.}_A \times 100 \dots \dots \dots (6)$$

280 where O.D._A was the absorbance value of control group, and O.D._B was the
281 absorbance value of sample group.

282 **3.3.2.6.2 Effect on the reduction of intracellular TNF- α**

283 HaCaTs (1×10^5 cells) were seeded into each well of a 24-wells plate in each
284 well for 96 h in an incubator at 37 °C, 95% humidified air/5% CO_2 . After that 300 μM
285 of aspirin (ASA; positive control), PPE (200 and 1,000 $\mu\text{g}/\text{mL}$), and DAV (200 and
286 1,000 $\mu\text{g}/\text{mL}$) were added to the cells for an hour. Then, the cell pellets were collected
287 to determine the TNF- α content using an ELISA assay kit.

288 **3.3.2.7 Determination of hair cell aggregation**

289 Cell aggregation behavior was performed by the modified method from
290 Kiratipaibonn et al., (2015) (118). Briefly, 8×10^3 cells of HFDPCs were seeded onto
291 each well of a 24-wells plate and incubated overnight under an incubator at 37 °C,
292 95% humidified air/5% CO_2 . The medium was replaced, and then HFDPCs were
293 treated with 1,000 $\mu\text{g}/\text{mL}$ PPE for 72 h in the sample group, while the control group
294 was treated with DMEM supplement. The cell aggregation was observed and
295 photographed under an inverted microscope (Nikon® T-DH, Nikon, Tokyo, Japan).

296 **3.3.3 Development of nanocarriers containing macromolecule for transdermal 297 delivery**

298 **3.3.3.1 Preparation of macromolecule-loaded nanocarriers**

299 **3.3.3.1.1 Preparation of LI and pegylated liposome (PEG-LI)**

300 The liposomal formulations were prepared by thin film hydration and
301 sonication methods (97). The proportional compositions of thin film for all
302 formulations were shown in **Table 1**. In brief, PC, Chol and DSPE-PEG2000 were
303 dissolved in CHCl_3 : MeOH (2:1) and mixed together in test tubes. The solvent was
304 evaporated to make lipid film by nitrogen gas and kept in desiccator for drying over 6
305 h. Then, 0.2% (w/v) of BSA-FITC dissolved in PBS pH 7.4 was added into the test
306 tubes, followed by mixing by a vortex mixer to formulate multi-lamellar LIs. All
307 formulations were sonicated on ice by a probe sonicator for 30 min (2 cycles) to
308 reduce the size of LI vesicles. The LI solution was centrifuged at 15,000 rpm, 4°C for
309 15 min to remove the excess component. The supernatant was collected and kept in a
310 refrigerator at 4-8 °C before use.

311 **Table 1** The compositions of LI and PEG-LI

Formulations	PC (mM)	Chol (mM)	DSPE-PEG2000 (mM)
LIs	10	2	-

3% PEG-LI	9.64	2	0.36
------------------	------	---	------

312

313 3.3.3.1.2 Preparation of NI and pegylated niosome (PEG-NI)

314 NIs were prepared by modified thin-film hydration and probe sonication
 315 methods (119). The proportional compositions of thin film for all formulations were
 316 shown in **Table 2**. Briefly, Span[®] 20 and Chol in ratio of 1.25 mM: 1.25 mM were
 317 dissolved in CHCl₃ and MeOH (1:1). After that, 3% of PEG2000-DSPE was added.
 318 The solvent was evaporated by nitrogen gas and put down in a desiccator over 6 h for
 319 completely dried. Then, 0.2% (w/v) of BSA-FITC in PBS pH 7.4 was added to form
 320 niosomal vesicles. These the size of the vesicles were reduced by a probe sonicator
 321 (40 kHz frequency, 40% amplitude) on ice for 30 min (2 cycles), followed by
 322 centrifuged at 15,000 rpm, 4°C for 15 min to remove an excess component. The
 323 supernatant which it was composed of NIs entrapped BSA-FITC, was collected and
 324 kept in a refrigerator at 4-8 °C before use.

325 **Table 2** The compositions of NI and PEGylated NI

Formulations	Span[®]20 (mM)	Chol (mM)	DSPE-PEG2000 (mM)
NIs	1.25	1.25	-
3% PEGylated NIs	1.25	1.25	0.075

326

327 3.3.3.1.3 Preparation of CS-TPP NP and CS-MHA-TPP NP

328 NPs such as CS-TPP and CS-MHA-TPP were prepared by ionic gelation
 329 method. The interaction between positively charged amino groups of CS and
 330 negatively charged of TPP was occurred (120). Briefly, CS or CS-MHA was
 331 dissolved in 1% (v/v) CH₃COOH. Afterward, TPP was dissolved in deionize water
 332 and dropped into the polymer solution containing BSA-FITC (0.2%, w/v) at pump
 333 rate of 0.15 time/min with probe-sonication for 30 min/time. The BSA-FITC was
 334 added to the polymer solution and stirred with magnetic stirrers for 24 h. The NPs
 335 were kept in a refrigerator at 4-8 °C before use.

336 3.3.3.2 The characterization of macromolecule-loaded nanocarriers

337 Particle size, polydispersity index (PDI), and zeta potential of nanocarriers
 338 were measured using a dynamic light scattering particle size analyzer (Zetasizer
 339 Nano-ZS, Malvern Instruments, Worcestershire, UK) with a 4 mW HeNe laser at a
 340 scattering angle of 173°. All samples were diluted at 1:20 with deionized water and
 341 examined in triplicate (n=3).

342 To determine the %EE and %LC, 2 mL of liposomal and niosomal
 343 formulations were added in a centrifugal filter tube (Amicron[®] 100K, Merck, USA),
 344 and centrifuged at 4,000 rpm, 4°C, 15 min. The BSA-FITC entrapped these
 345 formulations were collected from the filter device and then added to 0.1% Triton X-
 346 100 in the ratio of 1:1. Drug content was evaluated by fluorescence intensity using a
 347 fluorescence microplate reader at excitation/emission 485/535 nm. The %EE and
 348 %LC were calculated as the **equation (7)** and **(8)**, respectively.

$$349 \quad \% EE = \frac{BSA-FITC \text{ entrapped nanocarriers}}{\text{Initial BSA-FITC loaded}} \times 100 \dots \dots \dots (7)$$

$$350 \quad \% LC = \frac{BSA-FITC \text{ entrapped nanocarriers}}{\text{Total components of nanocarriers}} \times 100 \dots \dots \dots (8)$$

351 While %EE and %LC of the NPs were determined by modified indirect
 352 method. Briefly, 1.5 mL of BSA-FITC entrapped NPs was collected and centrifuged
 353 at 14,000 rpm, 4 °C for 30 min. The supernatant was collected and mixed with 2%
 354 (w/v) sodium citrate buffer in the ratio 1:1. The BSA-FITC content was determined
 355 by a fluorescence spectrophotometry (Victor Nivo™, PerkinElmer Inc, USA) at
 356 excitation/emission 485/535 nm. The results were calculated according to the
 357 **equation (9) and (10).**

$$358 \quad \% EE = \frac{\text{Total amount BSA-free amount BSA in supernatant}}{\text{Total amount BSA}} \times 100 \dots (9)$$

$$359 \quad \% LC = \frac{\text{Total amount BSA-free amount BSA in supernatant}}{\text{The weight of polymer}} \times 100 \dots \dots \dots (10)$$

362 3.3.3.3 *In vitro* skin permeation and deposition studies

363 Abdominal neonatal porcine skins were used as a model skin. The
 364 subcutaneous layer and hair shafts were carefully cut off by medical scissors. The
 365 thickness of the skin was 600-700 µm. The skins were kept in a refrigerator at -20°C
 366 and thawed in PBS pH 7.4 at room temperature before use.

367 Skin permeation of BSA-FITC was performed by vertical Franz-type diffusion
 368 cells. The porcine skins were inserted between the donor and receptor compartments.
 369 An aliquot of 6 mL of PBS pH 7.4 as a receptor medium was continuously stirred
 370 using a magnetic stirrer at 500 rpm, and the temperature was maintained at 32 ± 1°C.
 371 Two microliters of 0.2% (w/v) BSA-FITC loaded nanocarriers were added. A total of
 372 500 µL of receiver medium was collected at 1, 2, 4, 6, and 8 h for fluorescence
 373 analysis by a fluorescence microplate reader at an excitation wavelength of 485 nm
 374 and an emission wavelength of 535 nm. The same volume of PBS pH 7.4 was filled in
 375 each receiver compartment to maintain a constant volume. Each formulation was
 376 performed in triplicate (n=3).

377 After 8 h of permeation study, the extracted BSA-FITC deposited in the skin
 378 was measured. Briefly, the marked area of the skins was collected and extracted using
 379 a probe sonicator with a frequency of 40 kHz and a 40% amplitude for 10 min on an
 380 ice bath. Then, the samples were centrifuged at 5000 rpm for 5 min and collected the
 381 supernatant. The fluorescence intensity was analyzed by a fluorescence
 382 spectrophotometry (Victor Nivo™, PerkinElmer Inc, USA) at excitation/emission
 383 wavelength of 485/535 nm. All samples were repeated in triplicate (n=3).

384 3.3.4 Development of NIs loaded MSs serum

385 3.3.4.1 Preparation of NIs loaded MSs serum

386 0.2% (w/w) of the extract or BSA-FITC was loaded in NIs. NI formulation
387 was mixed with glycerin (4%w/v), microcare PHC (0.8%v/v), EDTA 2Na
388 (0.05%w/v), Sepimax Zen™ (0.54%w/v), and FIR water (5%v/v) to form a serum-
389 based formulation (NI serum). Subsequently, 1% (w/w) of MS was added to the
390 formulation (NI serum MS). Particle size, PDI and zeta potential of the nanovesicles
391 were analyzed as described above.

392 3.3.4.2 *In vitro* skin permeation study of NIs loaded MSs serum

393 Skin permeation of macromolecular proteins was performed by vertical Franz-
394 type diffusion cells, and 0.2% (w/w) of BSA-FITC was used as a model high-MW
395 protein loaded in NIs. One gram of each formulation was applied and gently
396 massaged onto the skin for 2 min (approximately 160 rubbing times/1.96 cm² of skin
397 area) using the forefinger with a medical glove, before inserting between the donor
398 and receptor compartments. An aliquot of 6 mL of PBS pH 7.4 as a receptor medium
399 was continuously stirred using a magnetic stirrer at 480 rpm, and the temperature was
400 maintained at 32 °C. A total of 500 µL of receiver medium was collected at 1, 2, 4, 6,
401 8, and 24 h for fluorescence analysis by a microplate reader at an excitation
402 wavelength of 485 nm and an emission wavelength of 535 nm. The same volume of
403 PBS was filled in the receiver compartment to maintain a constant volume. Each
404 sample was analyzed in triplicate.

405 3.3.4.3 CLSM study

406 In this study, BSA-FITC as a green fluorescent compound was used as a
407 model macromolecular protein, and Rh-PE was used as a red fluorescent probe for
408 niosomal membrane in the ratio of 1:100 mM. After 8 h of *in vitro* skin permeation,
409 the treated skin was washed with PBS to remove excess formulation. Formulation that
410 permeated through the whole skin was immersed in sufficient methyl salicylate and
411 then the top layer and permeation depth were visualized under a CLSM (an inverted
412 Zeiss LSM 800 microscope, Carl Zeiss, Jena, Germany) equipped with HeNe
413 (excitation wavelength 543 nm; emission wavelength 580 nm), Ar (excitation 488 nm;
414 emission 514 nm) and diode lasers (excitation 358 nm; emission 461 nm). Confocal
415 images were obtained using a × 10 objective lens. Whole skins were cross-sectioned
416 using a cryostat (Leica CM1850, Leica Instrument, Wetzlar, Germany). Each skin
417 sample was mounted on a metal sample holder using frozen section medium (Neg50,
418 Microm International, Waldorf, Germany). The frozen skin was cross-sectioned into
419 10 µm slices, and then placed on glass microscope slides. Finally, the tissues were
420 fixed on the slide using a fast-drying mounting (HI-MO, Bio-Optica Milano, Italy).
421 The cross-sectioned skins were visualized under a CLSM as described above.

422 3.3.5 Stability test

423 The stability of NI serum MSs containing (0.2%, w/v) DAV or (0.1%, w/v)
424 PPE was performed at three different temperature conditions, which the formulations

425 were stored in tight container and placed in a refrigerator (4 °C), at room temperature
 426 (25°C), and an oven (40°C) for 1 month. The stability results were analyzed by
 427 comparing values of size, PDI, zeta potential, protein content at day 0 and day 30 (1
 428 month) interval.

429 **3.3.6 *In vivo* human study**

430 *In vivo* human study was approved by an Investigational Review Board (No.
 431 COE 63.0803–056, Human Studies Ethics Committee, Silpakorn University Research,
 432 Innovation and Creativity Administration Office, Sanam Chandra Palace Campus).
 433 Twelve of healthy human volunteers (between 25 and 40 years old) agreed to
 434 participate in a clinical trial, that they were divided according to their genders as 5
 435 males and 7 females. Scalp skin and hair in a marked area were not applied with
 436 moisturizer products for at least 12 h before the measurement. A marked position was
 437 performed with an area of 1 cm² at the back of the head and a razor blade was used to
 438 cut off the hair shafts. The (0.2%, w/v) DAV or (0.1%, w/v) PPE-loaded NI serum
 439 MSs were applied and gently massaged onto the marked area for 2 min
 440 (approximately 120 rubbing times/marked skin area) by the forefinger. After applying
 441 the formulation for 14 days and 30 days, the melanin content, erythema and hydration
 442 of the skin were evaluated by the DermaLab[®] series (SkinLab Combo, Cortex
 443 Technology, Hadsund, Denmark), while change in hair length was observed using a
 444 Dino-Lite Edge digital microscope (AM7915 Series, Taiwan). All parameters were
 445 calculated from the percent change of treatment compared with non-treatment. The
 446 epidermal melanin content, termed as the melanin index (%MI) and skin erythema
 447 shown as the erythema index (% EI) were calculated according to **equation (11)** and
 448 **equation (12)**, where epidermal melanin content and skin erythema of normal skin
 449 were generated at 100%. The change in skin hydration (%Hydration) was calculated
 450 from **equation (13)**, while the change in hair elongation (%Hair elongation) was
 451 computed from **equation (14)**

$$452 \quad \%MI = 100 + ((Mt - M)/M) \times 100 \dots\dots\dots (11)$$

453 where Mt is the epidermal melanin content treated with the sample and M is the
 454 epidermal melanin content of non-treatment.

$$455 \quad \%EI = 100 + ((Et - E)/E) \times 100 \dots\dots\dots (12)$$

456 where Et is the skin erythema treated with the sample and E is the skin erythema of
 457 non-treatment.

$$458 \quad \%Hydration = (Ht - H)/H \times 100 \dots\dots\dots (13)$$

459 where Ht is the skin hydration treated with the sample and H is the skin hydration of
 460 non-treatment.

$$461 \quad \% \text{ Hair elongation} = ((Lt - L)/L) \times 100 \dots\dots\dots (14)$$

462 where Lt is the length of hair treated with the sample and L is the length of hair of
 463 non-treatment.

464 3.3.7 Statistical analysis

465 All data were shown as mean \pm standard deviation (S.D.). Statistically
466 significant differences were determined by one-way analysis of variance (ANOVA),
467 followed by Tukey's post hoc test. Independent student's t-test was used to determine
468 if the means of two sets of data were significantly different from each other. While the
469 in vivo human study was analyzed using the Wilcoxon signed rank test. Significant
470 difference was set at p value < 0.05 .



CHAPTER 4

RESULTS AND DISCUSSION

4.1 Appearance and SDS-PAGE analysis of DAV and PPE

DAV extract had a light red fibrous texture, while PPE extract exhibited a brown powder. The complex mixtures of proteins in the crude extracts of DAV and PPE were separated by the electrophoresis technique as shown in **Figure 12**. The gel matrix is a polyacrylamide gel and sodium dodecyl sulfate (SDS) that is an anionic (negatively charged) detergent to bind proteins. Proteins move through the pores in the gel matrix in response to an electrical field. Therefore, SDS-PAGE can be used to estimate the relative molecular mass of proteins (121). In our study, the gel showed bands of proteins in each crude extract with MWs ranging from 66 kDa to 6.5 kDa, representing the bands of high-MW proteins (i.e., Bovine serum albumin (BSA)) and polypeptides (i.e., growth factor).

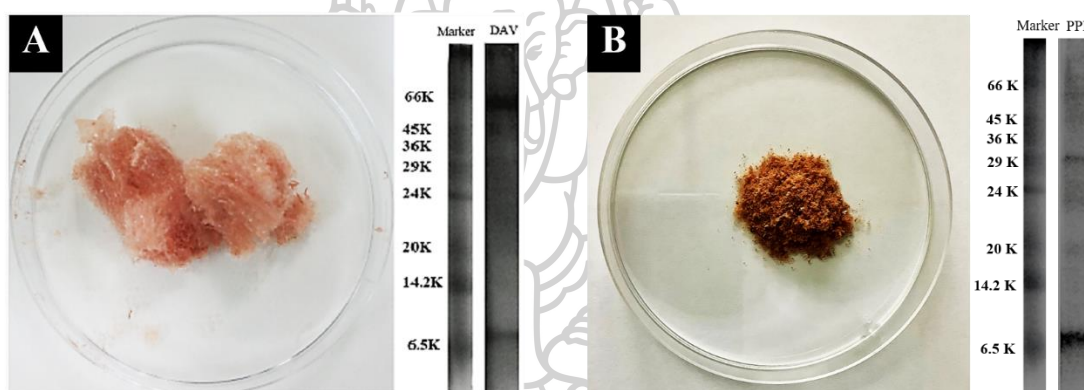


Figure 12 Image of appearance and proteins analysis using electrophoresis technique (SDS-PAGE) of DAV (A) and PPE (B)

4.2 Quantitative analysis of %Yield, total protein, GFs (FGF2, EGF, IGF-1, and TGF- β 1) and amino acids in DAV and PPE

% Yield of DAV and PPE were 5.64 ± 0.10 and 2.28 ± 0.16 %, respectively. Total protein, GFs (IGF-1, EGF, TGF- β 1, and FGF2), and amino acids content in these crude extracts are shown in **Table 3**. The total protein content of DAV (233.64 ± 5.55 mg/g) was higher than PPE (151.95 ± 3.40 mg/g). Moreover, the total content of GFs (IGF-1, EGF, TGF- β 1, and FGF2) in PPE was more than those in DAV. For amino acid determination, 12 types of amino acid were found in PPE as follows; cysteine > lysine > valine > leucine > glutamic acid > threonine > histidine > phenylalanine > isoleucine > serine > tyrosine > methionine. While DAV expressed 11 types of amino acid in the order of cysteine > lysine > glutamic acid > leucine > phenylalanine > tyrosine > isoleucine > histidine > serine > valine > methionine. To control the quality and standardization, the efficacy and safety of the extracts are necessary. Marker selection of the bioactive compound plays an important role in the quality control of the extracts sources or the extraction method (122). For anti-skin aging effect, total protein, EGF, and TGF- β 1 can be chosen as the bioactive markers

of the extracts because they are generally contained in the commercial cosmetic products (123). Whereas, IGF-1, EGF, and FGF2 are able to select as the bioactive markers for hair regeneration because of the hair growth promotion effect (124). In this study, we mentioned the regenerative effect of active ingredients to treat aging condition on skin and hair. Therefore, the total protein content, GFs and various amino acids were selected as bioactive markers in this study.

Table 3 Percent yield, total protein content and the quantitative content of GFs (IGF-1, EGF, TGF- β 1, and FGF2), and amino acids in DAV and PPE

	DAV	PPE
%Yield	5.64 \pm 0.10	2.28 \pm 0.16
Total protein (mg/g)	233.64 \pm 5.55	151.95 \pm 3.40
Growth factors		
- IGF-1 (ng/g)	36.87 \pm 10.04	40.38 \pm 6.00
- EGF (pg/g)	3.10 \pm 2.25	5.79 \pm 2.47
- TGF- β 1 (pg/g)	53.03 \pm 3.05	55.20 \pm 1.21
- FGF2 (pg/g)	28.36 \pm 6.40	65.34 \pm 6.56
Amino acids		
- Cysteine (nmol)	22.92	51.47
- Lysine (nmol)	4.14	25.31
- Valine (nmol)	0.24	21.95
- Leucine (nmol)	2.81	17.21
- Glutamic acid (nmol)	3.55	16.56
- Threonine (nmol)	-	16.22
- Histidine (nmol)	1.11	15.12
- Phenylalanine (nmol)	1.87	8.06
- Isoleucine (nmol)	1.64	6.21
- Serine (nmol)	0.39	5.40
- Tyrosine (nmol)	1.67	4.68
- Methionine (nmol)	0.01	4.10

4.3 Bioactivities of DAV and PPE on skin and hair rejuvenation

4.3.1 Effect of DAV and PPE on cell viability of NHFs, HaCaTs, and HFDPCs

As shown in **Figure 13 (A-C)**, various concentrations of DAV and PPE (1 – 4,000 μ g/mL) were non-toxic to NHFs and HFDPCs, while these crude extracts trended to decrease the cell viability of HaCaTs at the concentration of more than 100 μ g/mL. Both DAV or PPE exhibited significant difference in cell viability values at the concentrations over 1,000 μ g/mL ($p < 0.05$). MTT assay is generally the measurement method to evaluate the cell's metabolic activity for quantifying cellular proliferation. Therefore, the %cell viability of both extracts treated NHFs above 100% indicated that DAV and PPE might stimulate proliferation process (125).

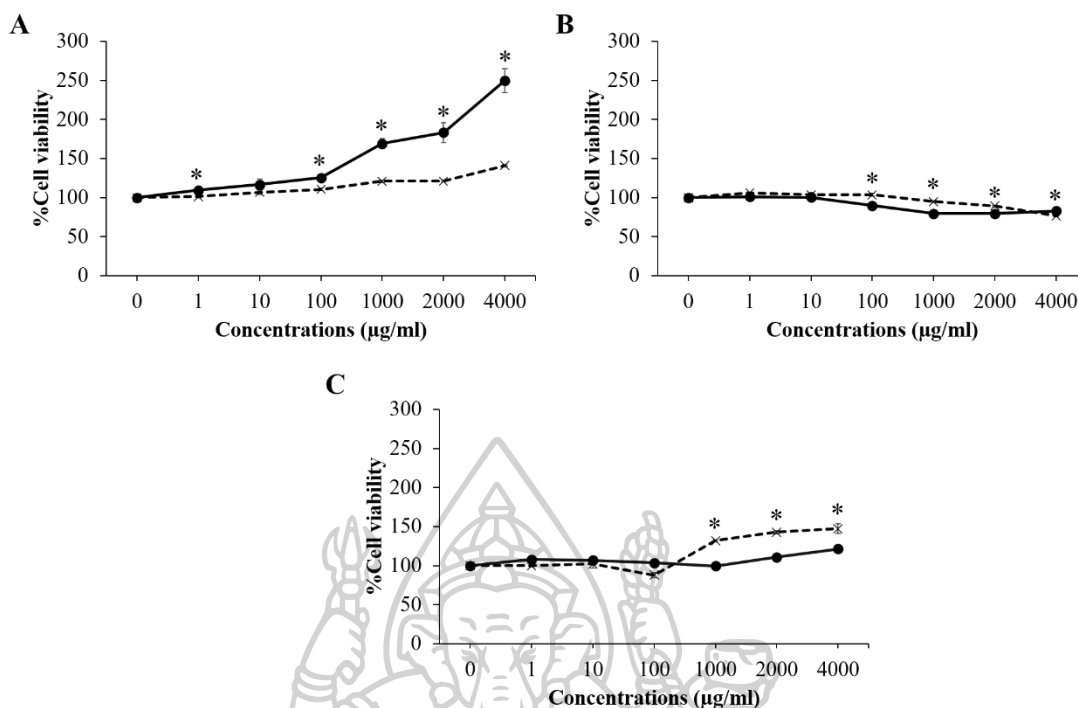


Figure 13 The %cell viability of NHFs (A), HaCaTs (B) and HFDPCs (C) treated with DAV (—●—) and PPE (---×---) at various concentrations (1-4,000 µg/mL). * expresses the significant difference between the treatment compound ($p < 0.05$).

4.3.2 Effect of DAV and PPE on cell proliferation of NHFs, HaCaTs, and HFDPCs

Keratinocyte cells are the constituents of the multilayered epidermis, which the epidermis is renewed by the proliferation and differentiation of the keratinocytes (126). On the other hand, dermal fibroblasts associate with the reconstructed epidermis in the generation and maintenance process (63). In the case of hair cells, HFDPCs are specialized mesenchymal cells of hair that play an important role in the morphogenesis and regeneration of hair growth (127). Additionally, the HFDPCs are involved with the activities of the keratinocytes to form the hair follicle and generate the hair shafts (128). For cell aging, both epidermal keratinocytes and dermal fibroblast of skin cells occurred loss of cell generation, while hair cell counts or hair cell densities declined with advancing age (129, 130). From the results shown in **Figure 14(A-B)**, DAV and PPE increased the proliferation of skin cells in a time-dependent manner. DAV enhanced the growth of keratinocytes and fibroblasts greater than PPE. In **Figure 14(C)**, both DAV and PPE were able to stimulate HFDPCs cell generation, but a high concentration of PPE at 4,000 µg/mL was toxic to the cells. Therefore, DAV at the concentration of 2,000 µg/mL and PPE at the concentration of 1,000 µg/mL were suitable to be used as regeneration compounds for skin and hair without causing cytotoxicity.

DAV and PPE contained a high content of GFs, in which FGF, IGF-1 and EGF have been found to stimulate cellular proliferation of human skin by DNA synthesis. These GFs also influenced multiple layers of keratinocytes arising from the

basal layer of the epidermis, providing an epidermal outgrowth (131). Besides, the mechanism of action of the peptides on cell renewal and ECM remodeling were related to activating the proliferation of the skin fibroblasts and deceleration of the aging process (132). In age-related hair regeneration, EGF and FGF were proved to increase the proliferative effect of papilla cells and hair root sheath fibroblasts (133). Moreover, IGF-1 is potent to stimulate hair-follicle growth by preventing hair follicles from entering the catagen phase (134).

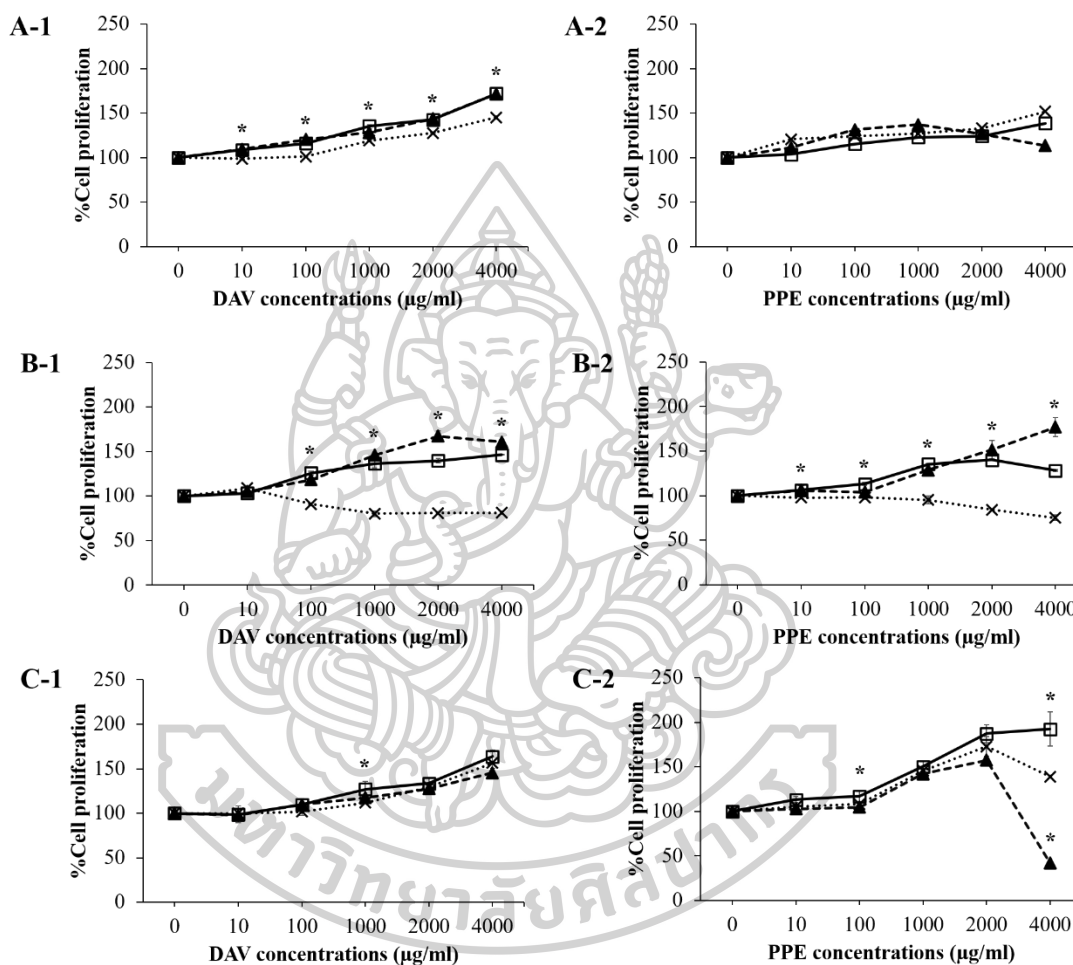


Figure 14 The % cell proliferation of skin and hair cells treated with DAV and PPE for 24 h (-----x-----), 48 h (—□—), and 72 h (---▲---): (A-1 and A-2) NHFs cell proliferation, (B-1 and B-2) HaCaTs cell proliferation, and (C-1 and C-2) HFDPCs cell proliferation. * represents the significant difference value compared to time 24 h ($p < 0.05$).

4.3.3 Effect of DAV and PPE on skin cell migration

Cell migration is essential for wound repair, in which the aging fibroblasts cause the loss of proliferative and migratory activity coupled with the loss of wound closure ability and skin repair (135). To evaluate a potential therapy for wound healing and skin recovery, 2,000 µg/mL of DAV extract and 1,000 µg/mL of PPE extract were used for *in vitro* scratch assay on skin fibroblast cells. As the result in

Figure 15, these extracts dramatically enhanced the migration of dermal cells at 24 h compared with the positive control (TGF- β 1) and negative control. Both DAV and PPE completely closed the width of the scratch area at 48 h. These results indicated that the extracts induced skin regeneration activity.

The skin regeneration ability declines with increased-age because of the structural and functional changes such as decreasing proliferation and migration effect of dermal cells and degrading collagen and elastin in the ECM (75). Bioactive factors such as proteins, peptides, GFs, and cytokines have significant biological activity involved in regulating cell growth and development, leading to an important role in both regeneration and repair (78). FGF family regulates the migration, proliferation, differentiation, metabolic activity, and survival in a wide variety of cells (136), while EGF influenced the growth and regeneration effect of skin cells (137). IGF-1 has been reported to improve skin fibroblast functions for example the inhibition of collagenase enzymes and the induction of collagen expression (138). In addition, TGF- β induced collagen biosynthesis and skin wound healing (139, 140). Thus, the DAV and PPE containing GFs and cytokines might play an important role to regenerate the skin cells (123).



Figure 15 Image-based monitoring of human skin fibroblasts migration at 0, 24 and 48 h for untreated cell (A), cells treated with TGF- β 1 (B), DAV 2000 μ g/mL (C), and PPE 1000 μ g/mL (D). All images were obtained at a magnification of 4 \times objective lens.

4.3.4 Repair of UVB-induced skin damage

Photo-aging is the main factor to induce oxidative stress, resulting in reduced cell growth, collagen metabolism, and degradation of elastin (73). UVB ray was reported to activate the expression of MMPs such as collagenase (MMP1), gelatinase (MMP2), stromelysin (MMP3), and gelatinase (MMP9), leading to degradation of the ECM and collagen (141). For MMP9 that was a transcription gene associated with collagen degradation (28). As seen in **Figure 16**, DAV and PPE stimulated the cell

growth after UVB-induced intracellular ROS. 2,000 $\mu\text{g/mL}$ of DAV and 1,000 $\mu\text{g/mL}$ of PPE showed the highest cell regenerative effect. Therefore, these concentrations were used to evaluate the mechanism of collagen metabolism. Pro-collagen I and MMP9 expression was used to determine collagen degradation. In **Figure 17**, pro-collagen I of the PPE-treated UVB-radiated cells were observed to be slightly higher than those of the untreated cells, while the DAV-treated UVB-radiated cells were significantly higher than non-treatment group. Down-regulation of MMP9 significantly decreased in both extracellular and intracellular after treatment with both extracts (**Figure 18**). Thus, PPE and DAV were able to restore the skin from photo-aging via the up-regulation of pro-collagen I and down-regulation of MMP9.

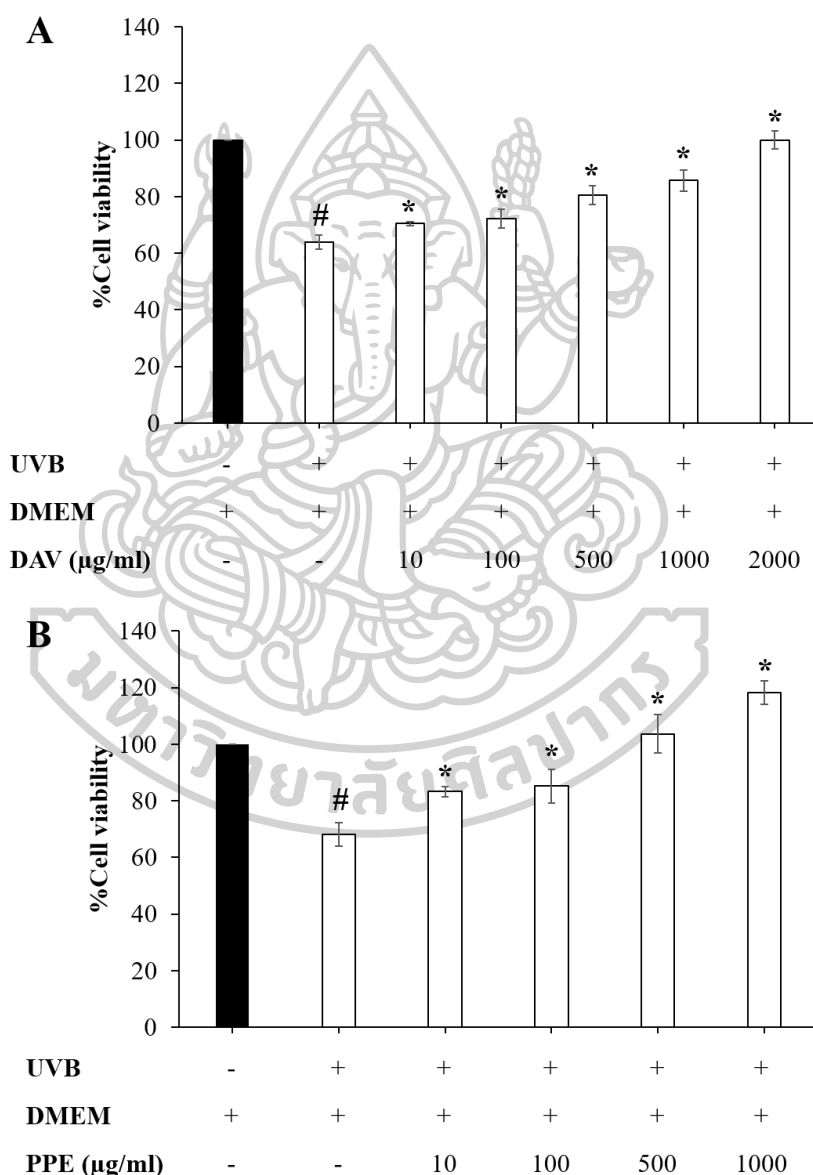


Figure 16 The % cell viability of UVB-irradiated cells treated with DAV (**A**) and PPE (**B**). The mark (+) indicated the samples exposure to the substance, while the mark (-) presented the samples have not been exposed to the substance. For statistical

symbols, # and * demonstrate the significant difference value between the control non-UVB-irradiated group and control UVB-irradiated group, respectively.

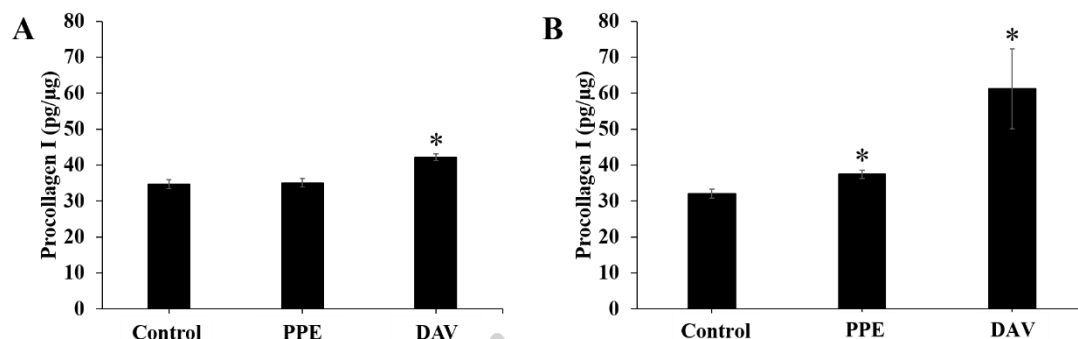


Figure 17 The extracellular procollagen I (pg/μg) level of the extracts-treated UVB-exposed NHF cells (A) and an intracellular procollagen I (pg/μg) level of the extracts-treated UVB-exposed NHF cells (B) compared with the control group (non-treatment). * exhibits statistically significant difference from the control ($p < 0.05$)

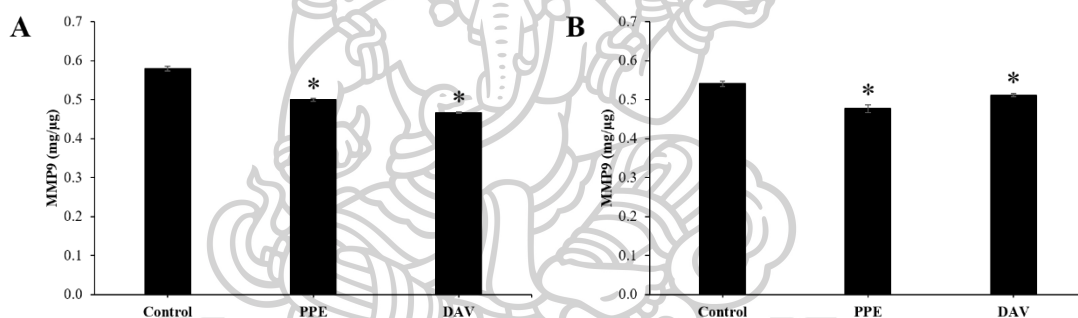


Figure 18 The extracellular MMP9 (mg/μg) level of the extracts-treated UVB-exposed HaCaTs cells (A) and an intracellular MMP9 (mg/μg) level of the extracts-treated UVB-exposed HaCaTs (B) compared with the control group (non-treatment). * show statistically significant difference from the control ($p < 0.05$)

4.3.5 Protective effect of DAV and PPE on skin cells

To evaluate the protective effect of skin cells, t-BHP has been used as a model compound to determine the mechanism of acute oxidative stress-induced DNA damage without cell death (142). In this study, cells were pretreated with DAV or PPE at various concentrations (10-2,000 μg/mL) for 1 h before being treated with 200 μM of t-BHP. The result showed that t-BHP significantly reduced the cell viability by around 50-60%, while pretreatment of keratinocyte cells with DAV or PPE at various concentrations did not affect the cell protection. Additionally, HaCaTs pretreatment with 100 μM of quercetin as a positive control significantly increased the viability of the cell and exhibited a cytoprotective effect against t-BHP-induced ROS production (Figure 19). Therefore, the pretreatment of HaCaTs with both DAV and PPE did not protect the cells against t-BHP-induced ROS production. In the previous report, protease enzymatic hydrolysate of antler velvet produced the peptides and showed potent peroxyl radical scavenging activity. Also, purified peptide (tetrapeptide,

Tryptophane (Trp)- Aspartic acid (Asp)- Valine (Val)- Lysine (Lys)) inhibited cellular damage, intracellular ROS production, presenting protective capacity against 2,2'-Azobis(2-amidinopropane) dihydrochloride (AAPH)-induced oxidative stress (143). While, homogenized PPE expressed the strong protective effect by protecting the HaCaTs from 2,4-dinitrochlorobenzene (DNCB)-induced ROS production (144). From the results of our study the active compounds in DAV were not performed the hydrolyzed process to obtain purified peptide. For PPE, we used different ROS stimulants and stimulation time, which may have an effect on stimulating cells to produce ROS.



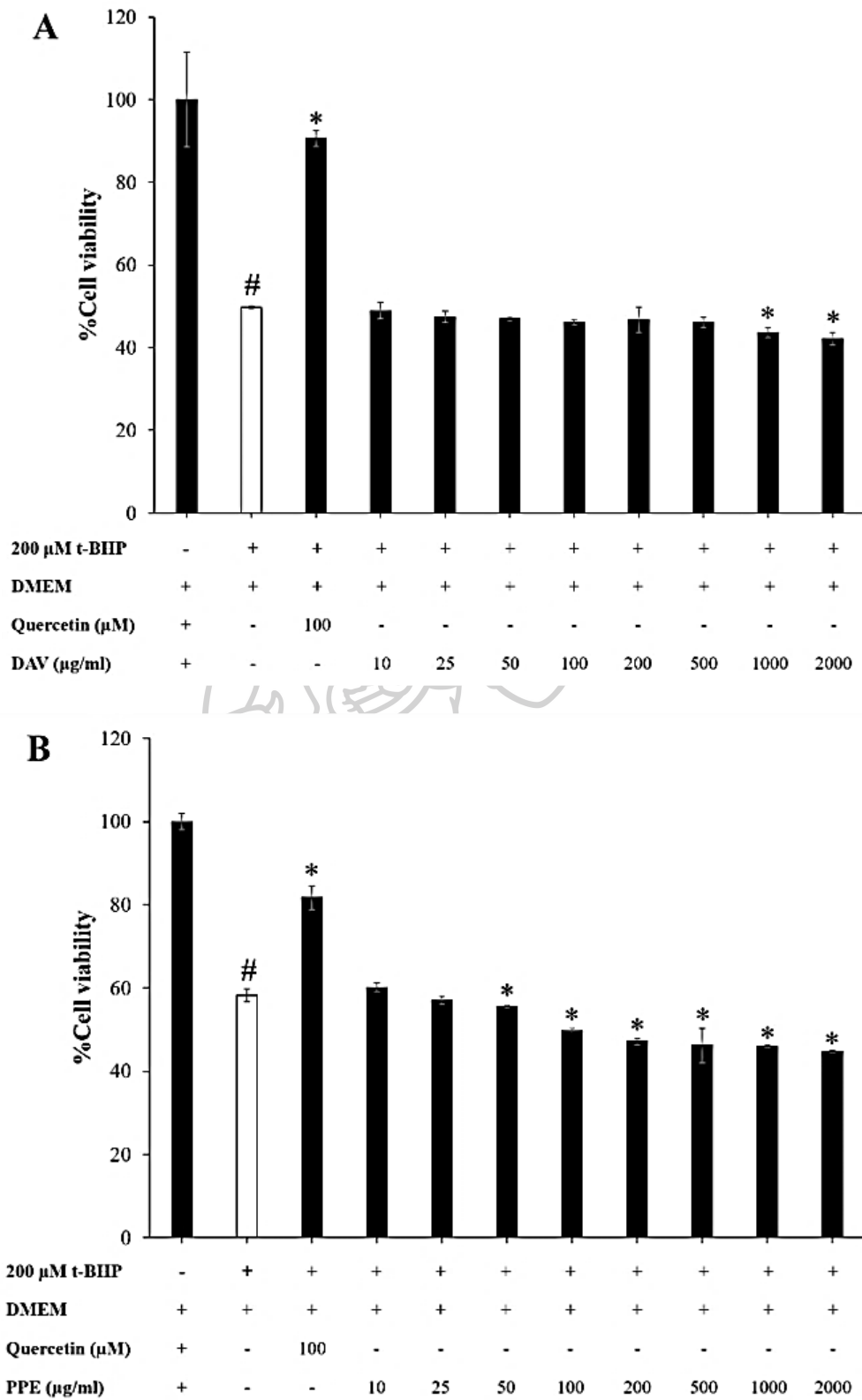


Figure 19 Protective effect of DAV (A) and PPE (B) on skin cells prior to 200 μ M t-BHP-exposed for 4 h. The mark (+) indicated the samples exposure to the substance, while the mark (-) presented the samples have not been exposed to the substance. #

and * demonstrate a significant difference value from the control non-t-BHP-exposed group and the control t-BHP-exposed group, respectively.

4.3.6 Effect of DAV and PPE on intracellular ROS reduction

To determine the effects of DAV and PPE on ROS generation in keratinocyte cells, t-BHP as a substance was used to induce oxidative stress in keratinocyte cells by modifying the redox status of the cells, resulting in the generation of ROS-stimulated skin aging. Fluorescence indicator (H₂DCFDA) was generally used as the intracellular ROS detection in living cells. After H₂DCFDA penetration into the cellular membrane, it becomes deacetylated by esterase enzymes and changes to a non-fluorescent compound (H₂DCF). Then, H₂DCF is oxidized with ROS into the fluorescent product DCF (145). After the cells were treated with 1mM t-BHP, the level of ROS generation significantly increased from non-pretreatment with t-BHP, suggesting that t-BHP had a strong ROS generation effect in HaCaTs. The positive control quercetin at a concentration of 100 μ M showed significantly decreased levels of 48%. Pretreatment of HaCaTs with DAV or PPE inhibited ROS production (**Figure 20**). The relative ROS levels exhibited significantly reduced with treatment of DAV at the concentrations of 25 and 200 μ g/mL were found to be 118% and 124%, respectively. PPE at a concentration of 25 μ g/mL also significantly inhibited the ROS level (130%). These results indicated that the DAV and PPE act as scavengers of ROS stimulated by t-BHP in HaCaTs. Recently, tetrapeptide (Trp-Asp-Val-Lys) of DAV inhibited intracellular ROS generation induced by AAPH when the its concentration increased between 0 and 400 μ g/mL (143). Whereas, the homogenized PPE (15 μ g/mL), which composed of protein component, decreased intracellular ROS production (146). F



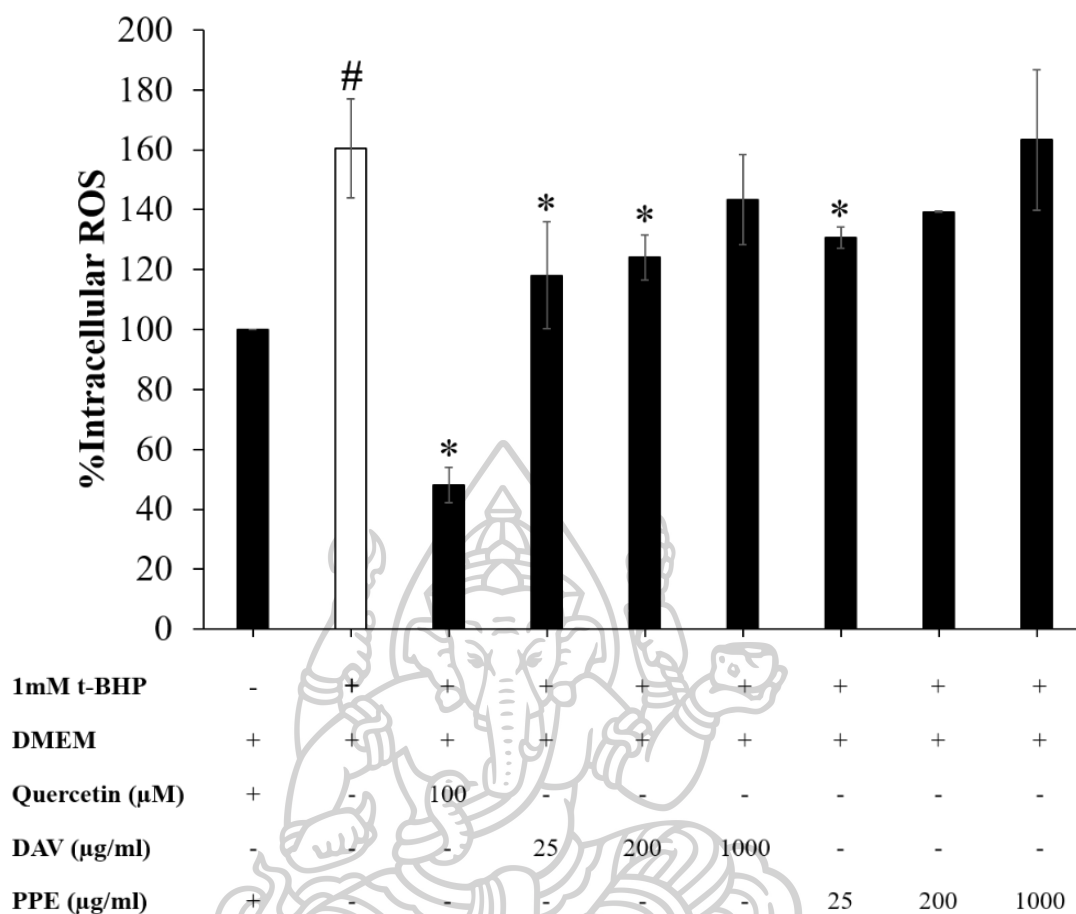


Figure 20 %Intracellular ROS reduction on HaCaTs pretreated with DAV, PPE and positive control (100 μM quercetin) after inducing ROS production with 1mM t-BHP. The mark (+) indicated the samples exposure to the substance, while the mark (-) presented the samples have not been exposed to the substance. # and * present the significant difference value compared to control non-treatment with t-BHP group and control t-BHP-induced HaCaTs cells group ($p < 0.05$), respectively.

4.3.7 Effect of DAV and PPE on anti-inflammation

4.3.7.1 Effect of DAV and PPE on inhibition of LOX enzyme

LOX plays an important role in ROS generation and the skin inflammation process. The enzyme regulates the metabolism of unsaturated fatty acids. In this study, LA was used as a substrate because it is rich in sphingolipid and ceramide of the epidermis, leading to maintain the barrier and prevent TEWL (147). When LOX interacted with LA, the peroxy radical as a product occurred (148). DAV and PPE could inhibit the reaction with the half-maximal inhibitory concentration (IC₅₀) of 157.40 ± 1.17 μg/mL and 185.9 ± 2.38 μg/mL, respectively, while the quercetin as a positive control showed IC₅₀ at the concentration of 0.0114 ± 0.0004 μg/mL. As seen in the results, both DAV and PPE extracts presented IC₅₀ values higher than quercetin. Hence, these extracts had the anti-inflammation activity through anti-LOX enzyme, suggesting that the extracts act as the inhibitor of LOX.

4.3.7.2 Effect of DAV and PPE on intracellular TNF- α reduction

Cytokines were reported in the stimulation of the inflammatory process. TNF- α was a proinflammatory cytokine found in the epidermis layer. The cytokines can cause the degradation of collagen synthesis and ECM protection (149). As shown in **Figure 21**, PPE extract at the concentration of 200 and 1,000 $\mu\text{g}/\text{mL}$ and ASA (positive control) significantly inhibited TNF- α production, while DAV extract exhibited no significant inhibition of TNF- α generation. In a previous report, protein hydrolysate correlated with anti-inflammation activity by inhibition of TNF- α production (150). Thus, PPE extract exhibited a potent anti-inflammation activity more than DAV extract.

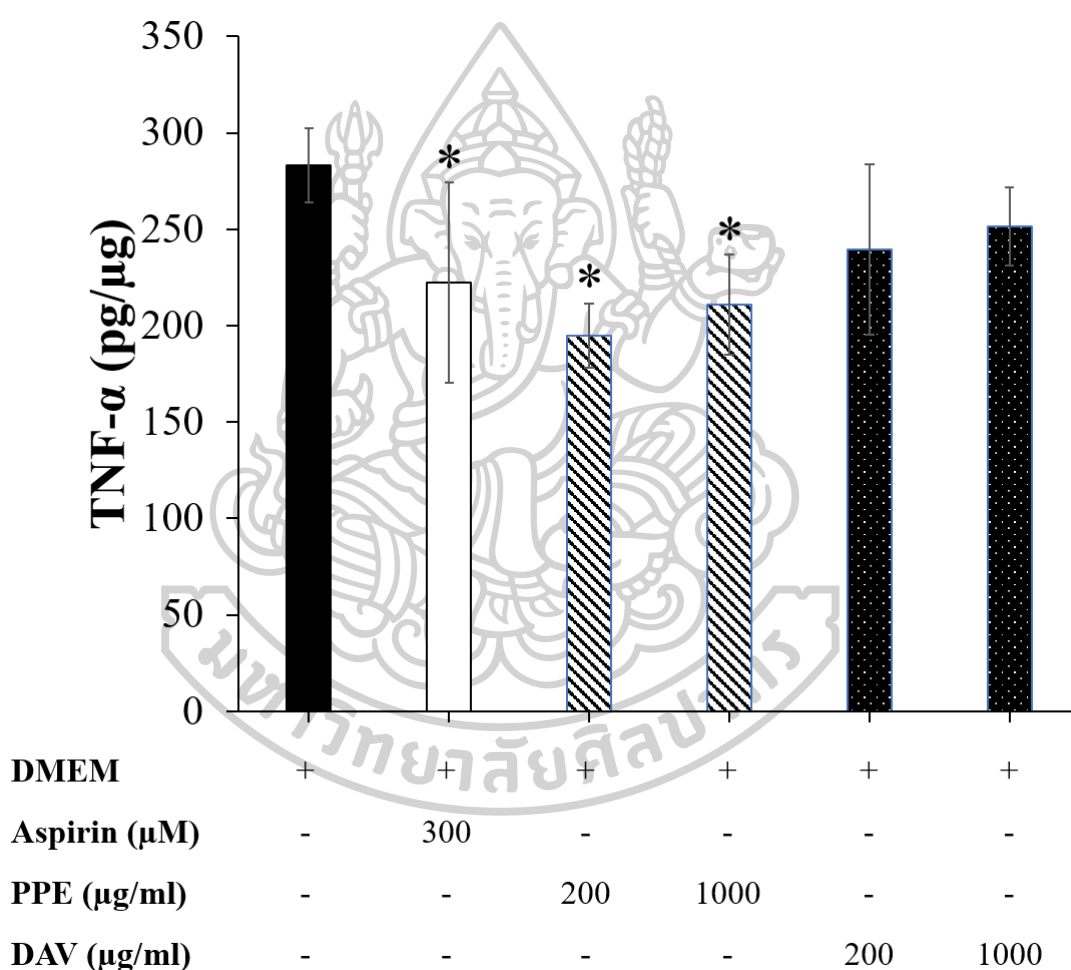


Figure 21 Effect of non-treatment group (negative control), 300 μM of ASA (positive control), PPE (200 and 1,000 $\mu\text{g}/\text{mL}$), and DAV (200 and 1,000 $\mu\text{g}/\text{mL}$) on intracellular TNF- α (n=3). The mark (+) indicated the samples exposure to the substance, while the mark (-) presented the samples have not been exposed to the substance. * exhibits the significant difference value from control ($p < 0.05$).

4.3.8 Effect of DAV and PPE on the aggregation of hair cell

Papilla cells were sub-cultured at low density into the plate, they showed a flattened morphology during migration. When the number of cells was increased, the cells became aggregated and condensed. Cells around the edges of condensed cells were arranged with their axes directed towards the center (151). From the results shown in **Figure 22**, the HFDPCs cells treated with DAV or PPE induced cell aggregation in a time-dependent manner, which the cell aggregation was found at a time of 24 h. GFs are an important role in the DP cell aggregative behavior. Some GFs are implicated to promote hair growth. EGF induces DP cell proliferation via promoting G1/S transition and accelerating the proliferation of DP cells. Moreover, the growth-stimulatory effect of EGF on DP cells is mediated via the Notch signaling pathway, associated with hair follicle development and hair growth (152).

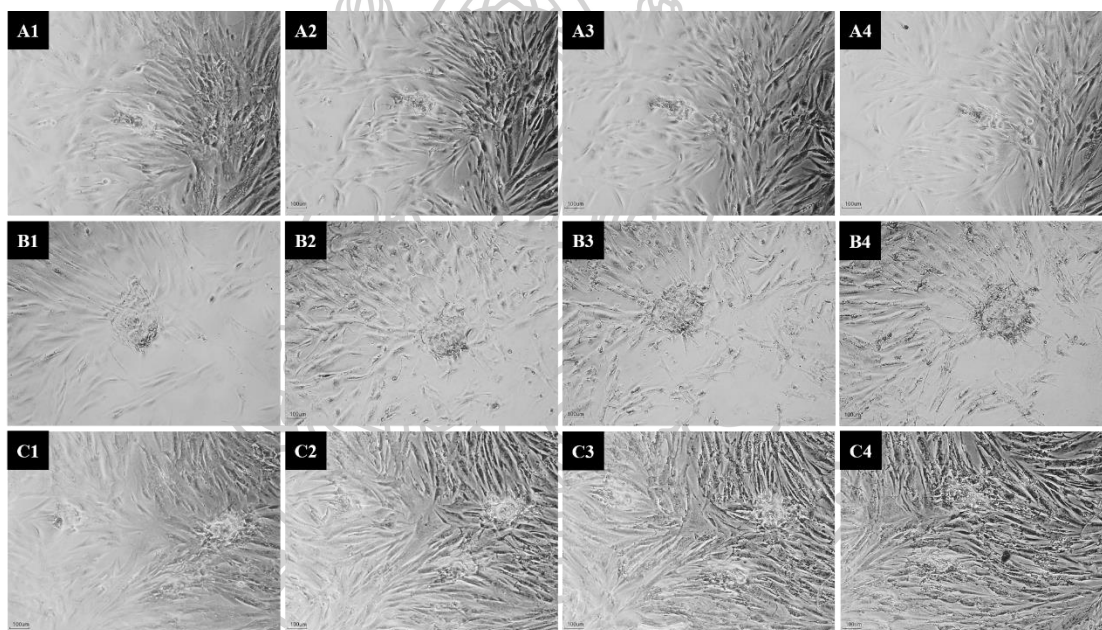


Figure 22 Effects of DAV and PPE on HFDPCs aggregation: (A1-A4) control group at time 0, 24, 48, 72 h, (B1-B4) the cells treated with 2,000 $\mu\text{g}/\text{mL}$ of DAV at time 0, 24, 48, 72 h, and (C1-C4) the cells treated with 1,000 $\mu\text{g}/\text{mL}$ of PPE at time 0, 24, 48, 72 h.

4.4 Development of nanocarriers for incorporation of a macromolecular protein

4.4.1 Physicochemical properties of nanocarriers

The physicochemical characteristics of the different nanocarriers are shown in **Table 4**. The particle size of all formulations ranged from 60 to 230 nm with a narrow size distribution ($\text{PDI} < 0.4$). The average particle size was in the order: liposomal formulation < niosomal formulation < NP formulation. In the case of PEG2000-DSPE grafted nanovesicles, PEG-NI was a smaller size than these vesicles without PEG2000-DSPE. PEG molecules could strongly decrease the attraction by van der

Waals forces and provide repulsive forces by steric, electrostatic, and hydration effects (153). Thus, the conjugation of PEG2000-DSPE on the LIs or NIs surface can reduce the aggregation of the vehicles resulting in smaller size (154). The zeta potential of the LI formulations was between -5.99 and -9.40 mV. Because the pH of the LI solution was 7.4, which was higher than the isoelectric point (pI) of PC (approximately 6-6.7). In addition, PC as a zwitterionic substance resulted in a negative surface charge (155). For NI formulations, the zeta potential ranged from -25.07 to -35.87 mV, which PEG grafted NIs decreased the negative charge relating to the increment in PEG chain length and the concentration ratio (156). CS-TPP and CS-MHA-TPP NPs expressed a positive charge because the pKa of CS is approximately 6.5; when the pH of the medium is less than 6, amines of CS are protonated reflecting the polycationic behavior of CS (98).

The %EE of the formulations were in the following order: LI > PEG-LI > CS-MHA-TPP NPs > NI > PEG-NI > CS-TPP NPs. BSA as a model protein is a hydrophilic compound and shows a negative charge in the body fluid (pH 7.4). The LI formulations can encapsulate hydrophilic compounds in an aqueous core, including adsorbed on uncharged (or neutral) LIs by hydrophobic interaction (157). While CS-MHA-TPP NPs highly entrapped protein by conjugating with thioether formation via maleimide groups (158). NIs with sorbitan monoester or Span were also used for protein drug delivery. Moreover, Chol is a lipid composition of NIs that influenced the encapsulation efficiency and showed a value of around 30% (159). For CS-TPP NPs, BSA encapsulation efficiency was significantly affected by the initial BSA concentration. The CS NPs could be loaded with protein ranging from 26 to 47 % by increasing the initial BSA concentration in the range from 0.2-2 mg/mL (160). However, the ratio of drug-loaded nanocarriers: to the mass of material was an important factor to for further investigation. In our study, maximum protein loading was found in NI formulation having %LC equal to 83, and followed by PEG-NI, CS-TPP NP, LI, CS-MHA-TPP NP, and PEG-LI.

Table 4 Characterization of nanocarriers in terms of the particle size (nm), PDI, zeta potential (mV), % EE, and %LC

Formulations	Drug	Size (nm)	PDI	Zeta potential (mV)	%EE	%LC
LI	0.2%BSA-FITC	62.50 ± 0.31	0.210 ± 0.01	-5.99 ± 0.93	65.57 ± 2.29	16.07 ± 0.52
PEG-LI	0.2%BSA-FITC	70.07 ± 0.35	0.202 ± 0.00	-9.40 ± 0.58*	61.83 ± 9.95	13.52 ± 2.12
NI	0.2%BSA-FITC	193.50 ± 4.20*	0.383 ± 0.07*	-35.87 ± 0.95*	38.13 ± 4.58*	83.63 ± 10.41*
PEG-NI	0.2%BSA-FITC	126.93 ± 1.03*	0.265 ± 0.01*	-25.07 ± 0.55*	35.80 ± 7.16*	64.03 ± 12.98*
CS-TPP NP	0.2%BSA-FITC	230.33 ± 72.54*	0.413 ± 0.08*	22.40 ± 0.10*	31.57 ± 2.79*	27.31 ± 1.11
CSM-TPP NP	0.2%BSA-FITC	218.50 ± 10.17*	0.381 ± 0.02*	23.40 ± 1.37*	60.34 ± 2.42	15.35 ± 0.94

Data present mean ± S.D. All samples were measured in triplicate. * exhibits the significant difference from conventional LIs ($p < 0.05$).

4.4.2 *In vitro* skin permeation and drugs deposited in the skin

Skin is a major organ in the human body, which consisted of 3 layers: epidermis, dermis, and subcutaneous. The SC acts as a rate-limiting barrier for transdermal drug delivery. In this study, vesicular nanocarriers were used to improve the skin penetration of macromolecules such as protein and GFs through the skin barrier (161, 162). In **Figure 23**, liposomal and niosomal formulations showed higher cumulative BSA-FITC permeated through the skin than NPs, suggesting that LIs and

NIs can penetrate through the skin via both transepidermal and transappendageal routes. PEG molecules hydrate the skin and change the water gradient, leading to increase skin permeation (97). Besides, the non-ionic surfactant is a composition of NIs and acts as chemical penetration enhancers. The surfactant interacts with the components of the SC, resulting in changing the structural organization of lipid bilayers. The drugs entrapped in NIs showed a good permeability and diffusion coefficient (163).

Although the skin permeation of BSA-FITC from all nanocarrier formulations was not significantly higher than the solution, the macromolecular protein-deposited in the skin layer is also the important target site to stimulate skin and hair regeneration. For *in vitro* drug-deposition in the skin at 8 h, the skin deposition of BSA-FITC loaded NI was higher than other formulations and significant difference from the solution (Figure 24). Thus, NI that exhibited higher skin permeation and deposition than other formulations was chosen to develop a suitable transdermal delivery system of macromolecules with another technique.

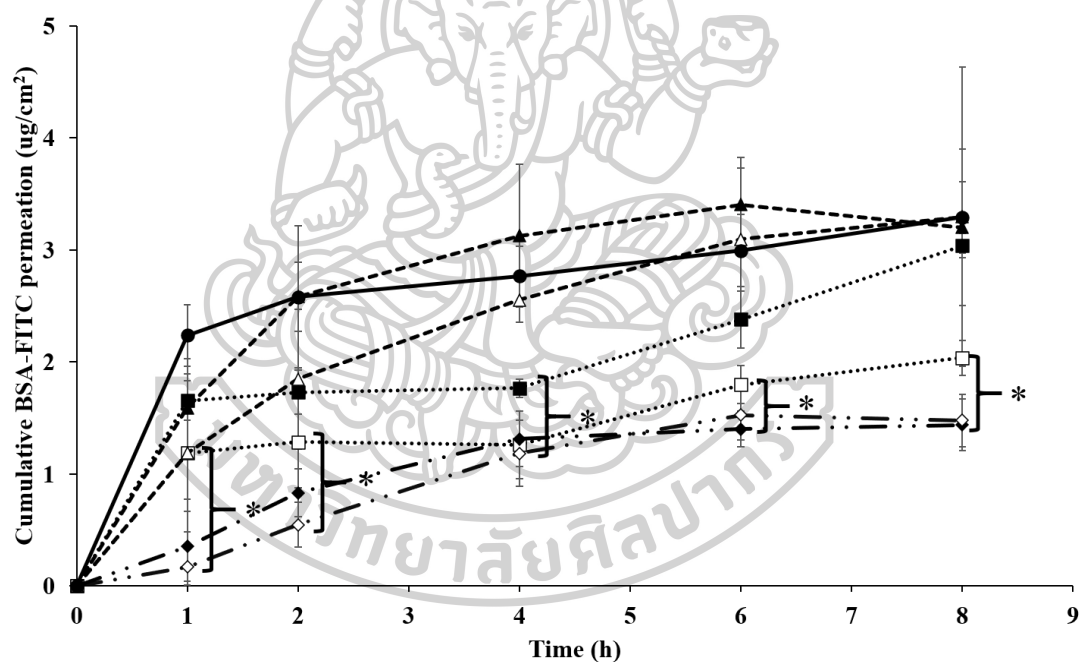


Figure 23 The cumulative permeation profile of BSA-FITC loaded nanocarriers: LI (---■---), PEG-LI (---□---), NI (---▲---), PEG-NI (---△---), CS-TPP NP (---◆---), CS-MHA-TPP NP (---◇---) at various time interval (0-8 h) compare to solution (---●---) (n=3). * presents the significant difference value compare to BSA-FITC solution.

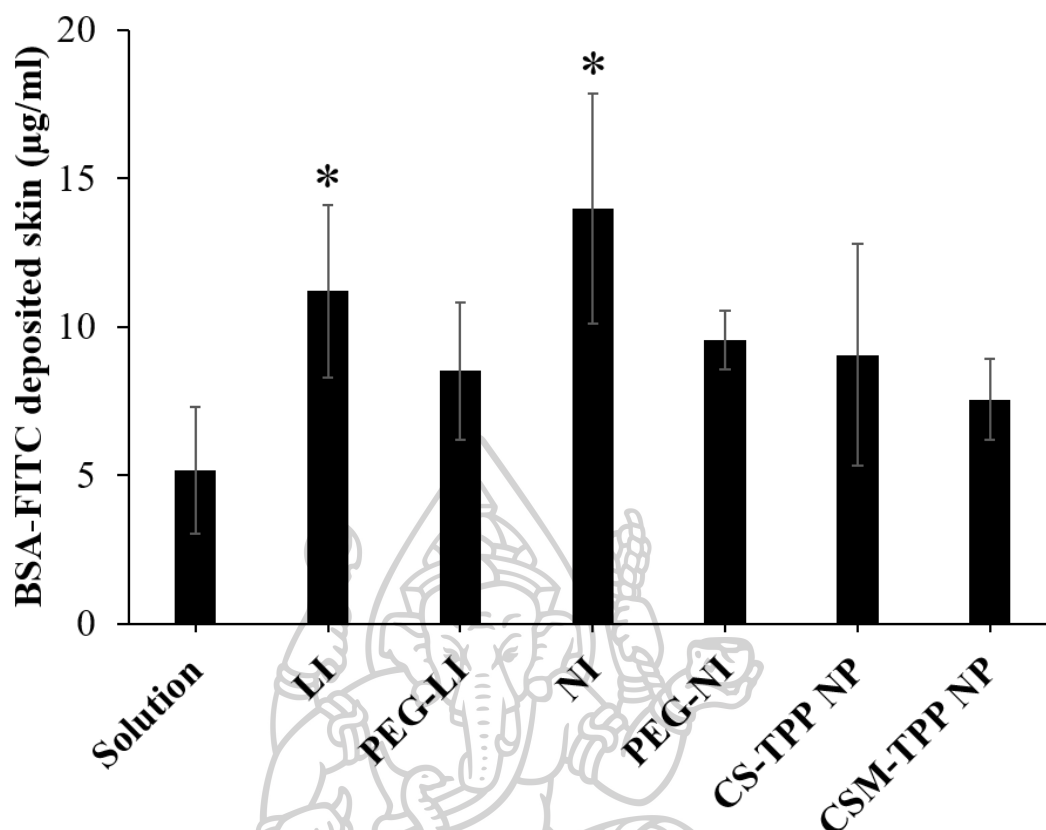


Figure 24 The profile of BSA-FITC deposited in the skin ($\mu\text{g/mL}$) in various types of nanocarriers containing BSA-FITC: LI, PEG-LI, NI, PEG-NI, CS-TPP NP, and CSM-TPP NP compared to BSA-FITC solution ($N=3$). * expresses the significant difference from solution form ($p < 0.05$).

4.5 Development of BSA-FITC-NIs loaded MSs serum

4.5.1 Physicochemical properties of niosomal formulations loaded BSA-FITC

The physicochemical properties of NI containing BSA-FITC are shown in **Table 5**. The particle size of NI formulations was in the nano range (193 – 232 nm) with narrow size distribution. The particle size of the serum was slightly higher than NI formulation, due to the presence of polyacrylate crosspolymer-6 (or SEPIMAX™ ZEN) which increased the viscosity (164). The zeta potential on the surface of these nanocarriers was negatively charged. The serum formulations were more negative than the solution due to the presence of polyacrylate crosspolymer-6 which neutralizes the zeta potential, resulting in uncoil s the carboxyl groups on the main chain.

Table 5 The physical properties of niosomal formulations.

Formulations	Sample	Size (nm)	PDI	Zeta potential (mV)
NI solution	-	144.23 \pm 1.96	0.340 \pm 0.02	-20.83 \pm 1.90
NI solution	0.2% (w/v) BSA-FITC	193.50 \pm 4.20	0.383 \pm 0.07	-35.87 \pm 0.95
NI serum	0.2% (w/v) BSA-FITC	227.33 \pm 13.46	0.618 \pm 0.07	-58.57 \pm 4.91

NI serum MSs	0.2% (w/v) BSA-FITC	232.83 ± 27.70	0.472 ± 0.02	-57.67 ± 1.97
--------------	---------------------	----------------	--------------	---------------

The data was represented as mean ± S.D. (n = 3). * presents the significance difference value from NI solution ($p < 0.05$).

4.5.2 *In vitro* skin permeation of niosomal formulations loaded BSA-FITC

To improve the skin permeability of macromolecular protein, both passive and invasive techniques of permeation enhancement have been exploited. As shown in **Figure 25**, the cumulative BSA-FITC permeation of NI serum MSs was significantly higher than other formulations ($p < 0.05$). In **Table 6**, the permeation flux (J), permeation coefficient (K_p), and enhancement ratio (ER) of NI serum MSs were also the highest, suggesting that MS in NI serum promoted the permeability of macromolecular proteins passed the skin.

Protein and GFs as the main bioactive compound are hydrophilic macromolecules, which limit skin penetration. SC is a rate-limiting step for transdermal drug delivery. Normally, the compound that can penetrate across by passive transport into the deeper skin should be small, moderate or potent lipophilic molecules (109). In this study, NIs with nonionic surfactant and Chol have been used to transport bioactive macromolecules for example protein and peptide, for their safety, efficient delivery and release (165). However, only NIs are not enough to deeply permeate the skin due to the alteration of the SC lipid structure (153). In this study, a combination of NIs with microneedling technique using MSs was developed to improve the skin permeability of bioactive macromolecules.

The thickness of the SC layer and the viable epidermis is approximately 10-20 μm and 50-100 μm , respectively (166). Microneedling can create a transportation pathway of bioactive macromolecules passed through the skin. MS has a needle-like structure with 11.89 μm diameter and 176.77 μm spicule length. MS was used as a microneedling technique because it can make deep punctures into the skin and deliver compounds passed the skin (167). After MS insertion into the skin, protein and GFs are transported through the pore, and bypass the tightly paced SC layer. Moreover, MS can also act as a microdermabrasion technique for resurfacing the SC, leading to improved skin permeability of bioactive macromolecules (110, 168).

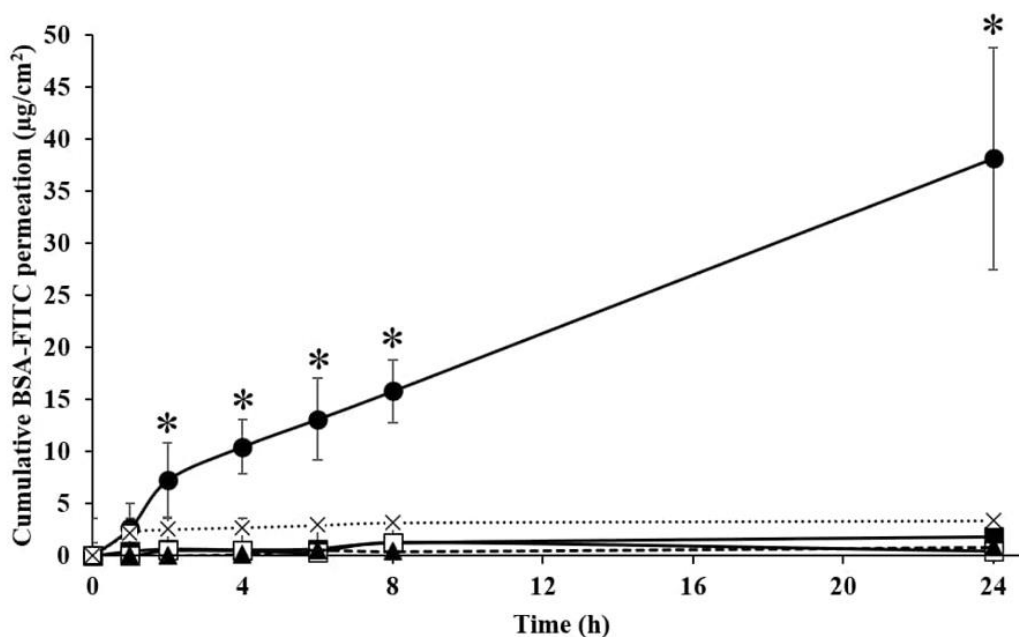


Figure 25 The cumulative BSA-FITC permeation-time profiles of NI serum MSs (—●—), NI serum (—■—), NI solution (---▲---), base (—□—), and solution (····×····). The data represent average \pm S.D. ($n = 3$). * presents significant difference values from solution (p -value < 0.05).

Table 6 The skin permeation parameters of the formulations: solution, base, NI solution, NI serum, and NI serum MSs

Formulations	Flux ($\mu\text{g}\cdot\text{cm}^{-2}\cdot\text{h}^{-1}$)	Kp ($\times 10^5$) ($\text{cm}\cdot\text{h}^{-1}$)	ER
Solution	0.0372 ± 0.02	1.86 ± 0.88	-
Base	0.0119 ± 0.01	0.60 ± 0.36	0.32
NI solution	0.0614 ± 0.06	3.07 ± 3.04	1.65
NI serum	0.0338 ± 0.01	1.69 ± 0.68	0.91
NI serum MSs	$1.2692 \pm 0.43^*$	$63.46 \pm 21.69^*$	34.11

The data was repeated in triplicate and showed the mean \pm S.D. ($n=3$). * represents significant difference from solution ($p < 0.05$)

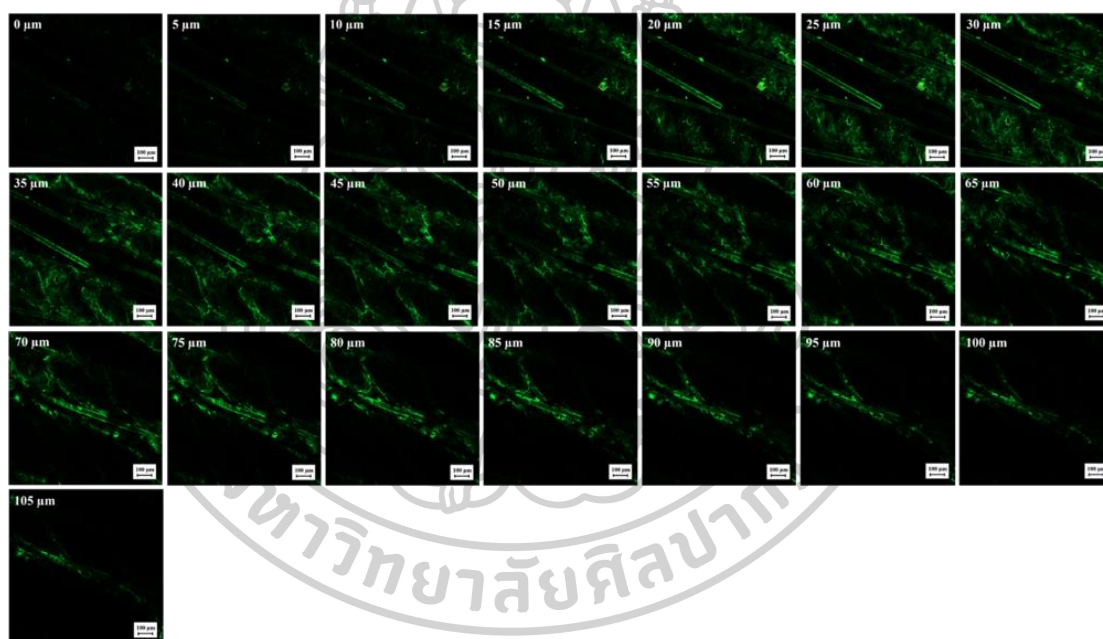
4.5.3 CLSM study

CLSM was used to analyze the skin penetration pathway and the permeation depth of the skin. In this study, Rh-PE was used to probe niosomal layer, which expressed red fluorescent color. While BSA-FITC as a model protein presented green fluorescent color. The x-z axis serial images are exhibited in **Figure 26**. Skin treated with NI serum MSs showed the deepest BSA-FITC delivery at a skin depth of 225 μm , while membrane vesicles were found in the top layer of the skin. In cross-sections of the skin, as shown in **Figure 26**, BSA-FITC solution showed the deposition of BSA-FITC in the skin and hair follicles, while BSA-FITC loaded NI also presented Rh-PE probed NI accumulated in the outermost layer of the skin and the hair follicular ducts. For BSA-FITC loaded NI serum MSs, BSA-FITC highly penetrated the skin and hair follicular ducts and Rh-PE was accumulated in the

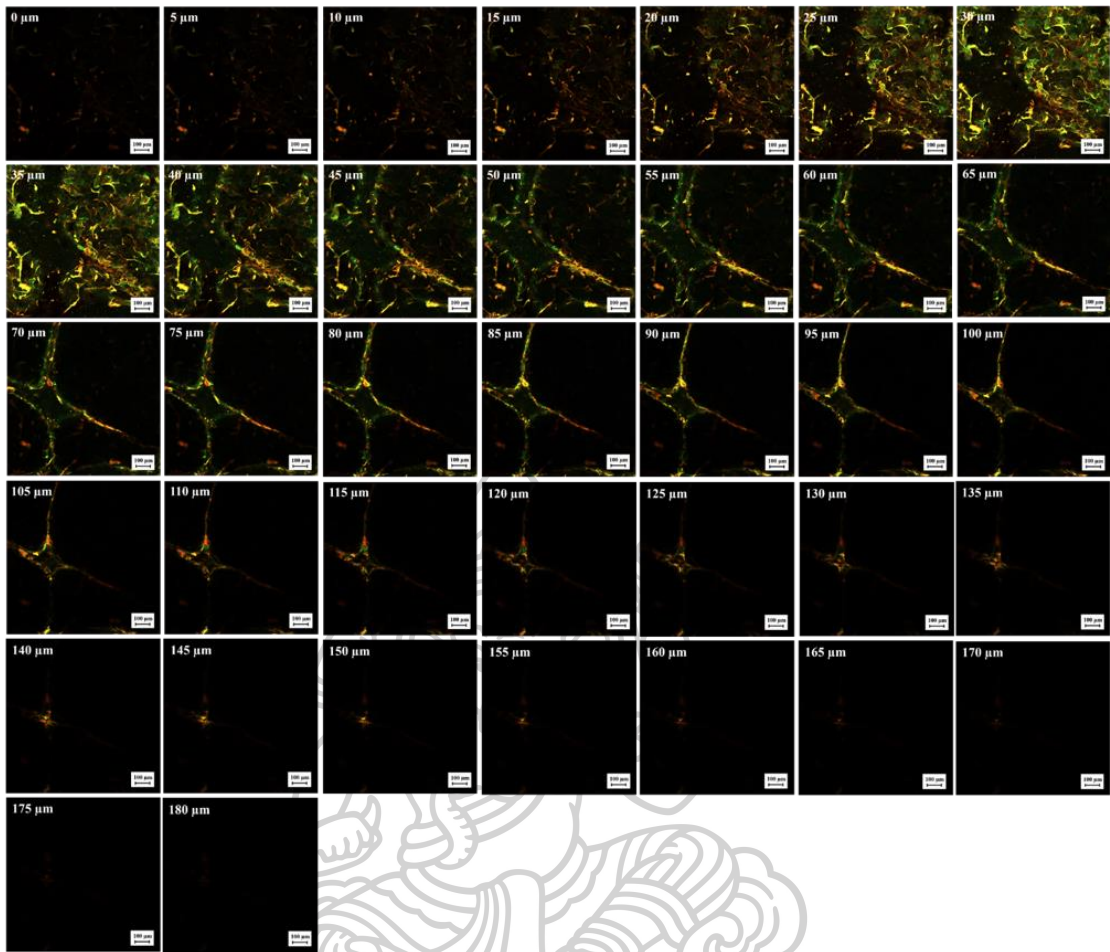
follicle openings and the SC. This indicated that a combination of MS and NI can improve the skin penetration and deposition of bioactive macromolecules.

Hydrophilic macromolecules have poor skin permeation because they are limited by the SC which is the rate-limiting barrier. However, distribution into corneocytes via the transcellular pathway and transfollicular pathway were identified as permeation mechanisms of these compounds (169, 170). In this study, NI was used to enhance the skin permeation of BSA-FITC. When NI was applied to the skin, the vesicles were absorbed into the skin and released the entrapped compound from the vesicles through the skin barrier (171).

Moreover, MS has an important role to improve the skin permeation of bioactive macromolecules by a minimally invasive technique. The creation of micropores into the epidermis and resurfacing of the SC increased bioactive macromolecule permeated through the skin (109). Therefore, NI serum MS presented a potential formulation for transdermal and transfollicular delivery of bioactive macromolecules. This formulation was optimal as a delivery system for DAV and PPE extract.



(A)



(B)



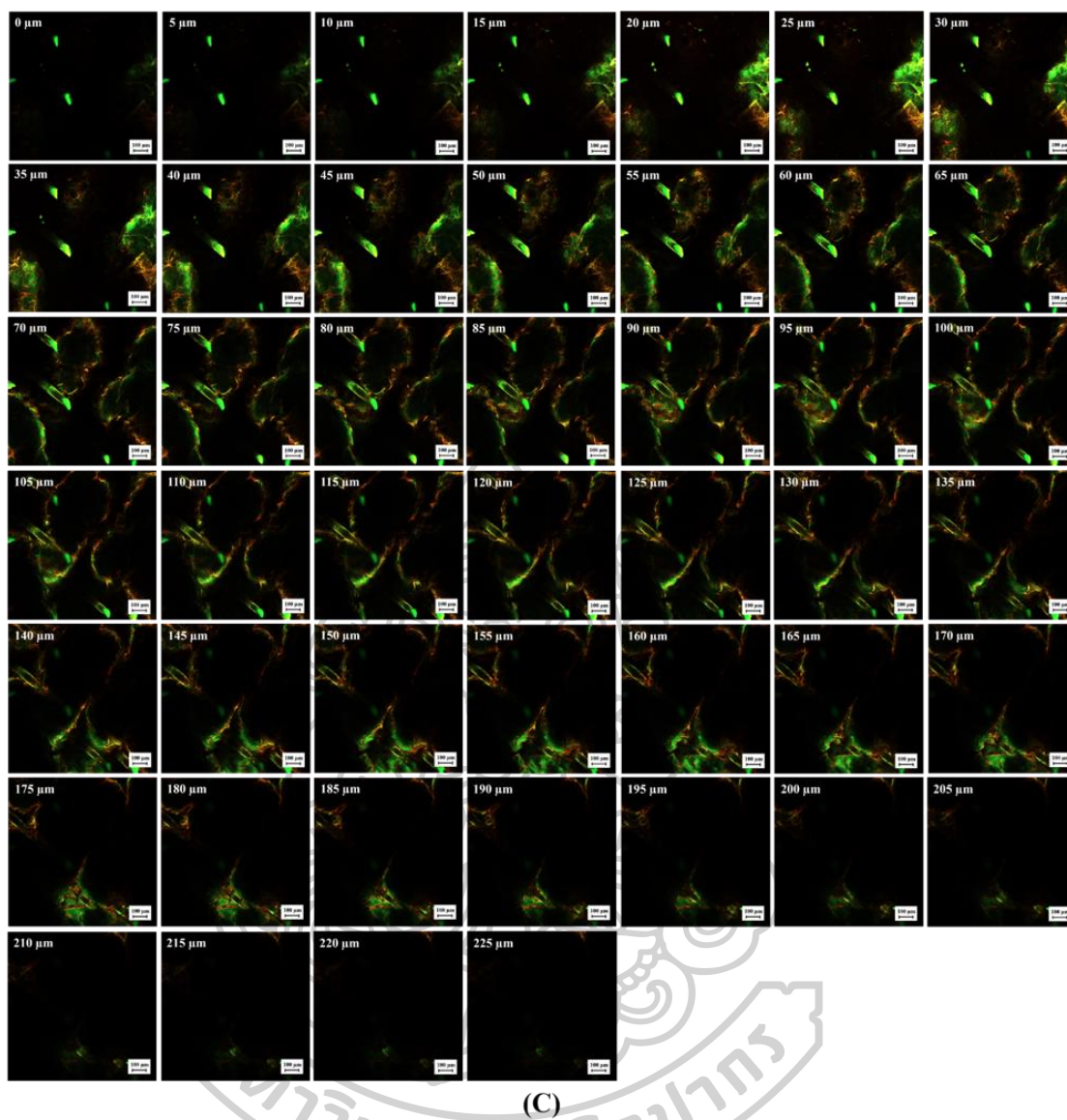


Figure 26 The x–z axis serial images from CLSM of skins treated with BSA-FITC solution (A), BSA-FITC-loaded Rh-PE-probed NI (B), and BSA-FITC-loaded Rh-PE-probed NI serum MSs (C) for 8 h. The images show green fluorescence of BSA-FITC and red fluorescence of Rh-PE (10 × objective lens).

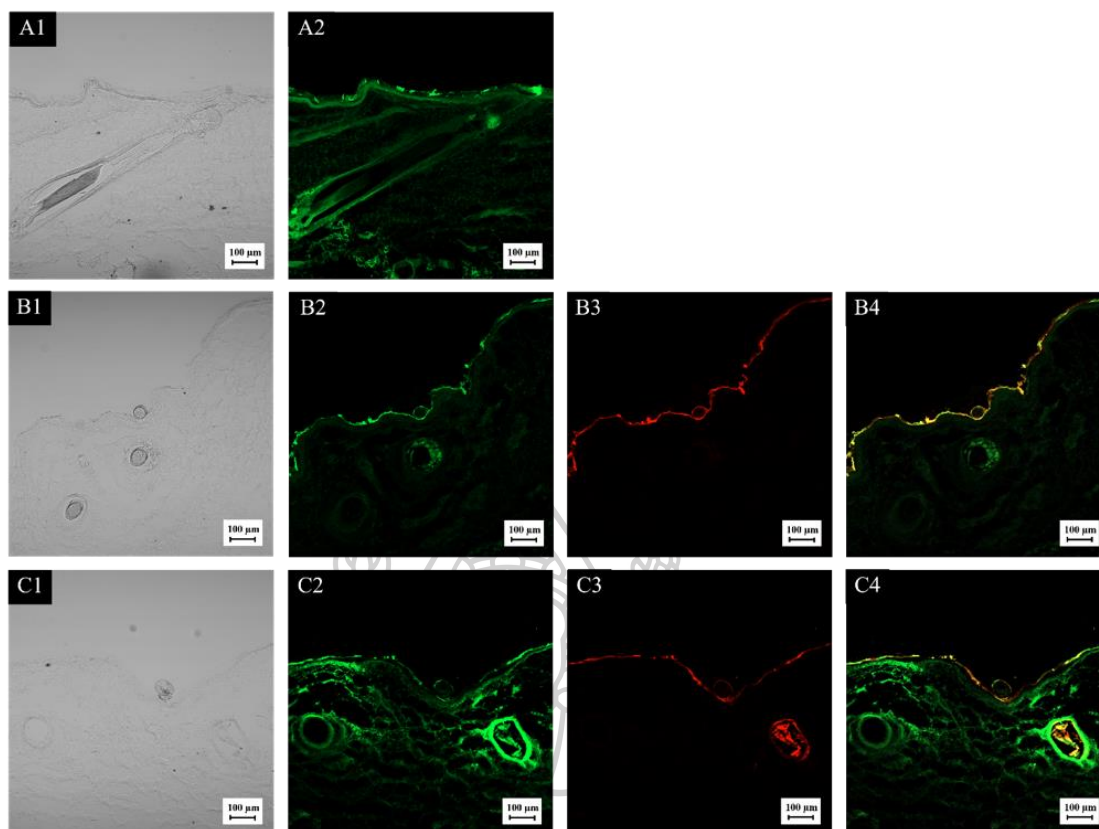


Figure 27 CLSM images of the skin cross-section after being treated with (A) BSA-FITC solution and BSA-FITC-loaded Rh-PE-probed nanocarriers: (B) NI solution and (C) NI serum MSs for 8 h. The images show (1) bright field, (2) green fluorescence of BSA-FITC, (3) red fluorescence of Rh-PE and (4) overlay of (2) and (3) (10x objective lens).

4.6 Stability study

The stability was evaluated in term of appearance of formulation, size, PDI, zeta potential, and protein content values at day 0 and after the one-month interval at three different temperatures (4 °C, 25°C, and 40°C). After 1 month, all the formulations were no changes in appearance and homogeneous at all studied temperatures (**Figure 28**). As seen in **Table 7**, the particle sizes, PDI, and zeta potential of both NI serum MSs containing PPE or DAV at all studied temperatures seem to have changed from day 0, suggesting that the serum based might interact with the nanovesicles and interfere the particle size analysis. However, all formulations exhibited small size in nanometer scale and negative surface charge after 1 month of all studied temperatures. For the remaining total protein (%), total protein in the formulation at test temperatures showed that significantly decreased when compared to the values at day 0. For the quality control of products, the thermal approaches are commonly used for accelerated stability testing. Formulations are kept in tight container and stored in an oven at high temperature between 40 °C and 60 °C for some weeks or months. Moreover, the destabilization processes e.g., creaming, flocculation, or coalescence were occurred, which can be checked by storing the

formulation at 25 °C and 45 °C for weeks. In addition, freeze-thaw-cycles and the droplet size analysis are able to apply for stability assessment (172). Therefore, NI serum MSs was a stable formulation for PPE and DAV.

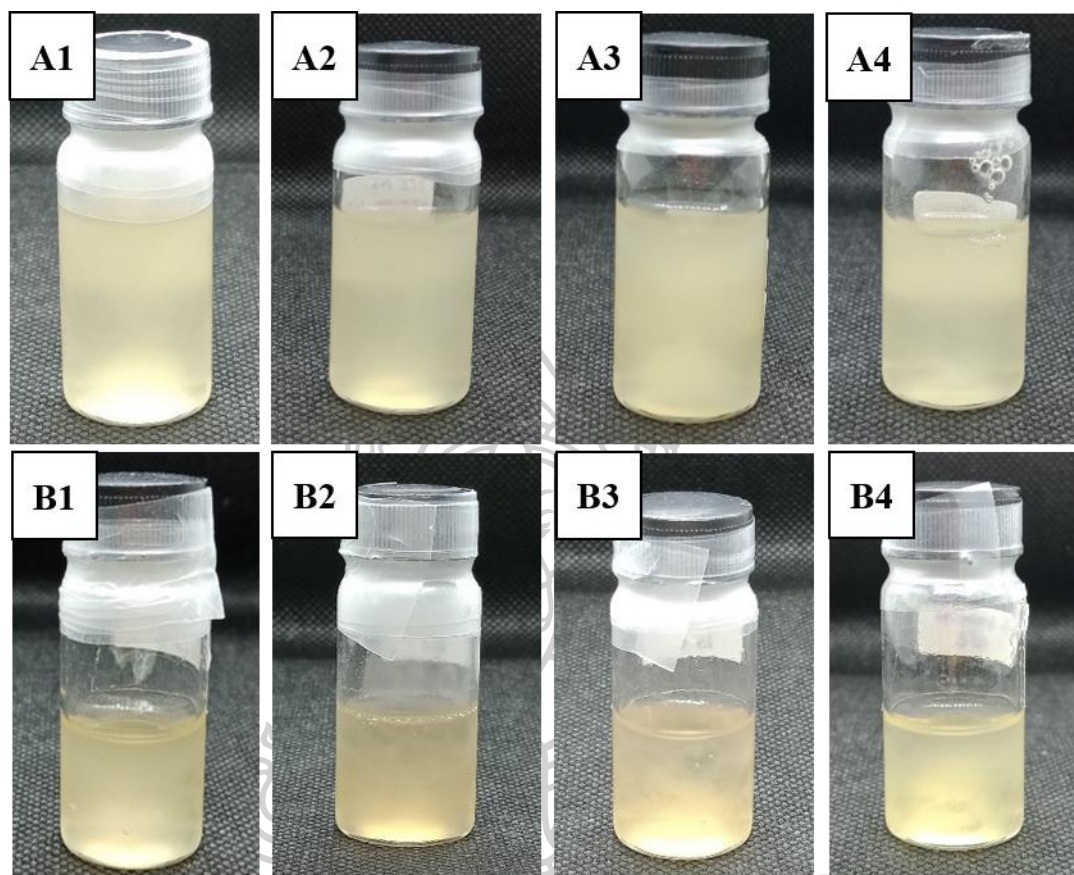


Figure 28 Appearance of NI serum MS containing (0.1%, w/v) PPE (A) or (0.2%, w/v) DAV (B) at day 0 (1) and after a 1 month at different temperature i.e., 4 °C (2), 25 °C (3), and 40 °C (4)

Table 7 The physicochemical characterization of NI serum MS containing (0.2%) DAV or (0.1%) PPE at day 0 and after a 1 month

Formulations	Time	Temperature (°C)	Size (nm)	PDI	Zeta potential (mV)	Remaining total protein (%)
NI serum MS containing (0.1%, w/v) PPE	Day 0	4	171.50 ± 1.08	0.33 ± 0.02	-28.5 ± 4.02	42.48 ± 2.50
		4	249.80 ± 7.95*	0.62 ± 0.08*	-49.40 ± 0.62*	33.04 ± 6.09
	1 month	25	320.00 ± 35.96*	0.73 ± 0.12*	-53.43 ± 0.64*	24.92 ± 7.82*
		40	231.63 ± 11.96*	0.54 ± 0.03*	-51.37 ± 3.81*	31.01 ± 1.64*
NI serum MS containing (0.2%, w/v) DAV	Day 0	4	252.87 ± 9.67	0.72 ± 0.06	-46.50 ± 1.59	51.62 ± 9.63
		4	257.43 ± 12.30	0.67 ± 0.03	-42.00 ± 1.21*	29.60 ± 3.38*
	1 month	25	248.33 ± 19.96	0.60 ± 0.07	-49.00 ± 1.78*	29.21 ± 2.05*
		40	229.40 ± 5.20*	0.75 ± 0.06	-53.00 ± 4.84	28.87 ± 3.11*

Data show mean ± S.D. Each sample was repeated in triplicate. * presents the significant difference when compared to the values at day 0 ($p < 0.05$).

4.7 *In vivo* human study

After applying DAV or PPE-loaded NI serum MSs onto the scalp skin of human volunteers for 30 days, hair growth increased after applying for 14 days and 30 days (**Figure 29**) and no unwanted symptoms were observed by visual appearances. Skin and hair growth parameters are presented in **Figures 30-31**. Changes in melanin content, erythema index, skin hydration, and hair elongation were presented in terms of %MI, %EI, %hydration, and %hair elongation, respectively.

Melanin content refers to the pigmentation level of skin and hair (173). In this study, the healthy human volunteers had dark brown or black hair color. After applying these formulations for 14 days and 30 days, the %MI of the treated skin was significantly higher than untreated skin ($p < 0.05$), indicating that there was an increase in hair pigment in the treatment area. The EI indicates the irritation and allergy reaction. The %EI of skin treated with the formulations for 30 days was significantly reduced, representing that NI serum MSs containing (0.2%, w/v) DAV or (0.1%, w/v) PPE did not stimulate redness or irritation in the skin. For skin hydration, %hydration of treated skin for 30 days was a higher value than for 14 days and the control group (untreated skin), suggesting that high moisture content of the skin (174). For hair promotion, %hair elongation indicates the hair growth after treatment with 14 days and 30 days. The results exhibited that NI serum MSs loading with (0.2%, w/v) DAV or (0.1%, w/v) PPE transported bioactive macromolecules passed the skin and hair follicles routes, leading to the promotion of hair growth and rejuvenation. DAV or PPE contained protein and GFs, which the GFs and their receptors were located in the skin and hair follicles. The exogenous GFs have an important role in hair follicle development and cycling (175). Hembree et al. (1996) reported that IGF-1 acted on follicle epithelial cells to maintain an anagen phase and stimulated hair growth. IGF-1 controlled insulin-like growth factor binding protein (IGFBP)-3 level, which IGFBP was IGF binding proteins that are produced and released in dermal papilla cells. The IGFBP-3 forms a complex with free IGF-1 to stimulate hair elongation and maintenance of the anagen phase (176). Local injection with IGF-1 increased hair follicle amount and prolonged the growth stage during the transition from of anagen stage to the telogen stage. Moreover, activating the regeneration of hair follicle cells during the anagen stage was also found. An effective stimulator of IGF-1 on hair follicle development would be a promising drug candidate for baldness therapy (177). Besides, subcutaneous injection of FGF induced hair growth on the dorsal skin of C57BK/6N mice via stimulating an anagen stage in resting hair follicles and presented the capacity of a hair growth-promoting agent (178). Consequently, NI serum MSs encapsulating (0.2%, w/v) DAV or (0.1%, w/v) PPE was suitable for a topical product on the scalp skin and hair. This formulation provided the effective skin permeability to transport bioactive macromolecules passed the skin and hair follicles route with a minimally invasive therapeutic technique and high efficacy for skin and hair rejuvenation.

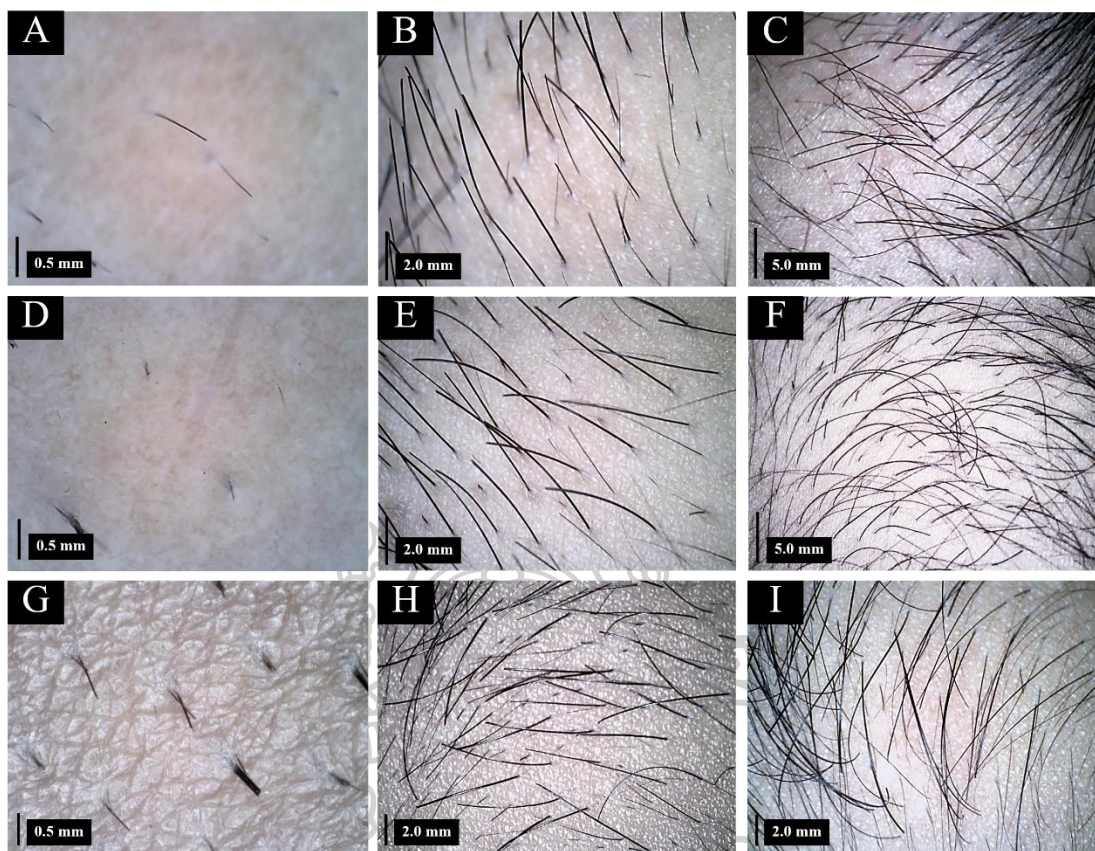


Figure 29 Images of change in the length of hair: non-treatment (A-C) at day 0 (A) (79.7x magnification), day 14 (B) (80.4x magnification), and day 30 (C) (14.4x magnification), after applying NI serum MSs containing (0.2%, w/v) DAV (D-F) at day 0 (D) (77.2x magnification), day 14 (E) (24x magnification), and day 30 (F) (10x magnification), and after applying NI serum MSs containing (0.1%, w/v) PPE (G-I) at day 0 (G) (69x magnification), day 14 (H) (19.8x magnification), and day 30 (I) (19.8x magnification).

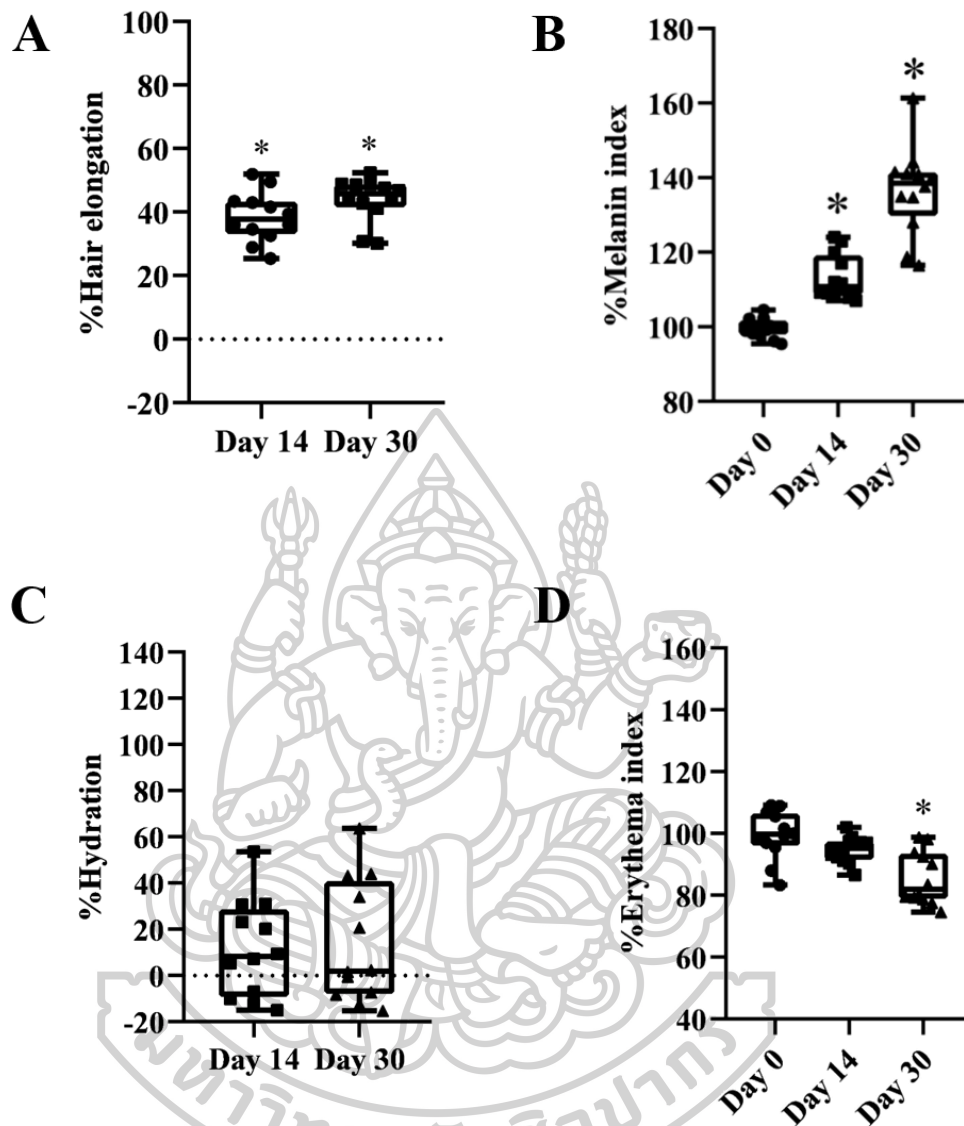


Figure 30 The percentage of hair elongation (% A), %MI (B) skin hydration (%Hydration, C) and, %EI (D), after treatment with NI serum MSs containing DAV extract for 14 days and 30 days. The data represents average \pm S.D. (n = 12). * present significance difference value from control (untreated skin) ($p < 0.05$).

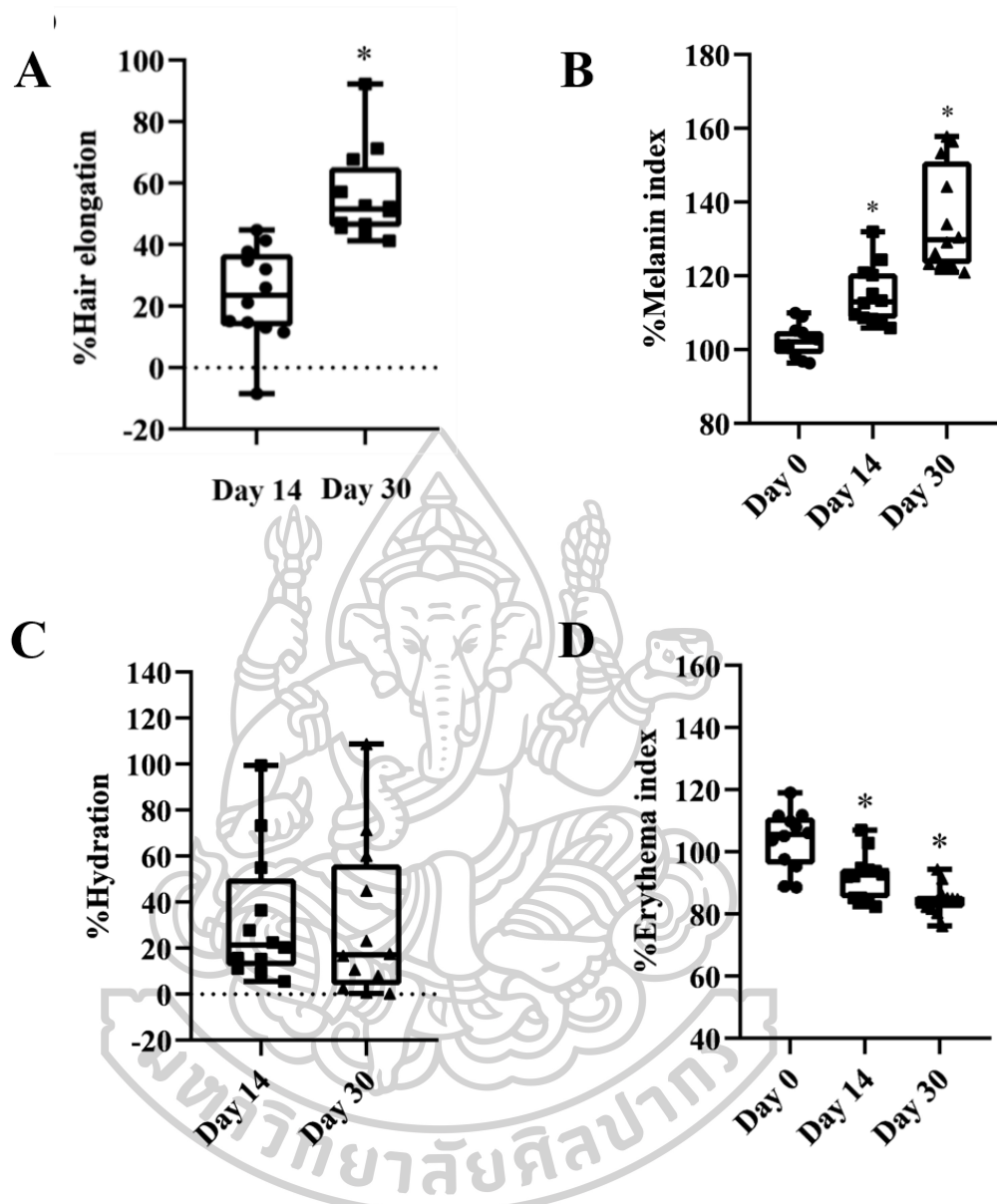


Figure 31 The percentage of hair elongation (%), A), %MI (B), skin hydration (%Hydration, C), and %EI (D) after treatment with NI serum MSs containing PPE extract for 14 days and 30 days. The data represents average \pm S.D. (n = 12). * present significance difference value from control (untreated skin) ($p < 0.05$).

CHAPTER 5

CONCLUSION

In this study, antler velvet of deer and placental of porcine were successfully extracted with the water-soluble active ingredients by the probe-sonication method. Protein, GFs, and amino acids were found in both of them. The extracts improved both skin and hair regeneration by inducing bioactivities on skin and hair cells such as proliferation, migration, anti-oxidant, anti-inflammation, and aggregation. To develop an effective transdermal delivery system of bioactive macromolecules, BSA-FITC was used as a model hydrophilic macromolecular protein. The nanocarriers and dermabrasion techniques were selected to enhance the skin permeation of macromolecules. NIs and sponge MSs in serum formulation were developed to effectively deliver macromolecular protein through and into the skin and hair follicles. The *in vivo* human study of serum NIs with sponge MSs containing these extracts showed the effectiveness of skin and hair regenerative improvement and safety information. The results of this study were able to conclude as follows:

5.1 Effect of DAV and PPE on skin and hair regeneration

The water-soluble bioactive ingredients of the DAV and the PPE could extract by a probe-sonication method. Protein, GFs (IGF-1, EGF, TGF- β , and FGF2), and various types the amino acid were found. For skin and hair rejuvenation activities, both of the extracts increased the cell growth of skin and hair cells such as HaCaTs, NHFs, and HFDPCs. The extracts could stimulate the movement of skin cells in a time-dependent manner. In addition, the extracts also have anti-oxidant activity via reducing intracellular ROS. After the skin cells were induced to increase ROS production by UVB, the extracts stimulated the cell proliferation and decreased MMP9 expression. Moreover, the extracts have an anti-inflammation effect by decreasing TNF- α production and inhibiting the activity of the LOX enzyme. For hair regeneration effect, extract-treated HFDPCs increased cell numbers, and then induced cell aggregation and condensation. Therefore, DAV and PPE play important roles to improve the bioactivity on skin and hair regeneration and repairment.

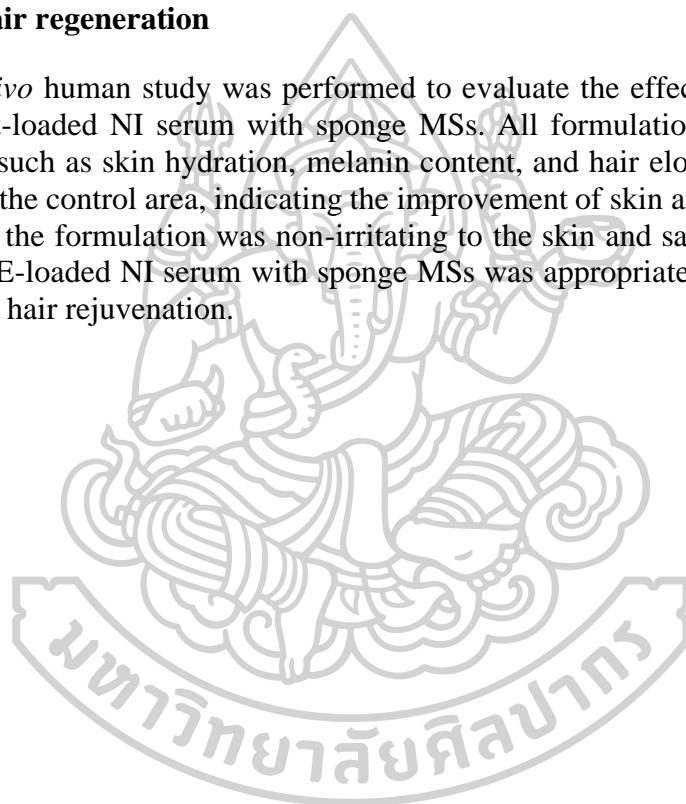
5.2 Effect of nanocarriers and dermabrasion techniques on skin permeation for macromolecules

In this study, the various types of nanocarrier such as LI, PEG-LI, NI, PEG-NI, CS-TPP NP, and CS-MHA-TPP NP were formulated to enhance the skin permeation of macromolecular protein and bioactive extracts. The physicochemical properties of these nanocarriers showed nano-scale size with narrow size distribution. The surface charge expressed the different values based on the composition of vesicles. LIs and NIs had a negative surface charge, while CS and CS-MHA NPs were a positive surface charge. The capacity of drug loading presented that NIs had the maximum protein loading. For the skin permeation and drug deposition studies, NIs enhanced the skin permeability and protein-deposited in the skin more than other formulations. Moreover, the combination of penetration-enhancing techniques might provide a synergistic effect. Thus, NIs were used as nanocarrier for macromolecular protein. To improve transdermal drug delivery of macromolecules, a dermabrasion

technique by using sponge MSs was added to the formulations. NI serum with sponge MSs was successfully developed to deliver BSA-FITC or bioactive extracts. The physicochemical characteristics showed that the vesicles were nano-size with narrow size distribution. The zeta potential was more negative charge than the solution form. For the skin permeation study, the values of J , K_p , and ER of BSA-FITC from NI serum with sponge MSs showed the highest values, suggesting that NI serum with sponge MSs could improve the transdermal delivery of macromolecular protein. Moreover, the skin penetration pathway and skin depth presented that the formulation can transfer BSA-FITC through the skin via transepidermal and transfollicular pathways with the highest skin depth.

5.3 The effectiveness of DAV and PPE-loaded NI serum with sponge MSs for skin and hair regeneration

In vivo human study was performed to evaluate the effectiveness of DAV or PPE extract-loaded NI serum with sponge MSs. All formulations could change the parameters such as skin hydration, melanin content, and hair elongation to be higher values than the control area, indicating the improvement of skin and hair regeneration. In addition, the formulation was non-irritating to the skin and safe to use. Therefore, DAV or PPE-loaded NI serum with sponge MSs was appropriate as a topical product for skin and hair rejuvenation.



REFERENCES

1. Kanasi E, Ayilavarapu S, Jones J. The aging population: demographics and the biology of aging. *Periodontology* 2000. 2016;72(1):13-8.
2. Kanaki T, Makrantonaki E, Zouboulis CC. Biomarkers of skin aging. *Reviews in Endocrine and Metabolic Disorders*. 2016;17(3):433-42.
3. Khavkin J, Ellis DAF. Aging skin: histology, physiology, and pathology. *Facial Plastic Surgery Clinics of North America*. 2011;19(2):229-34.
4. Panich U, Sittithumcharee G, Rathviboon N, Jirawatnotai S. Ultraviolet radiation-induced skin aging: the role of DNA damage and oxidative stress in epidermal stem cell damage mediated skin aging. *Stem Cells Int*. 2016;2016:7370642-.
5. Naidoo K, Birch-Machin MA. Oxidative stress and ageing: the influence of environmental pollution, sunlight and diet on skin. *Cosmetics*. 2017;4(1):4.
6. Kaddurah H, Braunberger TL, Vellaichamy G, Nahhas AF, Lim HW, Hamzavi IH. The impact of sunlight on skin aging. *Current Geriatrics Reports*. 2018;7(4):228-37.
7. Fuente DIM, Miquel J. An update of the oxidation-inflammation theory of aging: the involvement of the immune system in oxi-inflamm-aging. *Current Pharmaceutical Design*. 2009;15(26):3003-26.
8. Sajid S, Rahman S, Abbas G, Usman M, Salman A, Ateeq M, et al. Aging mechanisms: linking oxidative stress, obesity and inflammation. *Matrix Science Medica*. 2017;1:30-3.
9. Buffoli B, Rinaldi F, Labanca M, Sorbellini E, Trink A, Guanziroli E, et al. The human hair: from anatomy to physiology. *International Journal of Dermatology*. 2014;53(3):331-41.
10. Park AM, Khan S, Rawnsley J. Hair biology: growth and pigmentation. *Facial Plastic Surgery Clinics of North America*. 2018;26(4):415-24.
11. Trüeb RM. Pharmacologic interventions in aging hair. *Clin Interv Aging*. 2006;1(2):121-9.
12. Trüeb RM. The impact of oxidative stress on hair. *International Journal of Cosmetic Science*. 2015;37(S2):25-30.
13. Gainza G, Villullas S, Pedraz JL, Hernandez RM, Igartua M. Advances in drug delivery systems (DDSs) to release growth factors for wound healing and skin regeneration. *Nanomedicine: Nanotechnology, Biology and Medicine*. 2015;11(6):1551-73.
14. Ganceviciene R, Liakou AI, Theodoridis A, Makrantonaki E, Zouboulis CC. Skin anti-aging strategies. *Dermato-endocrinology*. 2012;4(3):308-19.
15. SHINGADE GM. Review on: recent trend on transdermal drug delivery system *Journal of Drug Delivery & Therapeutics* [Internet]. 2012 [cited 9Mar.2020]; 2(1). Available from: <https://jddtonline.info/index.php/jddt/article/view/74>.
16. Marwah H, Garg T, Goyal AK, Rath G. Permeation enhancer strategies in transdermal drug delivery. *Drug Delivery*. 2016;23(2):564-78.
17. Kumar R, Philip A. Modified transdermal technologies: breaking the barriers of drug permeation via the skin. *Tropical Journal of Pharmaceutical Research* [Internet]. 2007 [cited 9Mar. 2020]; 6(1):[633-44 pp.]. Available from: <https://www.ajol.info/index.php/tjpr/article/view/14641>.
18. Zsikó S, Csányi E, Kovács A, Budai-Szűcs M, Gácsi A, Berkó S. Methods to evaluate skin penetration In vitro. *Scientia Pharmaceutica*. 2019;87(3):19.

19. Ita K. Transdermal iontophoretic drug delivery: advances and challenges. *Journal of Drug Targeting*. 2016;24(5):386-91.
20. Amsden BG, Goosen MFA. Transdermal delivery of peptide and protein drugs: An overview. *AICHe Journal*. 1995;41(8):1972-97.
21. Chaulagain B, Jain A, Tiwari A, Verma A, Jain SK. Passive delivery of protein drugs through transdermal route. *Artificial Cells, Nanomedicine, and Biotechnology*. 2018;46(sup1):472-87.
22. Foldvari M, Baca-Estrada ME, He Z, Hu J, Attah-Poku S, King M. Dermal and transdermal delivery of protein pharmaceuticals: lipid-based delivery systems for interferon α . *Biotechnology and Applied Biochemistry*. 1999;30(2):129-37.
23. Morales JO, Fathe KR, Brunaugh A, Ferrati S, Li S, Montenegro-Nicolini M, et al. Challenges and future prospects for the delivery of biologics: oral mucosal, pulmonary, and transdermal routes. *The AAPS Journal*. 2017;19(3):652-68.
24. Bonté F, Girard D, Archambault J-C, Desmoulière A. Skin changes during ageing. In: Harris JR, Korolchuk VI, editors. *Biochemistry and Cell Biology of Ageing: Part II Clinical Science*. Singapore: Springer Singapore; 2019. p. 249-80.
25. Freitas-Rodríguez S, Folgueras AR, López-Otín C. The role of matrix metalloproteinases in aging: tissue remodeling and beyond. *Biochimica et Biophysica Acta (BBA) - Molecular Cell Research*. 2017;1864(11, Part A):2015-25.
26. Gilaberte Y, Prieto-Torres L, Pastushenko I, Juarranz Á. Chapter 1 - Anatomy and function of the skin. In: Hamblin MR, Avci P, Prow TW, editors. *Nanoscience in Dermatology*. Boston: Academic Press; 2016. p. 1-14.
27. Robert L, Labat-Robert J, Robert AM. Physiology of skin aging. *Pathologie Biologie*. 2009;57(4):336-41.
28. Zouboulis CC, Makrantonaki E. Clinical aspects and molecular diagnostics of skin aging. *Clinics in Dermatology*. 2011;29(1):3-14.
29. Tigges J, Krutmann J, Fritsche E, Haendeler J, Schaal H, Fischer JW, et al. The hallmarks of fibroblast ageing. *Mechanisms of ageing and development*. 2014;138:26-44.
30. Yang C-C, Cotsarelis G. Review of hair follicle dermal cells. *Journal of dermatological science*. 2010;57(1):2-11.
31. Chueh S-C, Lin S-J, Chen C-C, Lei M, Wang LM, Widelitz R, et al. Therapeutic strategy for hair regeneration: hair cycle activation, niche environment modulation, wound-induced follicle neogenesis, and stem cell engineering. *Expert opinion on biological therapy*. 2013;13(3):377-91.
32. Lei M, Chuong C-M. Aging, alopecia, and stem cells. *Science*. 2016;351(6273):559-60.
33. Pfl M, Farwick M, Mentel M, Köhler T, editors. *Preventing hair loss by balancing the hair cycle, strengthening the hair follicle, and improving scalp health 2014*.
34. Lupo MP. Cosmeceutical peptides. *Dermatologic Surgery*. 2005;31(s1):832-6.
35. Fabi S, Sundaram H. The potential of topical and injectable growth factors and cytokines for skin rejuvenation. *Facial Plast Surg*. 2014;30(02):157-71.
36. Peus D, Pittelkow MR. Growth factors in hair organ development and the hair growth cycle. *Dermatologic Clinics*. 1996;14(4):559-72.
37. Jeon B, Kim S, Lee S, Park P, Sung S, Kim J, et al. Effect of antler growth period on the chemical composition of velvet antler in sika deer (*Cervus nippon*). *Mammalian Biology*. 2009;74(5):374-80.

38. Kawtikwar P, Bhagwat DD, Sakarkar D. Deer antlers- Traditional use and future perspectives. *Indian Journal of Traditional Knowledge*. 2010;9:245-51.
39. Sui Z, Zhang L, Huo Y, Zhang Y. Bioactive components of velvet antlers and their pharmacological properties. *Journal of Pharmaceutical and Biomedical Analysis*. 2014;87:229-40.
40. Ko KM, Yip TT, Tsao SW, Kong YC, Fennessy P, Belew MC, et al. Epidermal growth factor from deer (*Cervus elaphus*) submaxillary gland and velvet antler. *General and comparative endocrinology*. 1986;63(3):431–40.
41. Zhou R, Li S. In vitro antioxidant analysis and characterisation of antler velvet extract. *Food Chemistry*. 2009;114(4):1321-7.
42. Je J-Y, Park P-J, Kim E-K, Kim H-A, Lim D-H, Jeon B-T, et al. Composition of biologically active substances and antioxidant activity of New Zealand deer velvet antler extracts. *Korean Journal for Food Science of Animal Resources [Internet]*. 2010; 30:[20-7 pp.].
43. Zhao L, Wang X, Zhang X-L, Xie Q-F. Purification and identification of anti-inflammatory peptides derived from simulated gastrointestinal digests of velvet antler protein (*Cervus elaphus* Linnaeus). *Journal of Food and Drug Analysis*. 2016;24(2):376-84.
44. Zhang L-Z, Xin J-L, Zhang X-P, Fu Q, Zhang Y, Zhou Q-L. The anti-osteoporotic effect of velvet antler polypeptides from *Cervus elaphus* Linnaeus in ovariectomized rats. *Journal of Ethnopharmacology*. 2013;150(1):181-6.
45. Guan S-W, Duan L-X, Li Y-Y, Wang B-X, Zhou Q-L. A novel polypeptide from *Cervus nippon* Temminck proliferation of epidermal cells and NIH3T3 cell line. *Acta biochimica Polonica*. 2006;53(2):395–7.
46. Chen X, Wang Y, Wu Y, Wang L, Li W. [Protective effects of peptides from velvet antler of *Cervus nippon* on acute ischemic myocardial injury in rats]. *Zhongguo Zhong Yao Za Zhi*. 2009;34(15):1971-4.
47. Zha E, Li X, Li D, Guo X, Gao S, Yue X. Immunomodulatory effects of a 3.2kDa polypeptide from velvet antler of *Cervus nippon* Temminck. *International Immunopharmacology*. 2013;16(2):210-3.
48. Kuo C-Y, Wang T, Dai T-Y, Wang C-H, Chen K-N, Chen Y-P, et al. Effect of the velvet antler of formosan sambar deer (*Cervus unicolor swinhoei*) on the prevention of an allergic airway response in mice. *Evidence-Based Complementary and Alternative Medicine*. 2012;2012:481318.
49. Chen J-C, Hsiang C-Y, Lin Y-C, Ho T-Y. Deer antler extract improves fatigue effect through altering the expression of genes related to muscle strength in skeletal muscle of mice. *Evidence-Based Complementary and Alternative Medicine*. 2014;2014:540580.
50. Burton GJ, Jauniaux E. What is the placenta? *American Journal of Obstetrics & Gynecology*. 2015;213(4):S6.e1-S6.e4.
51. Pan SY, Chan M, Wong M, Klokol D, Chernykh V. Placental therapy: an insight to their biological and therapeutic properties. *Journal of Medicine and Therapeutics*. 2017;1.
52. Moon P-D, Kim K-Y, Rew K-H, Kim H-M, Jeong H-J. Anti-fatigue effects of porcine placenta and its amino acids in a behavioral test on mice. *Canadian Journal of Physiology and Pharmacology*. 2014;92(11):937-44.
53. Yoshikawa C, Koike K, Takano F, Sugiur K, Suzuki N. Efficacy of porcine

- placental extract on wrinkle widths below the eye in climacteric women. *Climacteric*. 2014;17(4):370-6.
54. Hong K-B, Park Y, Kim JH, Kim JM, Suh HJ. Effects of porcine placenta extract ingestion on ultraviolet B-induced skin damage in hairless mice. *Korean journal for food science of animal resources*. 2015;35(3):413-20.
55. Wu CH, Chang GY, Chang WC, Hsu CT, Chen RS. Wound healing effects of porcine placental extracts on rats with thermal injury. *British Journal of Dermatology*. 2003;148(2):236-45.
56. Yoshikawa C. Effect of porcine placental extract on collagen production in human skin fibroblasts in vitro. *Gynecology & Obstetrics*. 2013;03.
57. JeungHi H, Kim M-R, Park Y, Hong YH, Suh HJ. Skin permeability of porcine placenta extracts and its physiological activities. *Korean Society for Food Science of Animal Resources [Internet]*. 2013; 33:[356–62 pp.].
58. Tang W-L, Zhang M, Fang Z. Optimization of ultrasound-assisted-extraction of porcine placenta water-soluble proteins and evaluation of the antioxidant activity. *Journal of food science and technology*. 2015;52(7):4042-53.
59. Lee H-Y, Chae H-J, Park S-Y, Kim J-H. Porcine placenta hydrolysates enhance osteoblast differentiation through their antioxidant activity and effects on ER stress. *BMC complementary and alternative medicine*. 2016;16(1):291.
60. Nam S-Y, Kim H-M, Jeong H-J. Anti-fatigue effect by active dipeptides of fermented porcine placenta through inhibiting the inflammatory and oxidative reactions. *Biomedicine & Pharmacotherapy*. 2016;84:51-9.
61. Tebakari M, Daigo Y, Ishikawa H, Nakamura M, Kawashima J, Takano F. Anti-inflammatory effect of the water-soluble portion of porcine placental extract in lipopolysaccharide-stimulated RAW264.7 murine macrophage cells. *Biological and Pharmaceutical Bulletin*. 2018;41(8):1251-6.
62. Gniadecki R. Regulation of keratinocyte proliferation. *General Pharmacology: The Vascular System*. 1998;30(5):619-22.
63. El-Ghalbzouri A, Gibbs S, Lamme E, Van Blitterswijk CA, Ponc M. Effect of fibroblasts on epidermal regeneration. *British Journal of Dermatology*. 2002;147(2):230-43.
64. Sennett R, Rendl M. Mesenchymal–epithelial interactions during hair follicle morphogenesis and cycling. *Seminars in Cell & Developmental Biology*. 2012;23(8):917-27.
65. Chi W, Wu E, Morgan BA. Dermal papilla cell number specifies hair size, shape and cycling and its reduction causes follicular decline. *Development (Cambridge, England)*. 2013;140(8):1676-83.
66. Farage MA, Miller KW, Elsner P, Maibach HI. Characteristics of the aging skin. *Advances in wound care*. 2013;2(1):5-10.
67. Sardesai VM. Role of Antioxidants in health maintenance. *Nutrition in Clinical Practice*. 1995;10(1):19-25.
68. Williams GM, Jeffrey AM. Oxidative DNA damage: endogenous and chemically induced. *Regulatory Toxicology and Pharmacology*. 2000;32(3):283-92.
69. Jannat S, Ali MY, Kim H-R, Jung HA, Choi JS. Protective effects of sweet orange, unshiu mikan, and mini tomato juice powders on t-BHP-induced oxidative stress in HepG2 cells. *Preventive Nutrition and Food Science [Internet]*. 2016; 21(3):[208–20 pp.].

70. Tu Y, Quan T. Oxidative stress and human skin connective tissue aging. *Cosmetics*. 2016;3(3).
71. Eruslanov E, Kusmartsev S. Identification of ROS using oxidized DCFDA and flow-cytometry. In: Armstrong D, editor. *Advanced Protocols in Oxidative Stress II*. Totowa, NJ: Humana Press; 2010. p. 57-72.
72. Chung JH, Kang S, Varani J, Lin J, Fisher GJ, Voorhees JJ. Decreased extracellular-signal-regulated kinase and increased stress-activated MAP kinase activities in aged human skin in vivo. *Journal of Investigative Dermatology*. 2000;115(2):177-82.
73. Cavinato M, Jansen-Dürr P. Molecular mechanisms of UVB-induced senescence of dermal fibroblasts and its relevance for photoaging of the human skin. *Experimental Gerontology*. 2017;94:78-82.
74. Cho Y-H, Bahuguna A, Kim H-H, Kim D-i, Kim H-J, Yu J-M, et al. Potential effect of compounds isolated from *Coffea arabica* against UV-B induced skin damage by protecting fibroblast cells. *Journal of Photochemistry and Photobiology B: Biology*. 2017;174:323-32.
75. Gosain A, DiPietro LA. Aging and wound healing. *World Journal of Surgery*. 2004;28(3):321-6.
76. Rittié L. Cellular mechanisms of skin repair in humans and other mammals. *Journal of cell communication and signaling*. 2016;10(2):103-20.
77. Ahtiainen L, Lefebvre S, Lindfors Päivi H, Renvoisé E, Shirokova V, Vartiainen Maria K, et al. Directional cell migration, but not proliferation, Drives Hair Placode Morphogenesis. *Developmental Cell*. 2014;28(5):588-602.
78. Zhou H, You C, Wang X, Jin R, Wu P, Li Q, et al. The progress and challenges for dermal regeneration in tissue engineering. *Journal of Biomedical Materials Research Part A*. 2017;105(4):1208-18.
79. Davinelli S, Bertoglio CJ, Polimeni A, Scapagnini G. Cytoprotective polyphenols against chronological skin aging and cutaneous photodamage. *Current Pharmaceutical Design*. 2018;24(2):99-105.
80. Borg M, Brincat S, Camilleri G, Schembri-Wismayer P, Brincat M, Calleja-Agius J. The role of cytokines in skin aging. *Climacteric*. 2013;16(5):514-21.
81. Jahoda CAB, Horne KA, Oliver RF. Induction of hair growth by implantation of cultured dermal papilla cells. *Nature*. 1984;311(5986):560-2.
82. Oliver RF, Jahoda CAB. The dermal papilla and maintenance of hair growth. In: Rogers GE, Reis PJ, Ward KA, Marshall RC, editors. *The Biology of Wool and Hair*. Dordrecht: Springer Netherlands; 1989. p. 51-67.
83. Mishra DK, Shandilya R, Mishra PK. Lipid based nanocarriers: a translational perspective. *Nanomedicine: Nanotechnology, Biology and Medicine*. 2018;14(7):2023-50.
84. Dragicevic N, Maibach H. Combined use of nanocarriers and physical methods for percutaneous penetration enhancement. *Advanced Drug Delivery Reviews*. 2018;127:58-84.
85. Kahraman E, Güngör S, Özsoy Y. Potential enhancement and targeting strategies of polymeric and lipid-based nanocarriers in dermal drug delivery. *Therapeutic Delivery*. 2017;8(11):967-85.
86. Bozzuto G, Molinari A. Liposomes as nanomedical devices. *International journal of nanomedicine*. 2015;10:975-99.

87. Pierre MBR, dos Santos Miranda Costa I. Liposomal systems as drug delivery vehicles for dermal and transdermal applications. *Archives of Dermatological Research*. 2011;303(9):607.
88. Ashtikar M, Nagarsekar K, Fahr A. Transdermal delivery from liposomal formulations – Evolution of the technology over the last three decades. *Journal of Controlled Release*. 2016;242:126-40.
89. Muzzalupo R, Tavano L. Niosomal drug delivery for transdermal targeting: recent advances. *Research and Reports in Transdermal Drug Delivery*. 2015;4:23-33.
90. Chen S, Hanning S, Falconer J, Locke M, Wen J. Recent advances in non-ionic surfactant vesicles (niosomes): fabrication, characterization, pharmaceutical and cosmetic applications. *European Journal of Pharmaceutics and Biopharmaceutics*. 2019;144:18-39.
91. Marianecchi C, Di Marzio L, Rinaldi F, Celia C, Paolino D, Alhaique F, et al. Niosomes from 80s to present: the state of the art. *Advances in Colloid and Interface Science*. 2014;205:187-206.
92. Howard MD, Jay M, Dziubla TD, Lu X. Pegylation of nanocarrier drug delivery systems: state of the art. *Journal of Biomedical Nanotechnology*. 2008;4(2):133-48.
93. Vllasaliu D, Fowler R, Stolnik S. PEGylated nanomedicines: recent progress and remaining concerns. *Expert Opinion on Drug Delivery*. 2014;11(1):139-54.
94. Lim SB, Banerjee A, Önyüksel H. Improvement of drug safety by the use of lipid-based nanocarriers. *Journal of Controlled Release*. 2012;163(1):34-45.
95. Ramadon D, McCrudden MTC, Courtenay AJ, Donnelly RF. Enhancement strategies for transdermal drug delivery systems: current trends and applications. *Drug delivery and translational research*. 2022;12(4):758-91.
96. Mahmoud NN, Al-Qaoud KM, Al-Bakri AG, Alkilany AM, Khalil EA. Colloidal stability of gold nanorod solution upon exposure to excised human skin: effect of surface chemistry and protein adsorption. *The International Journal of Biochemistry & Cell Biology*. 2016;75:223-31.
97. Rangsimawong W, Opanasopit P, Rojanarata T, Ngawhirunpat T. Terpene-containing pegylated liposomes as transdermal carriers of a hydrophilic compound. *Biological and Pharmaceutical Bulletin*. 2014;37(12):1936-43.
98. Nagpal K, Singh SK, Mishra DN. Chitosan nanoparticles: a promising system in novel drug delivery. *Chemical and Pharmaceutical Bulletin*. 2010;58(11):1423-30.
99. He W, Guo X, Xiao L, Feng M. Study on the mechanisms of chitosan and its derivatives used as transdermal penetration enhancers. *International Journal of Pharmaceutics*. 2009;382(1):234-43.
100. Rampino A, Borgogna M, Blasi P, Bellich B, Cesàro A. Chitosan nanoparticles: preparation, size evolution and stability. *International Journal of Pharmaceutics*. 2013;455(1):219-28.
101. Sahatsapan N, Rojanarata T, Ngawhirunpat T, Opanasopit P, Tonglairoom P. 6-Maleimidohexanoic acid-grafted chitosan: A new generation mucoadhesive polymer. *Carbohydrate Polymers*. 2018;202:258-64.
102. Kimura E, Kawano Y, Todo H, Ikarashi Y, Sugibayashi K. Measurement of skin permeation/penetration of nanoparticles for their safety evaluation. *Biological and Pharmaceutical Bulletin*. 2012;35(9):1476-86.
103. Nafisi S, Maibach HI. Chapter 3 Skin penetration of nanoparticles. *Emerging Nanotechnologies in Immunology* 2018. p. 47-88.

104. SHINGADE GM. Review on: recent trend on transdermal drug delivery system. *Journal of Drug Delivery and Therapeutics* [Internet]. 2012; 2(1).
105. Barry BW. Novel mechanisms and devices to enable successful transdermal drug delivery. *European Journal of Pharmaceutical Sciences*. 2001;14(2):101-14.
106. Zsikó S, Csányi E, Kovács A, Budai-Szűcs M, Gácsi A, Berkó S. Methods to evaluate skin penetration in vitro. *Scientia Pharmaceutica*. 2019;87(3).
107. Kumar R, Philip A. Modified transdermal technologies: breaking the barriers of drug permeation via the skin. *Tropical Journal of Pharmaceutical Research* (ISSN: 1596-5996) Vol 6 Num 1. 2007;6.
108. Prausnitz MR, Langer R. Transdermal drug delivery. *Nature Biotechnology*. 2008;26(11):1261-8.
109. Kalluri H, Banga AK. Transdermal delivery of proteins. *AAPS PharmSciTech*. 2011;12(1):431-41.
110. Villani M, inventor. Use of spongilla spicules as a dermabrasion device or resurfacing modality. United States patent US20100080853A1. 2010.
111. Andrews SN, Zarnitsyn V, Bondy B, Prausnitz MR. Optimization of microdermabrasion for controlled removal of stratum corneum. *International Journal of Pharmaceutics*. 2011;407(1):95-104.
112. Scott JA, Banga AK. Cosmetic devices based on active transdermal technologies. *Therapeutic Delivery*. 2015;6(9):1089-99.
113. Zhang S, Ou H, Liu C, Zhang Y, Mitragotri S, Wang D, et al. Skin delivery of hydrophilic biomacromolecules using marine sponge spicules. *Molecular Pharmaceutics*. 2017;14(9):3188-200.
114. Wadkhien K, Chinpaisal C, Satiraphan M, Wetwitayaklung P, Pongnimitprasert N. Anti-inflammatory effects of rhein and crude extracts from *Cassia alata* L. in HaCaT cells. 2018;Research.
115. Xu D, Hu M-J, Wang Y-Q, Cui Y-L. Antioxidant activities of quercetin and its complexes for medicinal application. *Molecules* (Basel, Switzerland). 2019;24(6):1123.
116. Alía M, Ramos S, Mateos R, Granado-Serrano AB, Bravo L, Goya L. Quercetin protects human hepatoma HepG2 against oxidative stress induced by tert-butyl hydroperoxide. *Toxicology and Applied Pharmacology*. 2006;212(2):110-8.
117. Chung LY, Soo WK, Chan KY, Mustafa MR, Goh SH, Imiyabir Z. Lipoxygenase inhibiting activity of some Malaysian plants. *Pharmaceutical Biology*. 2009;47(12):1142-8.
118. Kiratipaiboon C, Tengamnuay P, Chanvorachote P. Glycyrrhizic acid attenuates stem cell-like phenotypes of human dermal papilla cells. *Phytomedicine*. 2015;22(14):1269-78.
119. Pengnam S, Patrojanasophon P, Rojanarata T, Ngawhirunpat T, Yingyongnarongkul B-e, Radchatawedchakoon W, et al. A novel plier-like gemini cationic niosome for nucleic acid delivery. *Journal of Drug Delivery Science and Technology*. 2019;52:325-33.
120. Krauland AH, Alonso MJ. Chitosan/cyclodextrin nanoparticles as macromolecular drug delivery system. *International Journal of Pharmaceutics*. 2007;340(1):134-42.
121. Manns JM. SDS-polyacrylamide gel electrophoresis (SDS-PAGE) of proteins. *Current Protocols in Microbiology*. 2011;22(1):A.3M.1-A.3M.13.
122. Kushwaha S, Kushwaha N, Maurya N, Awani R. Role of markers in the

standardization of herbal drugs: a review. *Archives of Applied Science Research*. 2010;2.

123. Aldag C, Nogueira Teixeira D, Leventhal PS. Skin rejuvenation using cosmetic products containing growth factors, cytokines, and matrikines: a review of the literature. *Clin Cosmet Investig Dermatol*. 2016;9:411-9.

124. Herman A, Herman AP. Mechanism of action of herbs and their active constituents used in hair loss treatment. *Fitoterapia*. 2016;114:18-25.

125. Präbst K, Engelhardt H, Ringgeler S, Hübner H. Basic colorimetric proliferation assays: MTT, WST, and Resazurin. In: Gilbert DF, Friedrich O, editors. *Cell Viability Assays: Methods and Protocols*. New York, NY: Springer New York; 2017. p. 1-17.

126. Suter MM, Schulze K, Bergman W, Welle M, Roosje P, Müller EJ. The keratinocyte in epidermal renewal and defence. *Veterinary Dermatology*. 2009;20(5-6):515-32.

127. Driskell RR, Clavel C, Rendl M, Watt FM. Hair follicle dermal papilla cells at a glance. *Journal of cell science*. 2011;124(Pt 8):1179-82.

128. Morgan BA. The dermal papilla: an instructive niche for epithelial stem and progenitor cells in development and regeneration of the hair follicle. *Cold Spring Harbor perspectives in medicine*. 2014;4(7):a015180-a.

129. Rauch SD, Velazquez-Villaseñor L, Dimitri PS, Merchant SN. Decreasing hair cell counts in aging humans. *Annals of the New York Academy of Sciences*. 2001;942(1):220-7.

130. Gruber F, Kremslehner C, Eckhart L, Tschachler E. Cell aging and cellular senescence in skin aging — recent advances in fibroblast and keratinocyte biology. *Experimental Gerontology*. 2020;130:110780.

131. Bhora FY, Dunkin BJ, Batzri S, Aly HM, Bass BL, Sidawy AN, et al. Effect of growth factors on cell proliferation and epithelialization in human skin. *Journal of Surgical Research*. 1995;59(2):236-44.

132. Lin'kova NS, Drobintseva AO, Orlova OA, Kuznetsova EP, Polyakova VO, Kvetnoy IM, et al. Peptide regulation of skin fibroblast functions during their aging in vitro. *Bulletin of Experimental Biology and Medicine*. 2016;161(1):175-8.

133. Katsuoka K, Schell H, Wessel B, Hornstein OP. Effects of epidermal growth factor, fibroblast growth factor, minoxidil and hydrocortisone on growth kinetics in human hair bulb papilla cells and root sheath fibroblasts cultured in vitro. *Archives of Dermatological Research*. 1987;279(4):247-50.

134. Philpott MP, Sanders D, Kealey T. Cultured human hair follicles and growth factors. *Journal of Investigative Dermatology*. 1995;104(5, Supplement):44-5.

135. Kim D, Kim SY, Mun SK, Rhee S, Kim BJ. Epidermal growth factor improves the migration and contractility of aged fibroblasts cultured on 3D collagen matrices. *Int J Mol Med*. 2015;35(4):1017-25.

136. Maddaluno L, Urwyler C, Werner S. Fibroblast growth factors: key players in regeneration and tissue repair. *Development*. 2017;144(22):4047-60.

137. Ha J-M, Lim C-A, Han K, Ha J-C, Lee H-E, Lee Y, et al. The Effect of microspicule containing epidermal growth factor on periocular wrinkles. *Annals of dermatology*. 2017;29(2):187-93.

138. Noordam R, Gunn DA, Tomlin CC, Maier AB, Griffiths T, Catt SD, et al. Serum insulin-like growth factor 1 and facial ageing: high levels associate with reduced skin wrinkling in a cross-sectional study. *British Journal of Dermatology*. 2013;168(3):533-

8.

139. Barrientos S, Stojadinovic O, Golinko MS, Brem H, Tomic-Canic M. Perspective article: growth factors and cytokines in wound healing. *Wound Repair and Regeneration*. 2008;16(5):585-601.
140. Wolf NB, Küchler S, Radowski MR, Blaschke T, Kramer KD, Weindl G, et al. Influences of opioids and nanoparticles on in vitro wound healing models. *European Journal of Pharmaceutics and Biopharmaceutics*. 2009;73(1):34-42.
141. Kammeyer A, Luiten RM. Oxidation events and skin aging. *Ageing Research Reviews*. 2015;21:16-29.
142. Lima CF, Valentao PCR, Andrade PB, Seabra RM, Fernandes-Ferreira M, Pereira-Wilson C. Water and methanolic extracts of *Salvia officinalis* protect HepG2 cells from t-BHP induced oxidative damage. *Chemico-Biological Interactions*. 2007;167(2):107-15.
143. Ding Y, Ko S-C, Moon S-H, Lee S-H. Protective effects of novel antioxidant peptide purified from alcalase hydrolysate of velvet antler against oxidative stress in Chang liver cells in vitro and in a zebrafish model in vivo. *International Journal of Molecular Sciences*. 2019;20(20):5187.
144. Heo JH, Heo Y, Lee HJ, Kim M, Shin HY. Topical anti-inflammatory and anti-oxidative effects of porcine placenta extracts on 2,4-dinitrochlorobenzene-induced contact dermatitis. *BMC Complementary and Alternative Medicine*. 2018;18(1):331.
145. Gomes A, Fernandes E, Lima JLFC. Fluorescence probes used for detection of reactive oxygen species. *Journal of Biochemical and Biophysical Methods*. 2005;65(2):45-80.
146. Nensat C, Songjang W, Tohtong R, Suthiphongchai T, Phimsen S, Rattanasinganchan P, et al. Porcine placenta extract improves high-glucose-induced angiogenesis impairment. *BMC Complementary Medicine and Therapies*. 2021;21(1):66.
147. Kendall AC, Nicolaou A. Bioactive lipid mediators in skin inflammation and immunity. *Progress in Lipid Research*. 2013;52(1):141-64.
148. Czapski GA, Czubowicz K, Strosznajder RP. Evaluation of the antioxidative properties of lipoxygenase inhibitors. *Pharmacological Reports*. 2012;64(5):1179-88.
149. Binic I, Lazarevic V, Ljubenic M, Mojsa J, Sokolovic D. Skin ageing: natural weapons and strategies. *Evidence-based complementary and alternative medicine : eCAM*. 2013;2013:827248-.
150. Ahn C-B, Je J-Y, Cho Y-S. Antioxidant and anti-inflammatory peptide fraction from salmon byproduct protein hydrolysates by peptic hydrolysis. *Food Research International*. 2012;49:92-8.
151. Messenger AG, Jennifer Senior H, Bleehen SS. The in vitro properties of dermal papilla cell lines established from human hair follicles. *British Journal of Dermatology*. 1986;114(4):425-30.
152. Zhang H, Nan W, Wang S, Zhang T, Si H, Wang D, et al. Epidermal growth factor promotes proliferation of dermal papilla cells via Notch signaling pathway. *Biochimie*. 2016;127:10-8.
153. Kenworthy AK, Simon SA, McIntosh TJ. Structure and phase behavior of lipid suspensions containing phospholipids with covalently attached poly(ethylene glycol). *Biophysical Journal*. 1995;68(5):1903-20.
154. Rangsimawong W, Opanasopit P, Rojanarata T, Duangjit S, Ngawhirunpat T.

Skin transport of hydrophilic compound-loaded pegylated lipid nanocarriers: comparative study of liposomes, niosomes, and solid lipid nanoparticles. *Biological and Pharmaceutical Bulletin*. 2016;39(8):1254-62.

155. Chain E, Kemp I. The isoelectric points of lecithin and sphingomyelin. *The Biochemical journal*. 1934;28(6):2052-5.

156. Okore VC, Attama AA, Ofokansi KC, Esimone CO, Onuigbo EB. Formulation and evaluation of niosomes. *Indian journal of pharmaceutical sciences*. 2011;73(3):323-8.

157. Yokouchi Y, Tsunoda T, Imura T, Yamauchi H, Yokoyama S, Sakai H, et al. Effect of adsorption of bovine serum albumin on liposomal membrane characteristics. *Colloids and Surfaces B: Biointerfaces*. 2001;20(2):95-103.

158. Masuko T, Minami A, Iwasaki N, Majima T, Nishimura S-I, Lee YC. Thiolation of chitosan. Attachment of proteins via thioether formation. *Biomacromolecules*. 2005;6(2):880-4.

159. Ning M, Guo Y, Pan H, Yu H, Gu Z. Niosomes with sorbitan monoester as a carrier for vaginal delivery of insulin: studies in rats. *Drug Delivery*. 2005;12(6):399-407.

160. Xu Y, Du Y. Effect of molecular structure of chitosan on protein delivery properties of chitosan nanoparticles. *International Journal of Pharmaceutics*. 2003;250(1):215-26.

161. El Maghraby GM, Barry BW, Williams AC. Liposomes and skin: from drug delivery to model membranes. *European Journal of Pharmaceutical Sciences*. 2008;34(4):203-22.

162. El Maghraby GM, Williams AC. Vesicular systems for delivering conventional small organic molecules and larger macromolecules to and through human skin. *Expert Opinion on Drug Delivery*. 2009;6(2):149-63.

163. Münch S, Wohlrab J, Neubert RHH. Dermal and transdermal delivery of pharmaceutically relevant macromolecules. *European Journal of Pharmaceutics and Biopharmaceutics*. 2017;119:235-42.

164. Benderly D, Zolotarsky Y. Beyond thickening – use of alkyl acrylate crosspolymer in personal care formulations. *Polymers for Personal Care and Cosmetics*. ACS Symposium Series. 1148: American Chemical Society; 2013. p. 205-18.

165. Moghassemi S, Hadjizadeh A, Omidfar K. Formulation and characterization of bovine serum albumin-loaded niosome. *AAPS PharmSciTech*. 2017;18(1):27-33.

166. Sahle FF, Gebre-Mariam T, Dobner B, Wohlrab J, Neubert RHH. Skin diseases associated with the depletion of stratum corneum lipids and stratum corneum lipid substitution therapy. *Skin Pharmacology and Physiology*. 2015;28(1):42-55.

167. Udompataikul M, Wongniraspai M, Showpittapornchai U, Jariyapongsakul A. The study on effects and safety of *Spongilla lacustris* in 3% hydrogen peroxide solution on rat skin. *Journal of the Medical Association of Thailand = Chotmaihet thangphaet*. 2012;95 Suppl 12:S15-20.

168. Chen M, WANG D, inventors; XIAMEN UNIVERSITY, Xiamen (CN) assignee. Skin penetration enhancing method and its penetration enhancer. United States patent US10555896B2. 2020.

169. Patzelt A, Lademann J. Drug delivery to hair follicles. *Expert opinion on drug delivery*. 2013;10(6):787-97.

170. Rangsimawong W, Obata Y, Opanasopit P, Ngawhirunpat T, Takayama K.

- Enhancement of galantamine HBr skin permeation using sonophoresis and limonene-containing pegylated liposomes. *AAPS PharmSciTech*. 2018;19(3):1093-104.
171. Alvarez-Román R, Naik A, Kalia YN, Fessi H, Guy RH. Visualization of skin penetration using confocal laser scanning microscopy. *European Journal of Pharmaceutics and Biopharmaceutics*. 2004;58(2):301-16.
172. Lerche D, Sobisch T. Direct and Accelerated Characterization of formulation stability. *Journal of Dispersion Science and Technology*. 2011;32(12):1799-811.
173. Tobin DJ. Aging of the hair follicle pigmentation system. *International journal of trichology*. 2009;1(2):83-93.
174. Hua W, Fan LM, Dai R, Luan M, Xie H, Li AQ, et al. Comparison of two series of non-invasive instruments used for the skin physiological properties measurements: the DermaLab® from Cortex Technology vs. the series of detectors from Courage & Khazaka. *Skin Research and Technology*. 2017;23(1):70-8.
175. Danilenko DM, Ring BD, Pierce GF. Growth factors and cytokines in hair follicle development and cycling: recent insights from animal models and the potentials for clinical therapy. *Molecular Medicine Today*. 1996;2(11):460-7.
176. Hembree JR, Harmon CS, Nevins TD, Eckert RL. Regulation of human dermal papilla cell production of insulin-like growth factor binding protein-3 by retinoic acid, glucocorticoids, and insulin-like growth factor-1. *Journal of Cellular Physiology*. 1996;167(3):556-61.
177. Li J, Yang Z, Li Z, Gu L, Wang Y, Sung C. Exogenous IGF-1 promotes hair growth by stimulating cell proliferation and down regulating TGF- β 1 in C57BL/6 mice in vivo. *Growth Hormone & IGF Research*. 2014;24(2):89-94.
178. Lin W-h, Xiang L-J, Shi H-X, Zhang J, Jiang L-p, Cai P-t, et al. Fibroblast growth factors stimulate hair growth through β -catenin and Shh expression in C57BL/6 mice. *BioMed Research International*. 2015;2015:730139.





APPENDIX A

1. Standard curve for determination of BSA concentration

Standard: BSA
Method: BCA protein assay kit
Detector: The wavelength at 550 nm
Concentrations ($\mu\text{g/mL}$): 0, 25, 125, 250, 500, 1,000

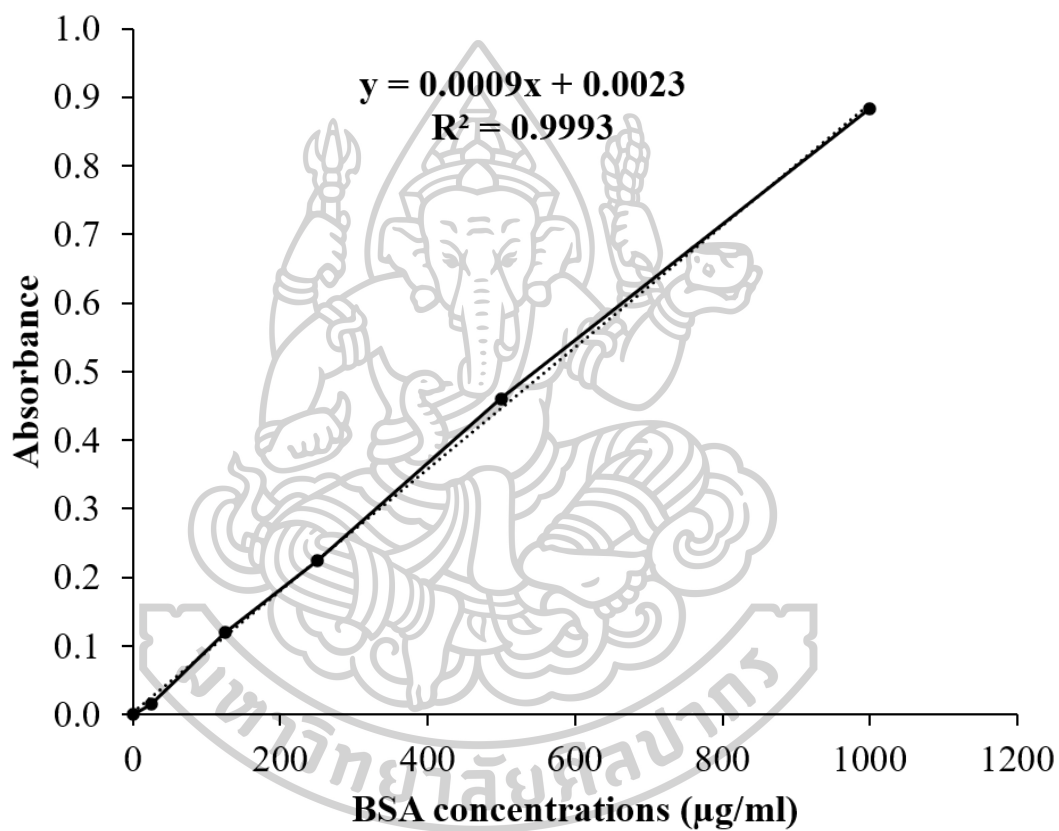


Figure A.1 Standard curve of BSA

2. Standard curve for determination of BSA-FITC concentration

Standard: BSA-FITC
Method: Fluorescence spectrophotometry
Detector: Excitation/emission wavelength 485/535 nm
Concentration(mg/mL): 0.01, 0.05, 0.1, 0.25, 0.5, 1, 2.5, 5

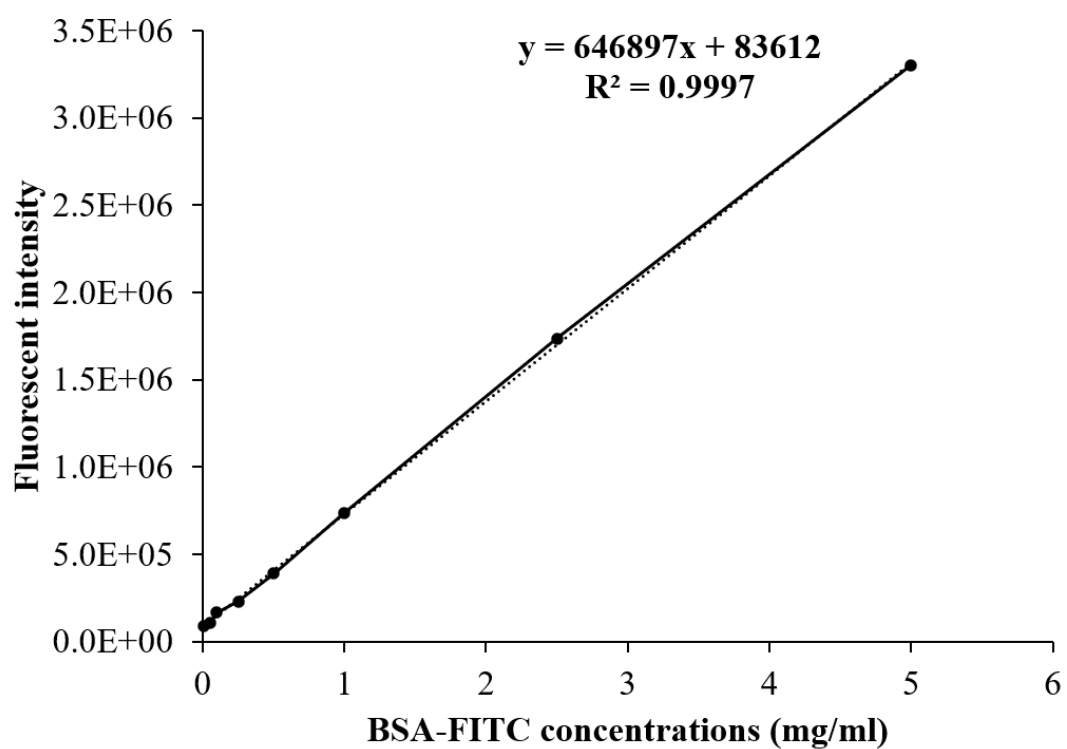


Figure A.2 Standard curve of BSA-FITC

3. Standard curve for determination of EGF

Standard: Recombinant human EGF
Method: ELISA assay kit
Detector: The wavelength at 450 nm
Concentrations (pg/mL): 0, 0.82, 2.05, 5.12, 12.8

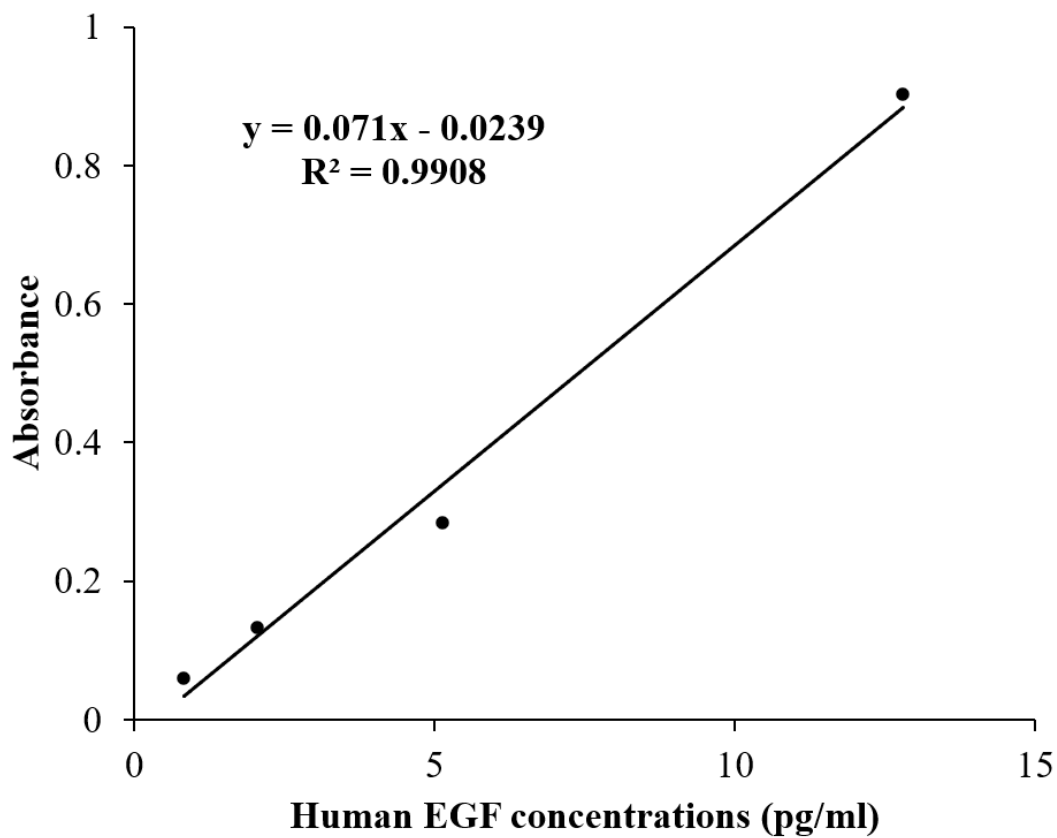


Figure A.3 Standard curve of EGF

4. Standard curve for determination of IGF-1

Standard: Recombinant human IGF-1
Method: ELISA assay kit
Detector: The wavelength at 450 nm
Concentrations (ng/mL): 0.123, 0.307, 0.768, 1.92, 4.8

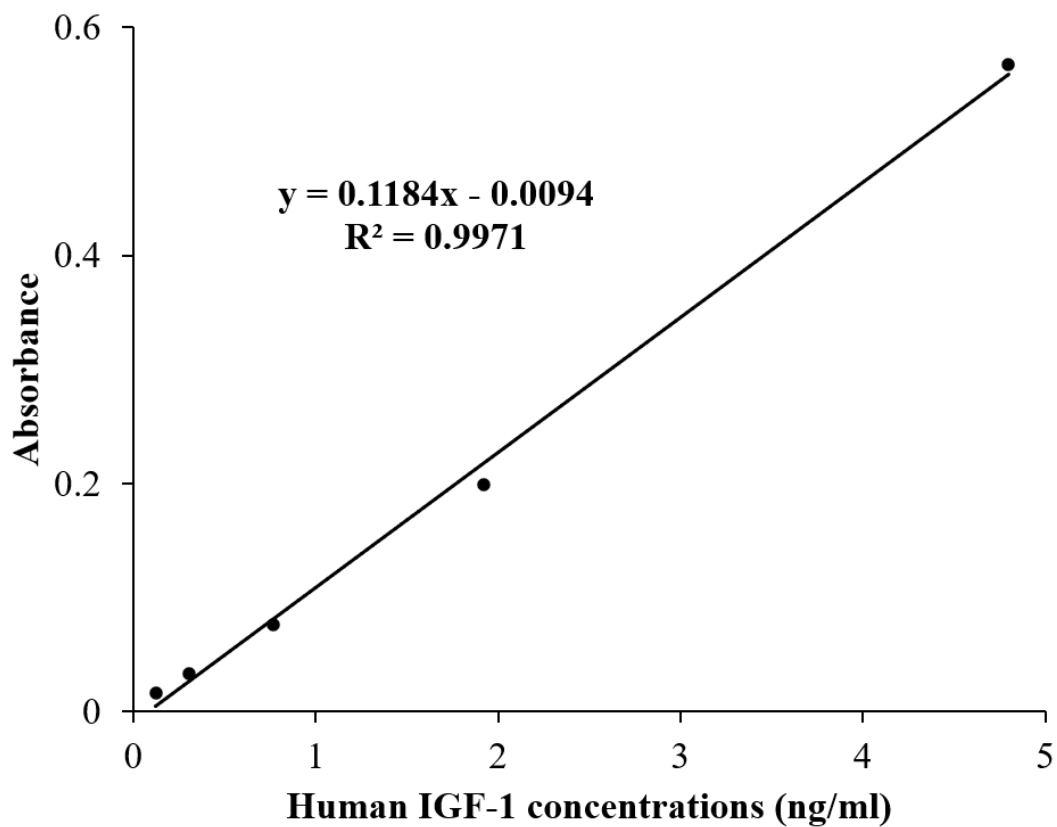


Figure A.4 Standard curve of IGF-1

5. Standard curve for determination of TGF- β 1

Standard: Recombinant human TGF- β 1

Method: ELISA assay kit

Detector: The wavelength at 450 nm

Concentrations (ng/mL): 0, 0.082, 0.247, 0.741, 2.222, 6.667

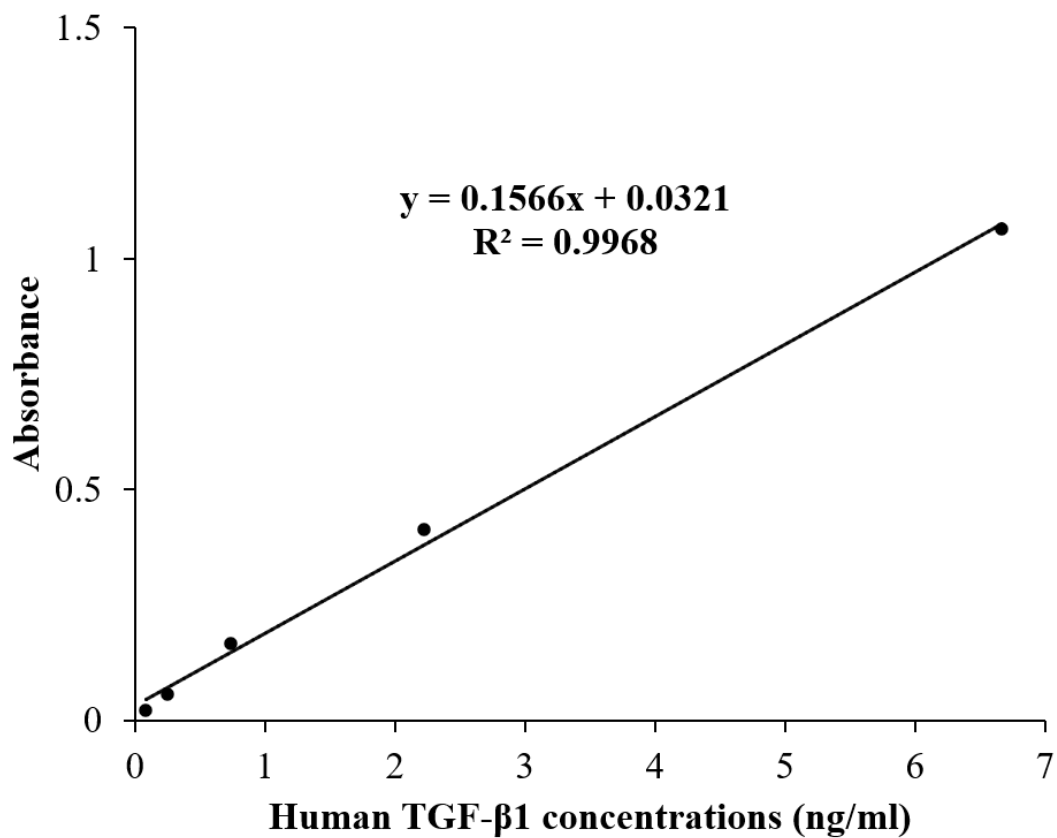


Figure A.5 Standard curve of TGF- β 1

6. Standard curve for determination of FGF2

Standard:	Recombinant human FGF2
Method:	ELISA assay kit
Detector:	The wavelength at 450 nm
Concentrations (pg/mL):	0, 102.4, 256, 640, 1,600, 4,000

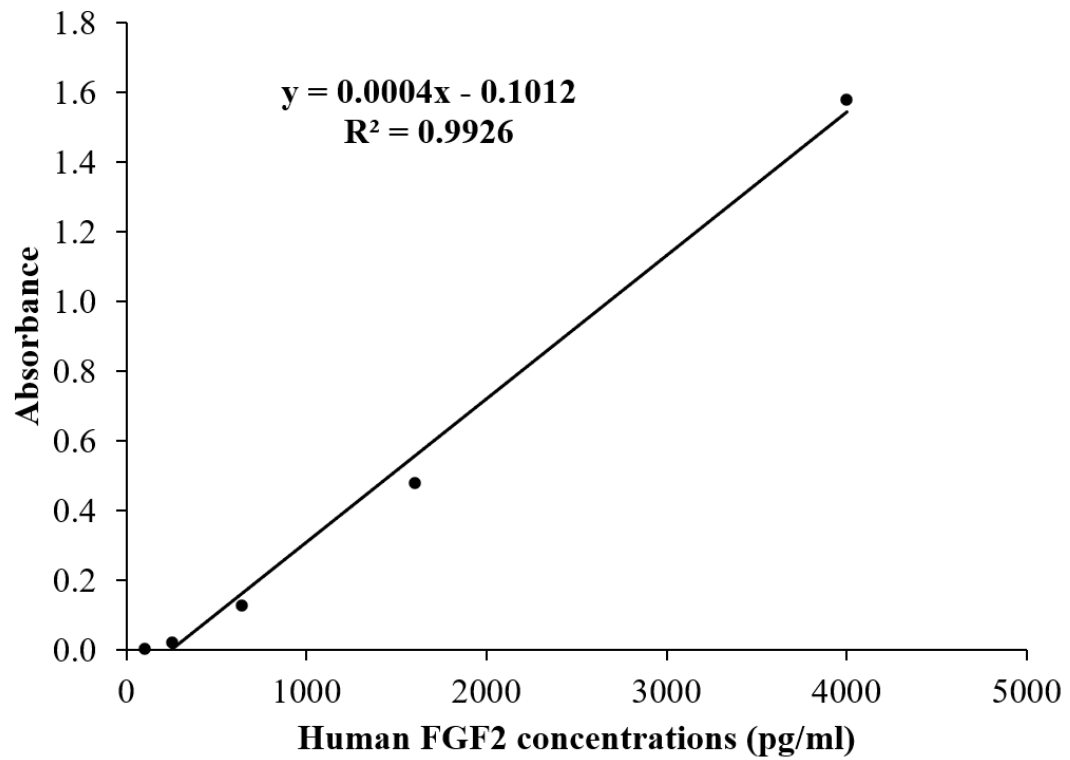


Figure A.6 Standard curve of FGF

7. Standard curve for determination of pro-collagen I

Standard: Human Pro-collagen I alpha I recombinant protein

Method: ELISA assay kit

Detector: Fluorescent intensity at excitation/emission 530/590 nm

Concentrations (pg/mL): 500, 1,000, 2,000, 4,000, 8,000, 16,000

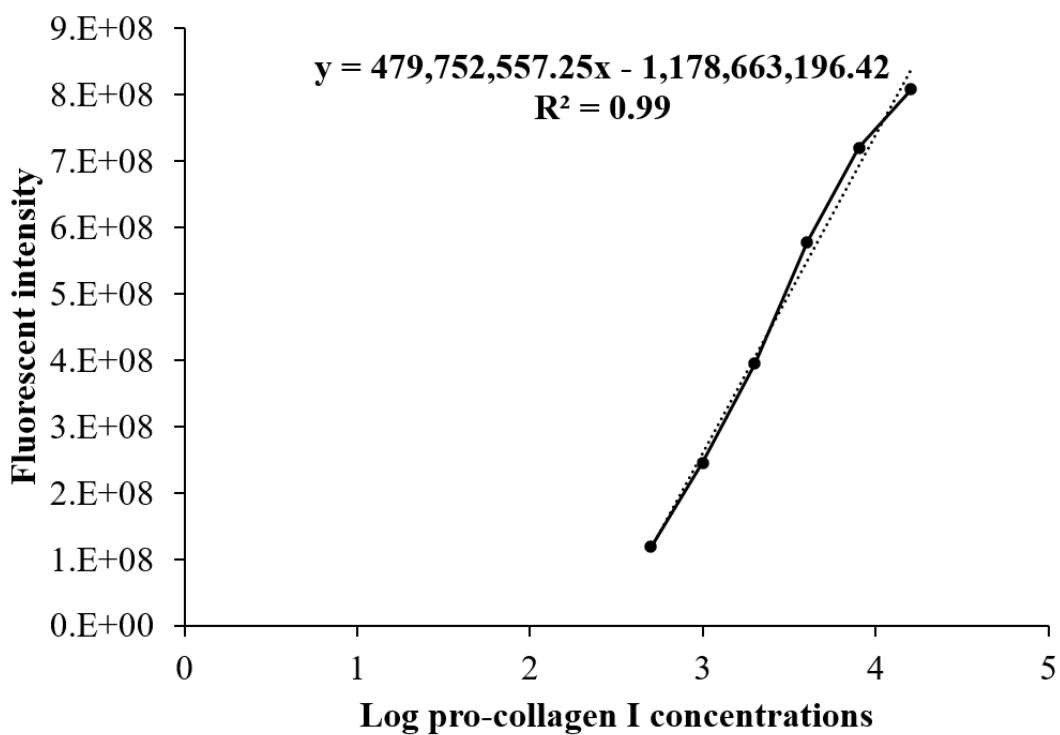


Figure A.7 Standard curve of pro-collagen I

8. Standard curve for determination of MMP9

Standard: Recombinant human MMP9

Method: ELISA assay kit

Detector: The wavelength at 450 nm

Concentrations (pg/mL): 0, 8.23, 24.69, 74.07, 222.2, 666.7

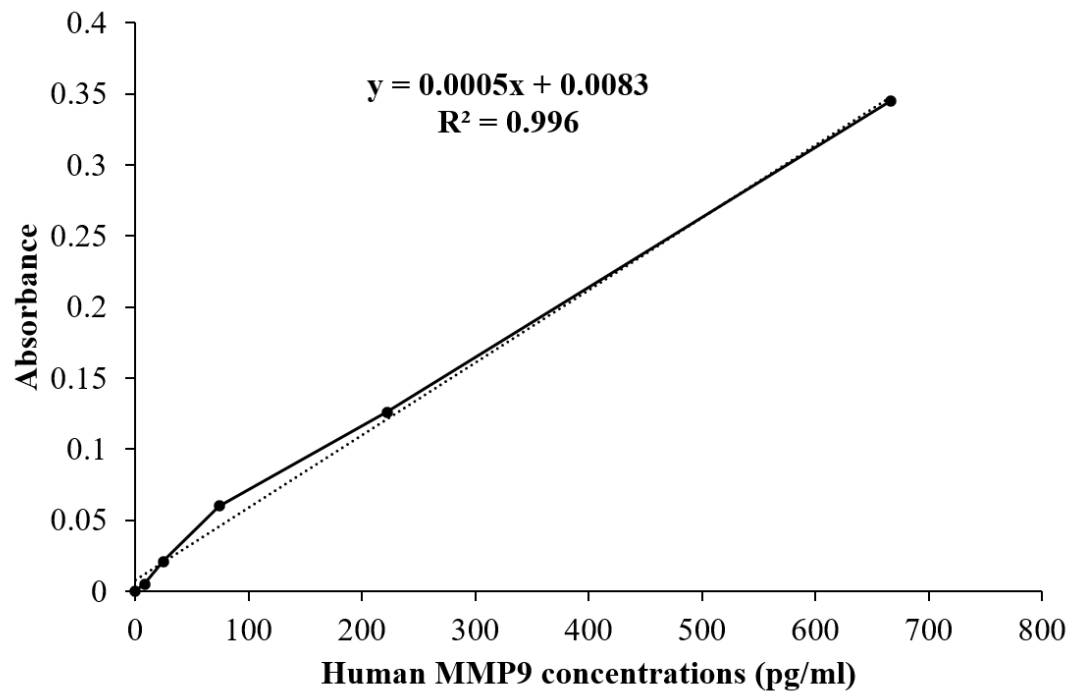


Figure A.8 Standard curve of MMP9

9. Absorbance spectra and wavelength of XO and the Fe³⁺-XO complex

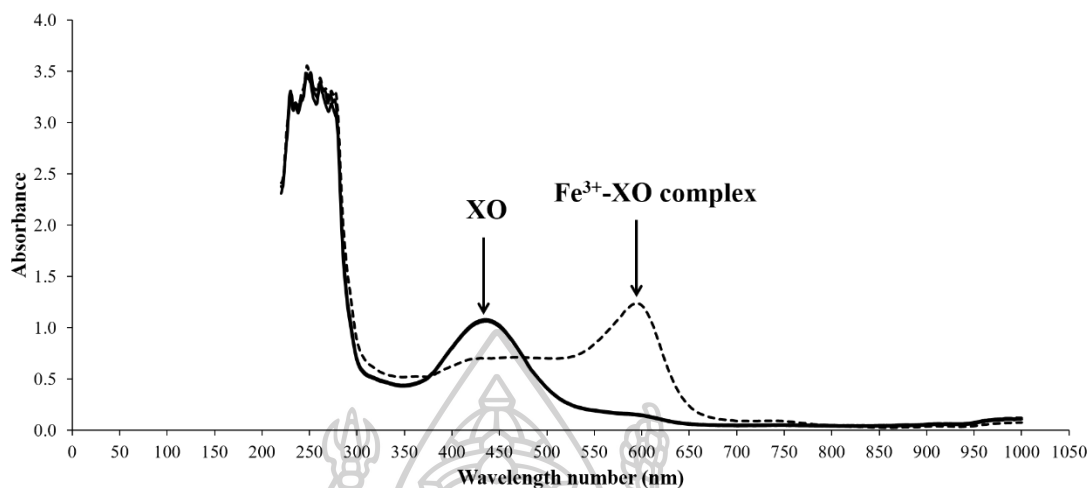


Figure A.9 Absorption spectra of XO (—) and the Fe³⁺-XO complex (-----) in aqueous Tris HCl pH 7.4. Reaction medium consisted of LOX enzyme (167 U/mL), LA (30 μ M), XO (100 μ M), ferric sulfate (Fe₂(SO₄)₃, 500 μ M), sulfuric acid (H₂SO₄, 30 mM) and methanol: water (9:1).



10. LOX inhibitory effect of DAV and PPE

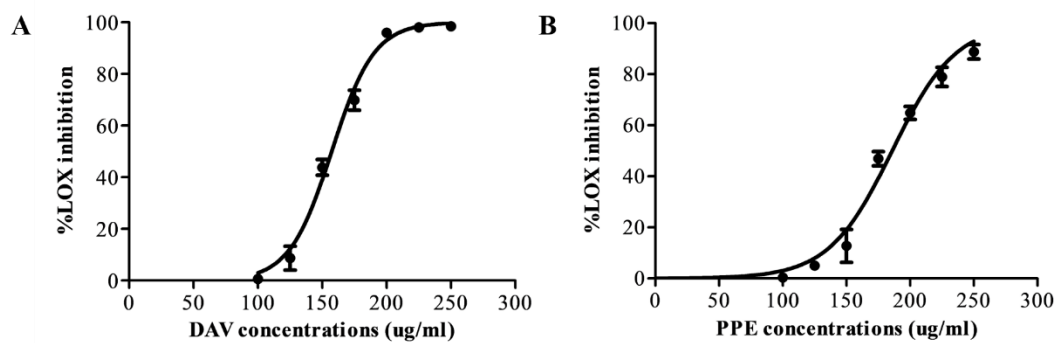


Figure A.9 Image shows the % LOX inhibition of various concentrations (0 - 250 µg/mL) of DAV (A) and PPE (B)



APPENDIX B

Table B.1 Cumulative skin permeation ($\mu\text{g}/\text{cm}^2$) of BSA-FITC-loaded nanocarriers: solution, LI, PEG-LI, NI, PEG-NI, CS-TPP NP, and CS-MHA-TPP NP at different time interval (0 - 8 h)

Time (h)	Solution	LI	PEG-LI	NI	PEG-NI	CS-TPP NP	CS-MHA-TPP NP
0	0	0	0	0	0	0	0
1	2.2367 \pm 0.28	1.6564 \pm 0.18	1.1886 \pm 0.41	1.5898 \pm 0.44	1.1876 \pm 0.71	0.3550 \pm 0.31	0.1715 \pm 0.16
2	2.5816 \pm 0.31	1.7313 \pm 0.20	1.2845 \pm 0.41	2.5852 \pm 0.63	1.8477 \pm 0.62	0.8311 \pm 0.21	0.5474 \pm 0.20
4	2.7652 \pm 0.27	1.7664 \pm 0.08	1.2602 \pm 0.30	3.1259 \pm 0.64	2.5521 \pm 0.20	1.3131 \pm 0.25	1.1853 \pm 0.29
6	2.9947 \pm 0.32	2.3802 \pm 0.25	1.7991 \pm 0.17	3.4054 \pm 0.33	3.0947 \pm 0.73	1.4023 \pm 0.16	1.5268 \pm 0.22
8	3.2916 \pm 0.32	3.0396 \pm 0.11	2.0366 \pm 0.15	3.2020 \pm 0.70	3.2972 \pm 1.34	1.4374 \pm 0.23	1.4799 \pm 0.23

Data present mean \pm S.D. Each formulation was repeated in triplicate.



Table B.2 Cumulative skin permeation ($\mu\text{g}/\text{cm}^2$) of BSA-FIT-loaded formulations (e.g., NI serum, base, NI, NI serum MSs, and solution) at different time interval (0 - 24 h)

Time (h)	NI serum	Base	NI	NI serum MSs	Solution
0	0	0	0	0	0
1	0.4372 ± 0.50	0.0090 ± 0.02	0.0000 ± 0.00	2.6785 ± 2.35	2.1791 ± 0.22
2	0.6449 ± 0.21	0.4942 ± 0.53	0.0095 ± 0.01	7.2764 ± 3.59	2.5352 ± 0.23
4	0.5906 ± 0.19	0.4994 ± 0.31	0.1318 ± 0.02	10.4912 ± 2.62	2.7337 ± 0.20
6	0.6614 ± 0.45	0.3301 ± 0.18	0.5635 ± 0.22	13.1156 ± 3.95	2.9439 ± 0.25
8	1.2483 ± 0.22	1.2581 ± 0.23	0.3965 ± 0.29	15.8188 ± 2.99	3.1972 ± 0.28
24	1.8405 ± 1.11	0.4650 ± 0.23	0.8075 ± 0.30	38.1665 ± 10.64	3.3962 ± 0.30

Data show mean \pm S.D. Each sample was repeated in triplicate.



Table B.3 The percent of hair elongation, MI, skin hydration, and EI after treatment with NI serum MSs containing (0.2%, w/v) DAV or (0.1%, w/v) PPE at day 0, day 14, and day 30.

Parameter	Day 0		Day 14		Day 30	
	DAV	PPE	DAV	PPE	DAV	PPE
%Hair elongation	0	0	38.56 ± 7.86	38.11 ± 40.23	43.87 ± 6.98	51.89 ± 18.65
%MI	99.85 ± 6.77	102.44 ± 4.33	94.73 ± 9.39	114.91 ± 7.93	95.88 ± 15.86	135.15 ± 13.99
%Hydration	14.38 ± 16.99	10.86 ± 12.35	26.79 ± 17.37	17.57 ± 16.53	32.24 ± 20.09	29.52 ± 16.97
%EI	99.22 ± 10.63	103.12 ± 8.42	98.18 ± 12.24	92.19 ± 7.44	97.38 ± 6.61	84.66 ± 4.72

Data represent mean ± S.D. (n=12).



VITA

NAME Kritsanaporn Tansathien

DATE OF BIRTH 04 August 1988

PLACE OF BIRTH Bangkok, Thailand

INSTITUTIONS ATTENDED Faculty of Pharmacy, Silpakorn University

HOME ADDRESS 8 Moo 5, Banmai, SamPhran, Nakorn Pathom, 73110

PUBLICATION

INTERNATIONAL JOURNAL

Tansathien K, Nuntharatanapon N, Jaewjira S, Pizon JRL, Opanasopit P, Rangsimawong W. Solid lipid nanoparticles containing Pueraria mirifica ethanolic extract for hair growth promotion. *Key Engineering Materials*. 2019;819:175-80.

Tansathien K, Suriyaaumporn P, Charoenputtakhun P, Ngawhirunpat T, Opanasopit P, Rangsimawong W. Development of sponge microspicule cream as a transdermal delivery system for protein and growth factors from deer antler velvet extract. *Biological and Pharmaceutical Bulletin*. 2019;42(7):1207-15.

Tansathien K, Chareanputtakhun P, Ngawhirunpat T, Opanasopit P, Rangsimawong W. Hair growth promoting effect of bioactive extract from deer antler velvet-loaded niosomes and microspicules serum. *International Journal of Pharmaceutics*. 2021;597:120352.

THAI JOURNAL

Tansathien K, Suriyaaumporn P, Ngawhirunpat T, Rangsimawong W, Opanasopit P. Effect of pegylated transfersomes containing macromolecular protein on transdermal delivery. *Interprofessional Journal of Health Sciences*. 2019;17(2):48-54.

CONFERENCE PROCEEDING

Tansathien K, Nuntharatanapong N, Sukma M, Rangsimawong W, Opanasopit P, Suksaeree J, Shuwisitkul D, editors. PEG2000-DSPE grafted niosomes for enhanced transdermal protein delivery. The International Conference and Exhibition on Pharmaceutical Sciences and Technology 2020 (PST2020) Proceeding supplement; 2020 May 19-20; College of Pharmacy Rangsit University, Thailand; 2020.